Università
Ca'Foscari
Venezia

Scuola Dottorale di Ateneo
Graduate School

Dottorato di ricerca
in Scienze Chimiche
Ciclo XXVI
(A.A. 2010/2011 – 2012/2013)

Advanced Materials for Inorganic Pollutants Electroanalysis

SETTORE SCIENTIFICO DISCIPLINARE DI AFFERENZA: CHIM/01
Tesi di Dottorato di Mardegan Andrea, matricola 955840

Coordinatore del Dottorato

Prof. Maurizio Selva

Tutore del Dottorando

Prof. Paolo Ugo

Co-tutore del Dottorando

Dott. Paolo Scopece

Contents

List of abbreviations

2D-NEE	Two dimensional ensembles of nanoelectrodes
3D-NEE	Three dimensional ensembles of nanoelectrodes
A_{act}	Active area
AdCSV	Adsorptive cathodic stripping voltammetry
AFM	Atomic Force Microscopy
A_{geom}	Geometric area
ASV	Anodic Stripping Voltammetry
Au-Nps	Gold Nanoparticles
Bi-AuE	Bismuth modified gold electrode
BiFEs	Bismuth film electrode
Bi-NEE	Bismuth modified NEE
CD	Critical dimension
C-MEMS	Carbon Micro Electro Mechanical System
CNT	Carbon Nanotubes
CV	Cyclic Voltammetry
D	Energy Dose
DI water	Deionized water
DL	Detection limit
DMG	dimethylglyoxyme
E_p	Peak Potential
$E_{p/2}$	Half wave potential
f	Fractional electrode area
FE-SEM	Field Emission - Scanning Electron Microscope
GBL	Gamma-butyloractone
GC	Glassy carbon
GNEE	Gold nanoelectrode ensembles
HMDE	Hanging mercury drop electrode
Hz	Hertz
IC	Integrated Circuit
ICP	Inductively coupled plasma
ICP-MS	Inductively coupled plasma – mass spectroscopy
ICP-OES	Inductively coupled plasma – optical emission spectroscopy

I_c	Capacitive current
I_F	Faradic current
I_{lim}	Limiting current
I_p	Peak Current
IR	Infrared
IUPAC	International Union of Pure and Applied Chemistry
$k°$	Standard rate constant for heterogeneous electron transfer
$k°_{app}$	Apparent rate constant for heterogeneous electron transfer
LR	Linear Range
m	Slope of the calibration plot
MEA	Microelectrode arrays
MEMS	Micro Electro Mechanical Systems
NEA	Nanoelectrode arrays
NEE	Nanoelectrode ensembles
NIST	National Institute of Standard and Technology (USA)
PC	Polycarbonate
PEB	Post-exposure baking
PPCE	Pyrolyzed photoresist carbon electrode
PVP	Polyvynilpyrrolidone
q	Surface density of nanodiscs in a NEE (nanodiscs cm^{-2})
R_a	Roughness
R^2	Linear Correlation Coefficient
rpm	Rotations per minutes
RSD	Relative Standard Deviation
SEM	Scanning Electron Microscope
SPS	Screen printed substrate
SWV	Square Wave Voltammetry
T	Polymer thickness
T_g	Glass transition temperature
TGA	Thermo gravimetric analysis
TO	Total overlap
UV	Ultraviolet
v	Scan rate
V	Volt

WHO	World Health Organization
XRD	X Ray Diffraction
ΔE	Separation between the peak potentials
γ	Activity coefficient
σ_b	Standard Deviation of the blank
ϑ	Fraction of blocked electrode surface

Lentamente muore chi diventa schiavo dell'abitudine, ripetendo ogni giorno gli stessi percorsi, chi non cambia la marcia, chi non rischia e non cambia colore dei vestiti, chi non parla a chi non conosce.

Muore lentamente chi evita una passione, chi preferisce il nero su bianco e i puntini sulle "i", piuttosto che un insieme di emozioni, proprio quelle che fanno brillare gli occhi, quelle che fanno di uno sbadiglio un sorriso, quelle che fanno battere il cuore davanti all'errore e ai sentimenti.

Lentamente muore chi non capovolge il tavolo, chi è infelice sul lavoro, chi non rischia la certezza per l'incertezza, per inseguire un sogno, chi non si permette almeno una volta nella vita di fuggire ai consigli sensati.

Lentamente muore chi non legge, chi non viaggia, chi non ascolta musica, chi non trova grazia in se stesso.

Muore lentamente chi distrugge l'amor proprio, chi non si lascia aiutare, chi passa i giorni a lamentarsi della propria sfortuna o della pioggia incessante.

Lentamente muore chi abbandona un progetto prima di iniziarlo, chi non fa domande sugli argomenti che non conosce, chi non risponde quando gli chiedono qualcosa che conosce.

Evitiamo la morte a piccole dosi, ricordando sempre che essere vivo richiede uno sforzo di gran lunga maggiore del semplice fatto di respirare.

Soltanto l'ardente pazienza porterà al raggiungimento di una splendida felicità...

[Pablo Neruda]

Sommario

Obiettivo di questo lavoro di tesi è lo sviluppo e l'applicazione di nuovi materiali elettrodici per l'analisi di inquinanti inorganici classificati dall'Organizzazione Mondiale della Sanità (WHO) come inquinanti prioritari.

Come materiali innovativi sono presentati ensemble di nanoelettrodi d'oro (NEE) ed elettrodi di carbonio prodotti attraverso la pirolisi di un fotoresist negativo (PPCE).

I NEE vengono fabbricati tramite deposizione *electroless* di oro all'interno dei pori di membrane *track-etched* di policarbonato (PC), commercialmente disponibili. La membrana, in questo caso, funge da stampo (*template*) per la crescita delle nanofibre metalliche.

Grazie alla loro struttura geometrica, i NEE operano in regime diffusivo di *total overlap* (TO) e, di conseguenza, sono caratterizzati da un elevato rapporto segnale/rumore che permette di raggiungere limiti di rivelabilità più bassi, rispetto ad elettrodi convenzionali, quando vengono usati in determinazioni "dirette", senza cioè uno step di preconcentrazione.

In questo lavoro è stato deciso di applicare per la prima volta questo tipo di elettrodi in voltammetria di stripping anodico (ASV); la prima applicazione analitica descritta in questa tesi, riguarda la determinazione di Arsenico inorganico in matrici acquose.

La bassa corrente capacitiva tipica dei NEE consente di raggiungere un limite di rivelabilità (DL) di 5 ngL^{-1} per As(III), circa due ordini di grandezza più basso di quello raggiungibile con un elettrodo convenzionale.

L'ASV permette l'analisi separata di entrambe le specie di As inorganico, che presentano gradi di tossicità molto diversi tra loro. Applicando un potenziale di deposizione opportuno si preconcentra all'elettrodo solo As^{3+}; in seguito, dopo riduzione chimica dell'As^{5+} ad As^{3+}, si determina la concentrazione dell'arsenico totale. Questa potenzialità delle tecniche elettrochimiche, unita alla possibilità di effettuare misure in campo e ai bassi costi le rende vantaggiose rispetto alle normali tecniche spettroscopiche.

Dato che la superficie elettrodica disponibile per la preconcentrazione è limitata, i NEE soffrono di facile saturazione anche a basse concentrazioni quindi il loro range dinamico lineare è molto ristretto. Per questa ragione viene anche proposta una diversa procedura di fabbricazione dei NEE nella quale i nanodischi sono sostituiti da nanofibre. Per questo scopo la membrana di policarbonato subisce un etching controllato portando così alla formazione di strutture tridimensionali (3D-NEEs). Gli *ensembles* di nanofibre (3D-NEEs) non soffrono di saturazione e sono applicati per la determinazione di arsenico inorganico in campioni reali.

I NEE sono stati anche integrati in un prototipo di cella in flusso, sempre per l'analisi di As(III) attraverso ASV. Quest'ultimo punto mette le basi per lo sviluppo di uno strumento da campo in cui il NEE sia l'elettrodo lavorante.

La seconda parte della tesi è focalizzata sulla modifica di elettrodi d'oro con bismuto per ampliarne la finestra accessibile di potenziale. L'oro, infatti, presenta una bassa sovratensione per la reazione di riduzione degli H^+ a idrogeno che interferiscono nell'analisi di quei metalli il cui potenziale di stripping è inferiore a -0.5V (Pb, Cd, …).
Per quanto riguarda il range catodico della finestra di potenziale, gli elettrodi a film di bismuto forniscono prestazioni elettroanalitiche, molto simili a quelle degli elettrodi di mercurio in termini di precisione, riproducibilità e stabilità dei segnali rappresentano quindi una valida alternativa all'impiego di un elemento tossico come il mercurio.
In quest'ottica, è stato deciso di modificare i NEE con bismuto e di usarli nella voltammetria di stripping anodico del Pb(II). Le caratteristiche geometriche dei NEE unite alle performance in voltammetria di stripping degli elettrodi a film di bismuto hanno portato a DL di 30 ng L^{-1}, che è il più basso tra quelli di letteratura che utilizzano metodi elettrochimici. In questo caso, sono stati confrontati metodi di deposizione di bismuto *in-situ* ed *ex-situ*, ottenendoriuslatti leggeremente migliori con la seconda metodologia.
Si è poi passati allo studio di un'altra tecnica analitica usata nell'elettroanalisi di metalli pesanti ovvero la voltammetria di adsorbimento e ridissoluzione catodica (AdCSV).
Dapprima è stata definita una metodica per la determinazione simultanea di Ni(II) e Co(II) attraverso AdCSV su elettrodi convenzionali d'oro. È stato sviluppato un protocollo di modifica dell'elettrodo *in-situ* che, a differenza della modifica *ex-situ*, rende l'analisi più semplice e più adatta per determinazioni sul campo.
Il metodo ottimizzato è risultato essere caratterizzato da limiti di rivelabilità di 97 e di 58 ng L^{-1} per Ni(II) e Co(II) rispettivamente. La metodologia analitica così sviluppata è stata infine applicata con successo alla determinazione di tracce di Ni(II) in campioni di acqua della laguna di Venezia.

L'ultima parte della tesi è stata focalizzata sullo sviluppo di elettrodi di carbonio prodotti per pirolisi di un fotoresist negativo ottenendo elettrodi denominati PPCE (Pyrolyzed Photorest Carbon Electrodes). Questi elettrodi sono stati ottenuti impiegando tecniche poco costose quali la fotolitografia ottica seguita da pirolisi in ambiente inerte.

La fotolitografia è una tecnica di microfabbricazione che si basa sulla rimozione selettiva di parti di un film sottile di un polimero (fotoresist) esposto – o non – alla luce UV.

In questa tesi, sono stati ottimizzati i parametri coinvolti nella pirolisi (temperatura finale e *dwell time*) perché questi hanno un grande impatto sulla struttura finale del materiale ottenuto, influenzando così il comportamento elettrochimico degli elettrodi ottenuti. Gli elettrodi prodotti in diverse condizioni sperimentali sono stati caratterizzati mediante spettroscopia Raman, diffrazione a raggi X (XRD), misure di resistenza elettrica e voltammetria.

È stato anche studiato l'effetto del substrato e dello spessore del film di fotoresist.

Al fine di verificare l'applicabilità dei PPCE all'analisi di inquinanti inorganici, questi elettrodi sono stati modificati con Bismuto per poi essere applicati per l'analisi di concentrazioni a livello di tracce di Cd(II) e Pb(II) (attraverso voltammetria di stripping anodico) e di Ni(II) e Co(II) (attraverso voltammetria di stripping catodico di adsorbimento). Infine, sono state eseguite delle promettenti prove preliminari volte a verificare la possibilità di modificare i PPCE con nanoparticelle d'oro e di applicarli per l'analisi di As(III) .

Per tutti gli analiti sono stati calcolati limiti di rivelabilità inferiori al μgL^{-1}. I risultati ottenuti indicano che i PPCE possono rappresentare una valida alternativa ad altri elettrodi ottenuti con tecniche di micro fabbricazione quali gli elettrodi *screen printed*.

Aims of the thesis

The main goal of this thesis is to exploit the capabilities of advanced materials and nanostructured devices, such as gold Nanoelectrode Ensembles (NEEs) and Pyrolyzed Photoresist Carbon Electrodes (PPCE), for the electroanalysis of some priority inorganic pollutants.

NEEs show remarkable advantages in comparison with conventional electrodes, thanks to their particular geometry. This distinctive feature makes them suitable for different uses; between them we'll concentrate on the possibility to improve the performances of conventional gold electrodes while used in anodic stripping voltammetry. By exploiting their particular geometry, these devices can be used for the determination of trace analytes in real samples at the subnanomolar concentration range.

In *Chapter 2*, NEEs are applied for the first time to the anodic stripping voltammetric determination of inorganic Arsenic. The use of these devices becomes convenient, compared with conventional spectroscopic methods, because they can perform oxidation state speciation and can be integrated in a portable and decentralized analyzer. This kind of electrodes is therefore also integrated in a flow cell with the prospect of developing a portable sensing station.

NEEs suffer from the fact that electrode surface useful for electrochemical accumulation of analytes is very limited. For this reason, a different NEE fabrication procedure in which the nanodisk electrodes are substituted by short nanofibers is proposed. The structure of the final ensemble changes from a 2-D structure into a 3-D one where gold nanowires protrude from the polycarbonate template. The electrochemical behavior of As(III) at 3D-NEE is compared and discussed.

Gold electrodes present a high hydrogen evolution at relatively low potential values. This fact makes very difficult the analysis of metals whose stripping peak is in the cathodic region.

In *Chapter 3*, the modification gold NEEs with Bismuth (whose electrochemical behavior is comparable to that of mercury) is studied and for the first time applied to the anodic stripping voltammetry of Pb(II) is performed. We'll discuss the advantages and limit of NEEs compared to conventional gold electrodes. We study the modification of gold NEEs with Bismuth obtaining, for the first time arrays of bismuth nanoelectrodes.

In *Chapter 4*, we report the simultaneous in-situ adsorptive cathodic stripping determination of Nickel and Cobalt at bismuth modified gold electrodes. This technique is useful and complementary to ASV, which we use in Chapter 2 and 3.
The morphology of the bismuth deposit onto the gold substrate, investigated by scanning electron microscopy, confirmed the successful deposition of bismuth microparticles onto the gold substrate. After optimization, a concentration below 1 μgL^{-1} Ni(II) is detected in real water samples taken from the lagoon of Venice.

The results achieved in the above chapters, constitute the basis and find further development in Ch*apter 5* which is devoted to the study and electroanalytical application of a new kind of electrode material named Pyrolyzed Photoresist Carbon.
Pyrolyzed Photoresist Carbon Electrodes (PPCE) are conveniently fabricated employing simple and inexpensive batch fabrication methodologies i.e., UV photolithography followed by pyrolysis. In this chapter, we optimize the pyrolysis conditions since they sensitively impact the microstructure of these electrodes, and as consequence they also influence the chemical and electrochemical behavior necessitating an optimization of the entire process. PPCEs give quasi-ideal electrochemical response and they display good reproducibility.
At the end of the chapter we'll demonstrate for the first time the applicability of pyrolyzed photoresist carbon electrodes for the analysis of heavy metals ions. To this aim, Bi-modified PPCE are used to analyze trace concentration of Cd(II) and Pb(II) via anodic stripping voltammetry (ASV) and Ni(II) and Co(II) by adsorptive cathodic stripping voltammetry. PPCE modified with gold nanoparticles are finally developed for performing preliminary tests on the possible ASV determination of trace As(III).
Advantages and limits of these approaches are compared and discussed, together with relevant prospects and further developments.

Chapter 1: Introduction

1.1 Modern Electroanalysis: a short overview

Electroanalysis can be classified as a special area of electrochemistry which is aimed on identification and on quantification of chemical substance(s) in the sample using electrochemical methods.

Historically, the real beginning of electroanalysis began in the first half of the 20th century, together with the rapid progress of Heyrovský's polarography [1] and techniques with modulated potential ramp [2-3], followed by invention of highly effective electrochemical stripping analysis [4] plus its further extension to the time-dependence mode [5]. Lately, the amperometric / coulometric detection in flowing streams [6] contributed to the expansion of electrochemical principles into the field of analytical separations.

In parallel with these current flow-based measurements, there were also other aspirants for wider applicability in electroanalysis. Within them, the dominant position was held by potentiometry [7] and by relatively recently proposed techniques, such as electrochemical impedance spectroscopy (EIS [8]), electrochemiluminescence analysis [9], and scanning electrochemical microscopy (SECM [10-12]).

Similarly as in other fields of instrumental analysis, the development and expansion of both electrochemistry and electroanalysis is tightly associated with the progress in instrumentation.

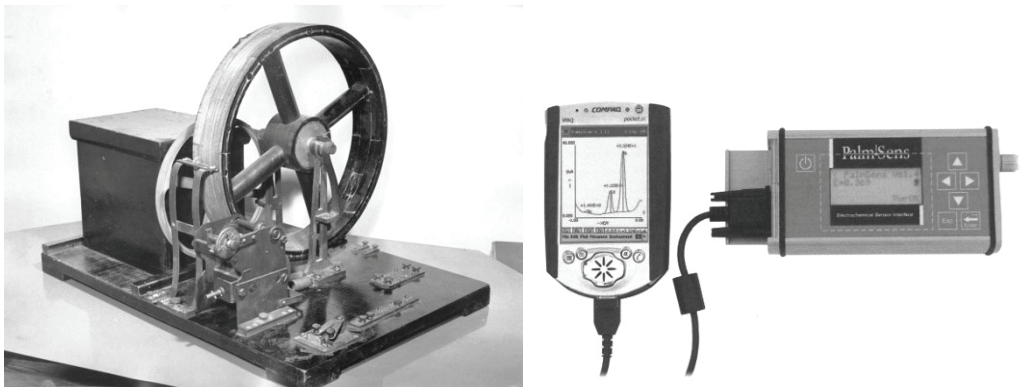

Figure 1.1. A) First polarograph by Heyrovský and B) modern portable miniaturized analyser.

However there is still margin for further progress in particular to improve sensitivity, specificity and miniaturization of electrochemical measurements. A key factor for this further progress is associated with the development of advanced working electrodes, which represent "the heart" of each electroanalytical system.

1.2 Stripping voltammetry

Stripping analysis is an analytical method that utilizes a bulk electrolysis step (*preelectrolyis*) to preconcentrate a substance from solution into the small volume of a mercury electrode or onto the surface of the working electrode (WE). After this electrodeposition step, the material is redissolved (*stripped*) from the electrode using some voltammetric technique. Different versions of the stripping analysis can be employed, depending on the nature of the deposition and measurement steps [13].

1.2.1 Anodic Stripping Voltammetry (ASV)

Anodic stripping voltammetry is the most widely used form of stripping analysis. The metals are preconcentrated by cathodic deposition at a controlled time and potential onto the WE. The metal ions reach the WE by diffusion and convection (achieved by electrode rotation or solution stirring), where they are reduced and concentrated. In the case of a mercury electrode the deposition could be written as follow:

$$Mn^{+} + ne^{-} + Hg \rightarrow M(Hg) \qquad (1.1)$$

After the deposition, the potential is scanned anodically with a selected potential waveform. During this anodic scan, the metals are reoxidized, stripped out of the electrode, and an oxidation current is observed:

$$M(Hg) \rightarrow Mn^{+} + ne^{-} + Hg \qquad (1.2)$$

Peak potentials serve to identify the metals in the sample. The peak current depends on various parameters of the deposition and stripping steps, as well as on the characteristics of the metal ion and on the electrode geometry.

The major type of interferences in ASV procedures are overlapping stripping peaks caused by similarity in the oxidation potentials (Pb, Tl, Cd, Sn or Bi, Cu, As), by the presence of surface-active organic compounds that adsorb on the electrode surface and inhibit the metal deposition, and by the formation of intermetallic compounds (e.g., Cu-As), which affects the

peak size and position. Knowledge of these interferences can lead to their prevention, through adequate attention to key operations.

1.2.2 Adsorptive Stripping Voltammetry (AdSV)

When the analyte reacts irreversibly or forms intermetallic compounds or cannot form an amalgam/alloy, the adsorptive stripping protocols can be an interesting approach [13-15]. The adsorptive stripping procedures commonly rely on the interfacial accumulation of target metal complexes onto a mercury drop or mercury film electrode, thus a large variety of metal analytes such as vanadium [16], chromium [17,18], molybdenum [19], aluminum [20], nickel, cobalt [21], etc. can be successfully determined.

In the case of Ni(II) and Co(II), complexed by dimethylglyoxyme (DMG), the mechanism for the adsorption and cathodic stripping voltammetry of M(II)-DMG_2 (M^{2+} is either Ni^{2+} or Co^{2+}) complexes can be explained as [22]:

$$M(II)\text{-}DMG_2\ (solution) \rightarrow M(II)\text{-}DMG_2\ (ads) \qquad (1.3)$$

After adsorption on the electrode surface the application of cathodic potential scan results in the reduction of the metal complex represented by the equation:

$$M(II)\text{-}DMG_2\ (ads) + ne^- \rightarrow M(II)\text{-}DMG_2^{n-} \qquad (1.4)$$

In reaction (1.4), both the metal ion and complex are reduced. The first step is the reduction of the central metal

$$M(II)\text{-}DMG_2(ads) + 2e^- \rightarrow M(0) + 2\ DMG^-\ (ads) \qquad (1.5)$$

followed by a four electron reduction of the glyoximate ligands.

1.3 Electrochemical Measurements in Environmental Analysis

Main Topics, Problems and Strategies

Undoubtedly, a discipline that includes the identification, quantification, and monitoring of various species in the environment is also one of the largest areas of electroanalysis [23-25]. The reason is that there is a wide variety in choice of the: measuring techniques and approaches applicable; principles of the respective methods and procedures; electrodes, sensors, and detection units; samples to be analysed.

Main Approaches in Electroanalysis of Environmental Samples

Together with classification of the individual analytes, samples, typical topics and trends, environmental electroanalysis can also be characterised by the way of performing the respective measurements and observations. In this optics, the following categories can be outlined:

(1) *Preliminary / orientation screening of the substance(s) of interest*. In experiments of this kind, sufficient selectivity towards the target analyte is the primary requirement, whereas the overall performance or detection capabilities of the corresponding method(s) are of secondary importance. This opens certain possibilities for some less effective techniques, such as (equilibrium) potentiometry, or even classical polarography, whose advantages remain in tradition, simple equipment, and very low expenses.

(2) *Identification and quantification of the analyte / Determination of its total content*. In routine analysis, the proper identification of the analyte of interest and, mainly, its quantitative determination is the key information. With respect to the fact that a majority of environmental determinations belongs to trace analysis selected technique(s) and the corresponding method must obey quite strict criteria with respect to sufficiently high selectivity and sensitivity, good reproducibility, and the adequate analytical performance, hand in hand with economical balance. Moreover, some more effective measurements with rather expensive instrumentation, e.g. those based electrochemical stripping analysis (ESA) or one-purpose highly effective analysers should offer yet further benefits, such as certain number of samples per time period, ability of simultaneous analysis, remote control and full compatibility with PC, or even automation of the whole analytical procedure.

(3) *Chemical speciation of the individual forms of the substance in the sample*. In certain simplification, chemical speciation can be made either as differentiation between two typically behaving species, or also complete speciation of all the existing forms and its actual distribution in the sample. Analyses of this kind are always a challenging task requiring the adequate approach to the sample collection and pre-treatment, right choice of instrumental technique, as well as to the proper analysis and evaluation of the results.

(4) *Field monitoring / Outdoor analysis*. A rather specific area of environmental analysis, where highly powerful but large, heavy, and expensive instrumentation typical e.g. for spectral and separation techniques may become a principal limitation in being used out of lab, in the field monitoring. In contrast to this, modern electrochemical instrumentation involves a number of portable analysers and miniaturised devices [26] that may offer surprisingly good performance in relation with generally less comfort of use and unfavourable conditions of outdoor experimentation.

1.3.1 Requirements on the Working Electrodes

(a) *metrological properties*: precision and accuracy; reproducibility / repeatability of the signal (in trace analysis, typically within ± 5-10 %); stability of the response.
(b) *electroanalytical performance* that means proportionality / linearity of the signal with concentration; sensitivity / detection characteristics; selectivity vs. interference profile; base-line character and the actual signal-to-noise ratio as apparently the most specific parameters of each particular detection / sensing system.
(c) *other features* such as mechanical stability and resistance; friendly-to-use construction with simple handling; compatibility with modern instrumentation, including capability of being miniaturised and/or employed in automated and remote-control systems; reasonable price; ecological acceptability and maximal harmony with the principles of green analytical chemistry.

1.4 Electrode materials alternative to mercury

1.4.1 Bismuth, antimony and amalgam electrodes

Mercury electrodes are widely described in the literature and the three main configurations are hanging mercury drop electrode (HMDE), stationary hanging mercury drop and mercury film electrodes [13, 27-29]. The advantages of mercury electrodes over electrodes made of other materials are high hydrogen overvoltage and good reproducibility of the surface; drawbacks are the toxicity and low redox potential. Mercury electrodes are used principally for the determination of metal ions which form an amalgam with Hg.
Seemingly unshakeable position and real dominance of the mercury-drop and mercury-film based electrodes in practical electroanalysis [30-35] had abruptly deteriorated with the

commencement of the new millennium and massive propagation of ecologically oriented analysis propagating the principles of "*green analytical chemistry*". The turbulence around this breakpoint has been quickly reflected in the respective activities of electroanalysts, having introduced **bismuth**- [36-38] or **antimony**-based electrodes [39,40] that became soon very popular as the most promising alternative to mercury electrodes.

Meanwhile, since liquid metal became almost unwanted, some efforts to keep mercury in electroanalytical practice in the form of non-toxic **amalgams** has been performed [41-43].

1.4.2 Carbon electrodes

The advantages of carbon electrodes include low cost, wide potential window, relatively inert electrochemistry, and electrocatalytic activity for a variety of redox reactions. Of particular relevance are oxidations and reductions of organic and biological molecules in both aqueous and nonaqueous media, for which the electrochemical properties of carbon electrodes are often superior to those of noble metals. However, only special forms of carbon / graphite - e.g., glassy carbon and wax-impregnated pyrolytic graphite [44] or carbon paste [45] - could compete with to the precious metals with respect to the overall electroanalytical performance.

Otherwise, in response to the advances in new technologies, also other interesting materials came to the fore; some of them attracting considerable attention. This is the case of boron-doped diamond [46], carbon inks for screen-printed electrodes [47], or carbon nanotubes as the self-catalysing and easy-to-modify electrode substrate [48,49].

A kind of low cost C-based electrodes which are finding wide application also at a commercial level are the screen-printed electrodes (SPE). A screen-printed sensor is generally formed by layers (or films) of special inks or pastes deposited sequentially onto an insulating support or substrate. The film is applied through a mask contacting the substrate, and deposited films are obtained by pattern transfer from the mask. After the printing step, the next stage is to dry the printed film. Conventionally, thick-film sensors were baked at temperatures ranging from 300 and 1200 °C. After drying, the films retain a rigid pattern on the substrate and are relatively immune to smudging. As it is visible in Figure 1.2, an insulating layer is then applied in order to expose only the active area of the sensor.

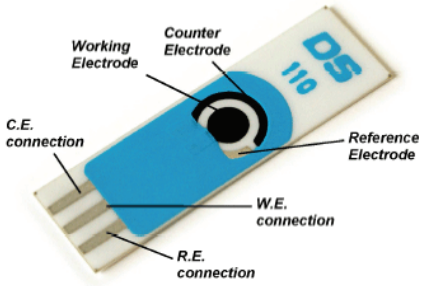

Figure 1.2. Photograph of a commercially available screen printed electrode (DropSens)

Screen printed electrodes has been widely used for the electroanalysis of heavy metal ions such as chromium [50,51], lead and cadmium [52-54], zinc [55], mercury [56], nickel and cobalt [57,58] and arsenic [59].

Also some drawback of SPE has to be listed, which are intrinsic in the fabrication method: the resistance of the binders, which increase the overall resistance of the electrode, the poor control of the micro-structure of the carbon and the impossibility to miniaturize the device under the millimeter scale.

In order to overcome the above limits, further new forms of carbon are intensively investigated for electroanalytical purposes; typical examples being graphene (especially for transparent electrodes) [60], pyrolyzed photoresist carbon [61,62] and electrospun nanofibers [63].

1.4.3 Noble Metals Electrodes

The use of these electrodes in stripping analysis is limited because of low hydrogen overvoltage at platinum, gold and palladium electrodes [64]. Another limitation of these kind of electrodes is the formation of oxide layers or dissolution of metals. Gold disk electrodes (mm-sized or μm-sized) are used, in particular, for determination of arsenic [65-67], cadmium [68-70], copper [71,72], mercury [73-76].

1.5 Miniaturization of the electrode surface

The ability to build micro-and nanostructures on electrode surfaces has given rise to new electrochemical devices in which the properties of the electrode are tailored for specific purposes [77]. In principle, this is a very attractive prospective for developing electrochemical sensors suited especially for environmental analysis in complex matrices, where the presence of numerous interferences hinders the reliable use of "classical" electrodes.

It is well known indeed that geometry, surface structure and material constituting an electrode have a profound effect on the electrochemical behavior of electroactive species and as a consequence influence the electrochemical response. The size of working electrodes also affects the response of the electrode, due to mass transport effects of the active species to and from the electrode. Electrodes miniaturization, is one of the main trends in the field of electrochemistry of the last decades. Electrodes can be classified as "macro" (having dimensions greater than 100 μm), "micro" (having at least one dimension below 100 μm) and "ultramicro" (having one dimension less than the diffusion layer, therefore below to 25 μm) [78,79]. When such miniaturization is taken to the extreme, nanoelectrodes (NE) can be obtained. A nanoelectrode has one dimension which is in the same range-scale of the charging double layer, therefore less than 50 nm [80].

Besides the obvious practical advantage of the small size, allowing smaller sample volumes to be used and application to *in-vivo* measurements, microelectrodes offers a number of advantages such as high current density, low background charging current and enhanced mass transport efficiency.

A drawback in the use of microelectrodes can be related to the extremely low currents obtained. One way to overcome this problem is to use arrays of micro- or nanoelectrodes (MEA and NEA respectively), whereby multiple electrodes are operated in parallel. The shapes and the geometry of the MEA/NEA are mainly limited by their fabrication technique and can be conveniently classified according to the design and application they are designed for. Individual electrodes in the array may assume random arrangements in this case the array is more properly defined as an ensemble of micro or nanoelectrodes (MEE and NEE respectively) as first termed by Martin and co-workers [81] The main advantage of random configurations is their easy fabrication, since usually it does not require expensive and technologically demanding instrumentation. The main drawback is the random geometry of the electrode, which makes difficult a clear comparison with theoretical models. Moreover the

random spacing between the individual electrodes can lead to different diffusion mechanisms on the same ensemble. The design of arrays with well-defined geometry and interelectrodic spacing is highly preferred as far as electroanalytical applications are concerned [82], nonetheless the fabrication of such arrays is not always practical and requires special equipment which are not always present in chemistry laboratories.

1.6 Techniques for the micro- and nanofabrication of advanced electrodes surfaces.

1.6.1 MEAs Fabrication techniques

Assembly of electrode materials

The simplest approaches involve the embedding of micro sized electrodic materials in insulating matrices. Wu et al. [83] fabricated a gold circular microarray by wrapping a gold minigrid around precast cylinders. Bond and coworkers [84] made a 10x10 MEA by embedding gold wires in epoxy resin layer-by-layer.

Angnes et al. [85] developed a method to transform inexpensive electronic chip into a MEA. In this procedure, the chips are sawed through their middle leading to the destruction of the silicon circuit and to the cutting of the gold wires that connect it with the external terminals. By embedding in resin and polishing the surface of the sawed chip it is possible to obtain a linear array where the tips of the gold wires (typically 25 μm in diameter), are the electrodes of the array. More recently, Szunertis and coworkers [86] described the fabrication of an ordered microelectrode array based on an etched optical fiber bundle. Such devices present an interesting combination of optical and electrochemical properties. In Figure 1.3 SEM images of the bundle before (a) and after (b) electrophoretic paint deposition and a schematic representation of the MEA are reported (c).

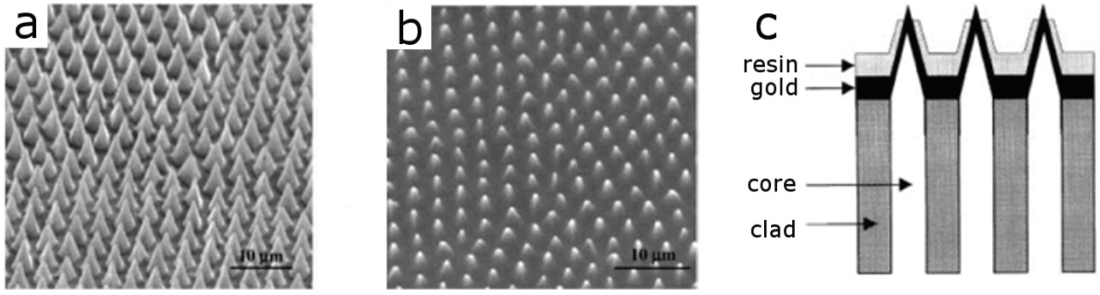

Figure 1.3. SEM picture of a metalized optical fiber bundle (a) and of resin coated fiber bundle (b). Schematic representation of a optical fiber MEA cross section (c).

Not only metallic MEA were prepared by electrode assembly methods. Martin et al. reported a procedure for preparing a carbon microdiscs array by filling the pores of a microporous membrane (3, 8 and 13 μm pores diameter) with carbon paste [87,88].

Photolithography

Photolithography is the most diffused technique for the fabrication of regular arrays of microelectrodes. Photolithography is a microfabrication technique, which is based on the selective removal of parts of thin films (photoresist) exposed to UV light. This procedure allows one to obtain regular arrays of micro electrodes with high spatial resolution, nonetheless this technique requires special and expensive equipment besides, photolithographic process requires access to a clean room.

The basic principles of photolithography are illustrated in Figure 1.4. Two types of photoresist are used. Positive photoresist are insoluble polymers that become soluble in a developer solution on irradiation, while negative photoresist are initially soluble and become insoluble on irradiation. The chemistry of negative photoresist is fully described in section 1.6.3.

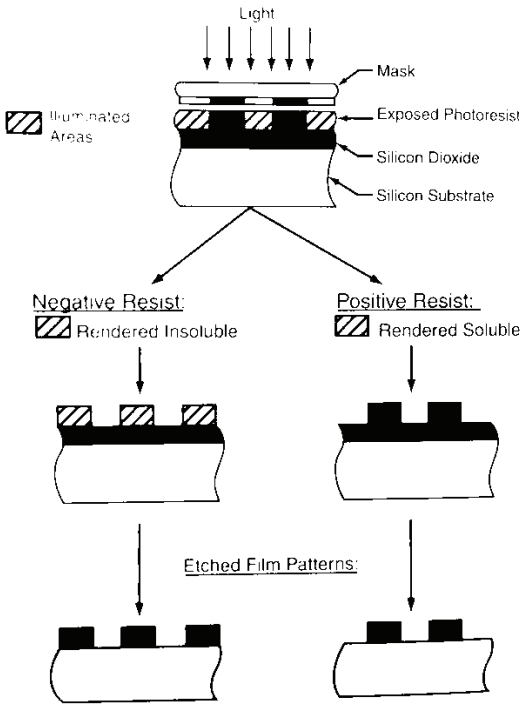

Figure 1.4. Positive and negative resist: exposure, development and pattern transfer. Positive resist develop in the exposed region. Negative resist remain in the exposed region. From [84].

A number of different photolithographic procedures for the production of gold microelectrode arrays were reported [89-93]. Besides gold, platinum [94], iridium [95] and carbon [96] were also used as metal electrode material. The most important advantage of this technique is that the size, shape and interelectrode spacing can be designed according to the requirements of its final application.

1.6.2 Templated synthesis of nanoelectrode ensembles

The membrane templated synthesis is based on the idea that the pores of a host material can be used as a template to direct the growth of new materials. Historically, the template synthesis in track-etched materials was introduced by Possin [97] and Williams and Giordano [98], who prepared different metallic wires with diameter as small as 10 nm within the pores of etched nuclear damaged tracks in mica. The first synthesis of NEEs prepared by using nanoporous membranes as templating material, was described by Menon and Martin [99] who deposited gold nanofibres with a diameter as small as 10 nm within the pores of track etched polycarbonate (PC) membranes by chemical (electroless) method, obtaining a random ensemble of metal nanodisks surrounded by the insulating polymer. All the nanoelectrodes

were interconnected each other so that they all the experienced the same electrochemical potential.

Afterwards, various examples of membrane templated electrochemical deposition of nanowires of semiconductors [100], metals (e.g. Ni and Co) [101], oxides and conducting polymers [102] appeared in the literature.

In the template synthesis of nanoelectrodes, each pore of the membrane is filled with a metal nanowire or nanofiber. The metal fibers growth can be performed both using electrochemical [101] or electroless [99,103,104] deposition methods.

In both deposition methods, the pore density in the template, determines the number of metal nanoelectrode elements on the NEE surface and, correspondingly, the average distance between them; while the diameter of the pores in the template determines the diameter of the individual nanoelectrodes. Since track-etched membranes are characterized by randomly distributed pores, unless special procedures are applied [105], by this method it is only possible to obtain random ensembles of nanoelectrodes, i.e. NEE.

The polymeric membranes most widely used to this goal are fabricated by the *track-etching* method which consists of two different steps. In the first step (the *tracking* step), a thin polymeric membrane is tracked by nuclear fission fragments of heavy elements or by accelerated ion beams. The tracking of the membrane is then followed by chemical *etching*, during which the pore formation takes place. The removal of the tracked zones is achieved by a chemical etching agent, typically a solution of a strong alkali.

The time of tracking determines the pore density [106,107], while the chemical etching influences the pores size and shape [106,108,109]. The polymeric materials most widely used to fabricate track-etched membranes are polycarbonate, polyethylene terephthalate and polyimide [106].

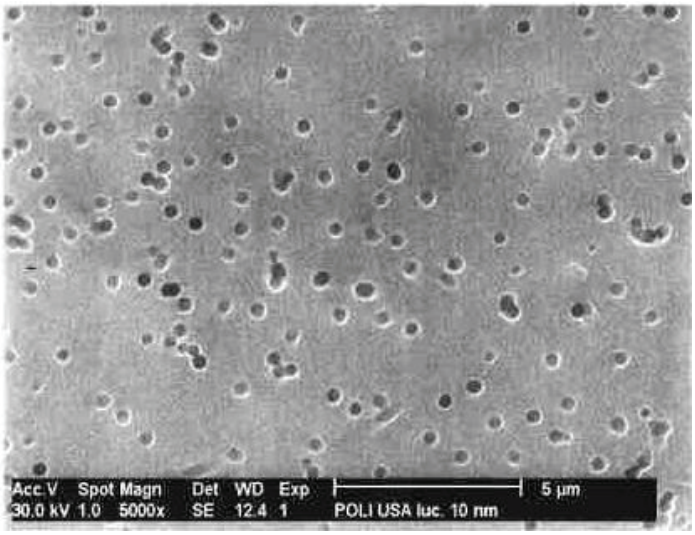

Figure 1.5. SEM image of a commercially available track-etched polycarbonate membrane.

NEEs are prepared by filling the pores of a template with metal nanowires so that in the final ensemble only the surface of the nanodisk is exposed to the sample solution. Specific details about the typical assembly used to transform a piece of a golden membrane into a handy NEE are shown in Figure 1.6 and reported in the first original papers [99,110] as well as in recent modifications [103,111,112].

In this kind of NEEs all the nanoelectrodes are connected to each other by a back metal current collector, so that all the nanoelectrodes experience the same applied potential.

As illustrated in Fig. 1.7, depending on whether the template is completely kept on site, partially etched or fully removed, it is possible to obtain nanoelectrodes ensembles with very different geometries [113,114].

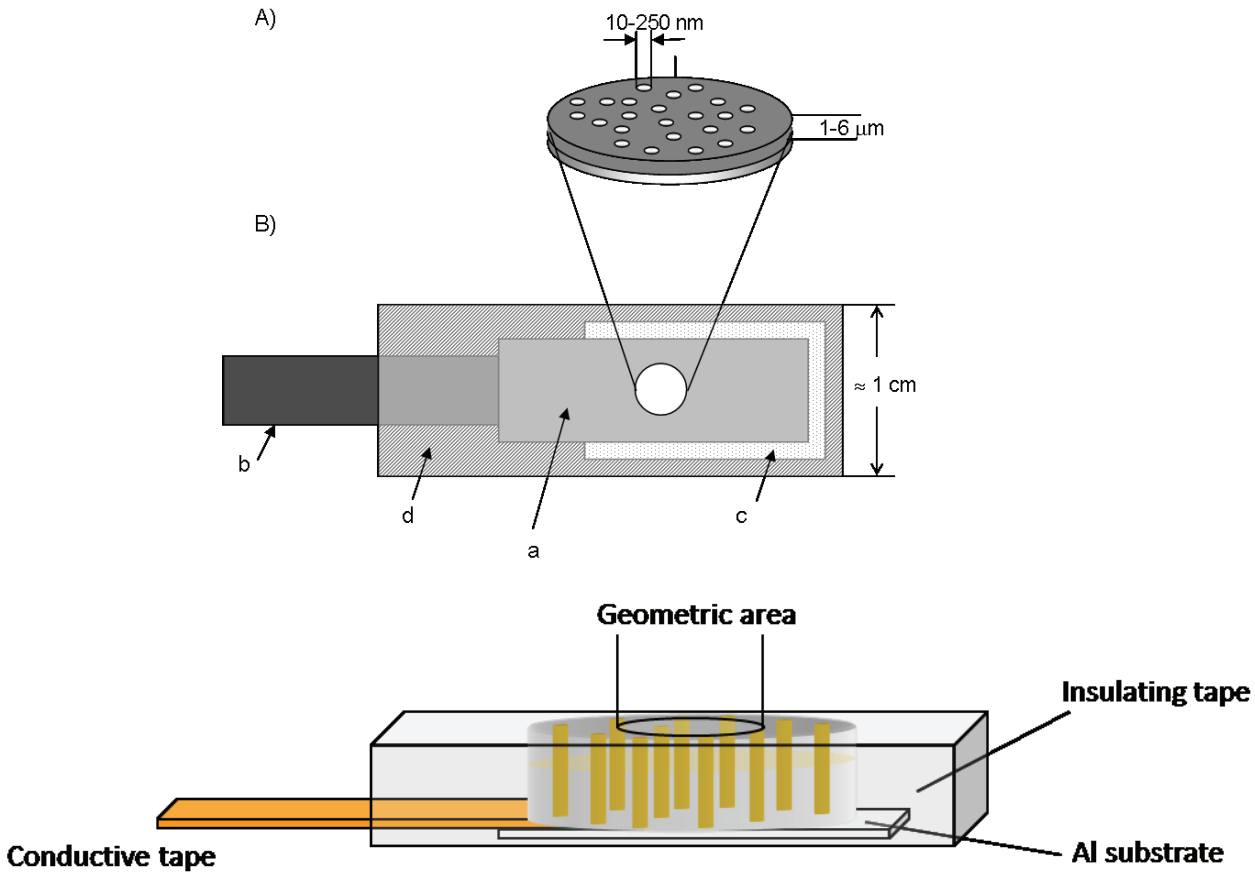

Fig. 1.6. Scheme of a Au-NEE prepared using a track-etched polycarbonate membrane as template (A). Particular of the section of the active area; (B) top view, (C) section of the all NEE ready for use as working electrode. a) Track-etched golden membrane; b) copper adhesive tape with conductive glue to connect to instrumentation; c) aluminum adhesive foil with non-conductive glue; d) insulating tape. Not all details (namely, the nanoelectrodes dimension) are in scale.

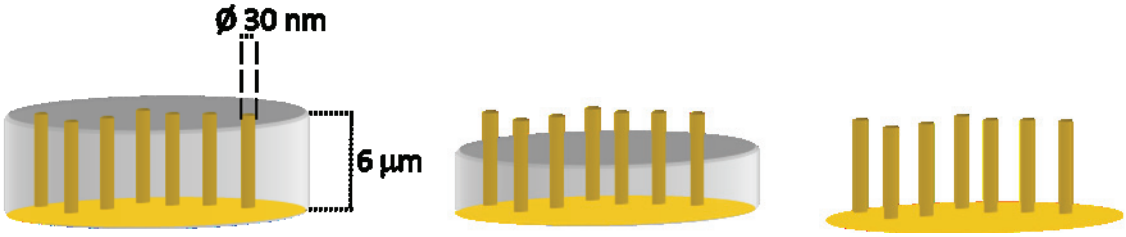

Fig. 1.7. Different geometries for template nanoelectrode ensembles: a) ensemble of nanodisks; b) ensemble of partially naked nanowires; c) ensemble of completely naked nanowires.

Electroless deposition of metals

Electroless metal deposition involves the use of chemical reducing agents which allow the plating of a metal from a solution onto a specific surface. The kinetic of this process plays a key role since the homogeneous electron transfer from the reducing agent to the metal ions is very slow respect to the reduction on the surface. A catalyst that accelerates the rate of ion

reduction is then applied to the surface to be coated. As a consequence, the metal is reduced preferentially at the surface incorporating the catalyst so that only the surface of interest, activated with the catalyst, is finally plated. The thickness of the metal layer can be controlled by varying the plating time [115].

The electroless deposition of gold [99] consists of three different steps. The first is the "sensitization" of the membrane. During this process, Sn^{2+} is applied to the surface (pore walls plus outer faces of the membrane) of the template by immersion of the membrane into an acidic solution containing $SnCl_2$. The adhesion of the cations occurs through coordination with amino and carbonyl functionalities probably of the polyvynilpyrrolidone (PVP) which is added as wetting agent to commercial membranes (PC is hydrophobic, but impregnation with PVP makes the surface hydrophilic).

The sensitized membrane is subsequently activated by immersion into an aqueous silver-ammonia solution: during this step the surface bound Sn(II) is oxidized to Sn(IV) and Ag^+ is reduced to elemental Ag, according to the reaction

$$Sn^{2+} + 2Ag^+ \rightarrow Sn^{4+} + 2Ag^0$$

As a result, the pore walls and both membrane faces are coated with Ag nanoparticles.

The Ag-coated membrane is finally immersed into an Au plating bath, where the silver particles are galvanically displaced by gold and all the surface is coated with Au particles.

$$Au^+ + Ag^0 \rightarrow Au^0 + Ag^+$$

These particles act as catalytic sites for the further reduction of Au(I) on the membrane surfaces, performed using formaldehyde as the reducing agent.

$$2Au^+ + CH_2O + 3OH^- \rightarrow 2Au^0 + HCOO^- + 2H_20$$

With this procedure, the metal growth starts from the pore walls to continue up to the complete filling of the porosities. This is the reason why stopping the deposition after a short time, Au nanotubes can be obtained [103,111,116], while, the complete filling to obtain nanowires is achieved if the plating step is extended up to 24 h. In order to slow down the kinetics of the deposition, the plating is performed at 0° C.

Electrochemical properties of NEEs

The electrochemical characteristics that distinguish NEEs from conventional macro (mm-sized) or even ultramicro (μm-sized) electrodes are the dramatic lowering of the double layer charging current [99,117] and the extreme sensitivity to the kinetics of the charge transfer process [118] which means capability to measure very high charge transfer rate constants [119].

Since these characteristics are specific for ensemble of nanodisks electrodes the lack of some of these characteristics, such as the persistence of high capacitive currents, should be taken as a diagnostic indication for a failure in the preparation procedure [103].

From a voltammetric view point, NEEs can be considered as ensembles of disc ultramicroelectrodes separated by an electrical insulator interposed between them. An ultramicroelectrode is considered as an electrode with at least one dimension comparable or lower than the thickness of the diffusion layer (typically < 25 μm). At such small electrodes, edge effects from the electrode become relevant and diffusion from the bulk solution to the electrode surface is described in terms of radial geometry instead of the simpler linear geometry used for larger electrodes. Under radial diffusion control, the voltammogram displays a typical sigmoidal shape; a limiting current (I_{lim}) instead of a peak, is the relevant analytical parameter related directly to the analyte concentration.

The density (q) of nanodisks/surface in a NEE is dramatically large (10^6-10^8 elements/cm^2); for this reason, all the nanoelectrodes are statistically equivalent and the different contribution of the elements at the outer border of the ensemble is negligible [120,121], even in NEEs of overall area as small as 10^{-2}-10^{-3} cm^2.

NEEs can exhibit three distinct voltammetric response regimes depending on the scan rate or reciprocal distance between the nanoelectrode elements [122,123]. When radial diffusion boundary layers overlap totally (radius of diffusion hemisphere larger than average hemidistance between electrodes, slow scan rates) NEEs behave as planar macroelectrodes with respect to Faradaic currents (total overlap conditions). When diffusion hemispheres become shorter (higher scan rates), the current response is dominated by radial diffusion at each single element (pure radial conditions). At very high scan rates, the linear active regime is reached in which the current response is governed by linear diffusion to the individual nanodisk.

Fig. 1.8 shows the situations encountered for the total overlap (TO) and pure radial regimes, being characterized by higher signal to background current ratios. These two regimes are those typically used for analytical and sensing applications.

TO regime is the regime usually observed at NEEs prepared from commercial track-etched membranes, with high pore density [99]. Transition from one regime to the other as a function of nanoelements distance was demonstrated experimentally [122] using specially-made membranes.

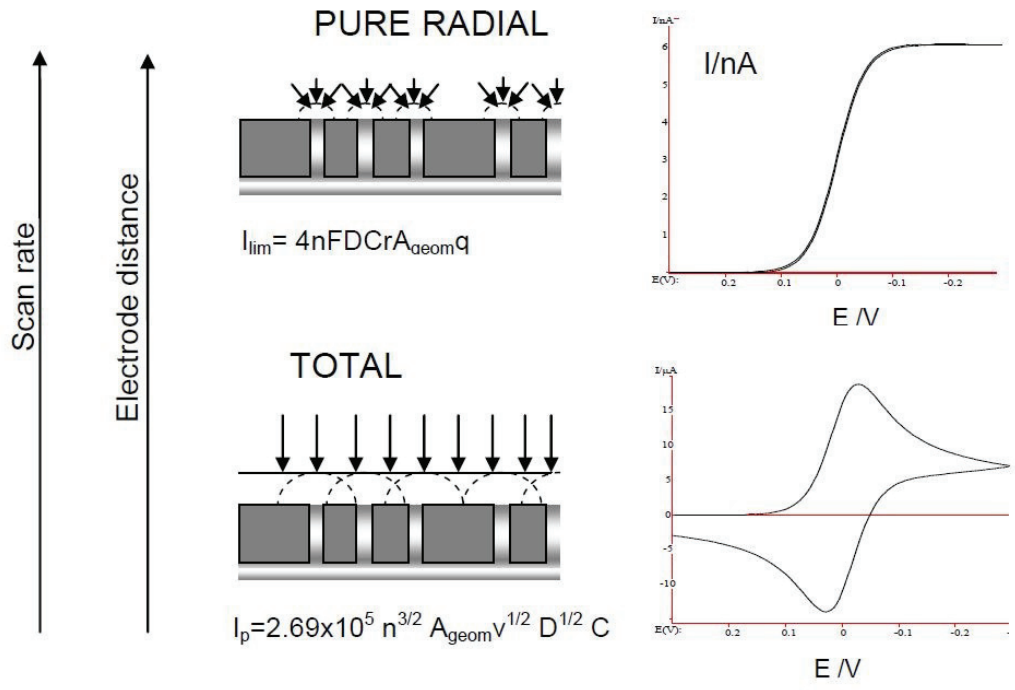

Figure 1.8. Typical diffusive regimes observed at nanoelectrode ensembles as a function of the scan rate and/or nanoelectrodes distance. See the list of abbreviations for symbols in the equations.

Under TO conditions, the Faradaic current (I_F) is proportional to the geometric area of the electrode (A_{geom}, nanodisks plus insulator) of the ensemble while the capacitive current (Ic) is proportional only to the active area (A_{act}), which corresponds to the summation of the area of all the nanodisks exposed to the sample solution.

The Faradic-to-capacitive current ratios at a NEE and a conventional electrode with the same geometric area are compared by the equation (1):

$$(I_F/I_C)_{NEE} = (I_F/I_C)_{conv} \times A_{geom}/A_{act} \quad (3)$$

This ratio at the NEE is higher than that at the conventional electrode by a factor that is the reciprocal of the fractional electrode area (f), defined as

$$f = A_{act} / A_{geom} \quad (4)$$

Typical f values for NEEs are between 10^{-2} and 10^{-3}. Therefore signal to background current ratios at NEE are 2-3 order of magnitude higher than at conventional electrodes of the same geometric area. As a consequence detection limits at NEEs are 2-3 orders of magnitude lower than with conventional electrodes [99,117,124].

It was shown that improvements in signal/background current ratios at NEEs are independent on the total geometric area of the ensemble [120]; this is true if the fractional area is kept constant and if the dimensions of the ensemble are lowered to a size still large enough to contain a large number of nanoelements (for instance, NEE with A_{geom} of 0.005 cm^2 contains $4.8x10^6$ nanoelectrodes). Note that NEEs warrant such independence on the ensemble size for overall geometric areas much lower than those required for achieving comparable results with arrays of micrometer sized electrodes [121]. This is because the real nanometer size of the electrodes and very high number of elements per cm^2.

For a given geometric area, it is evident that the I_F/I_C is maximum when the TO regime is operative, being lower in the case of a pure radial regime. In this case, in fact, only a certain percentage of the geometric area of the ensemble contribute to producing a Faradaic current while, in the total overlap regime, this percentage is 100%. On the other hand, it is worth stressing that for NEEs or NEAs with the same active area, higher Faradaic currents are achieved when operating under pure radial conditions [121]; this is the regime of choice for obtaining the maximum improvement of detection limits when there is no constrain in increasing the distance between the nanoelectrode elements and/or the overall geometric area of the ensemble.

When using NEE for trace analysis the accessible potential window is limited by the formation of a surface oxide layer on the positive side at about 0.7 V vs Ag/AgCl [99]. On the negative side it depends on the hydrogen evolution reaction and shifts negatively by increasing the solution pH (e.g., approximately -0.75 V vs Ag/AgCl at pH 7) [124].

It was demonstrated that NEEs can be used not only as bare electrodes, but also as polymer coated devices [117]. For instance, the overall surface of a NEE (insulator and nanodisks) can be easily coated by a thin layer of an ionomer coating. In the cited literature example [117], the ionomer of choice was the polyestersulphonate Eastman AQ55®, which was applied as a water dispersion, i.e. using a solvent which does not damage the NEE surface (the polycarbonate template can be damaged by organic solvents). Such an approach showed that

it was possible to combine successfully the preconcentration capabilities of ionomer coated electrodes with the increased Faradaic/capacitive current ratio typical of NEEs.

The ability of NEEs to furnish well resolved cyclic voltammograms for trace redox species has interesting consequences also for adsorption related problems, as in the case of small organic redox molecules and some biomacromolecules as well. If adsorption is concentration dependent, then lowering the solution concentration below the adsorption limit can sometime overcome the problem. This was demonstrated to be the case for some phenothiazines [124], commonly used as redox mediators in biosensors, and for the heme-containing enzyme cytochrome *c* [125].

An important characteristic of NEEs is that electron transfer kinetics appear slower than at a conventional electrode with continuous metallic surface [99]. Being composed of a large number of nanodisks metal elements surrounded by a large surface of insulating material (the guest membrane), NEEs act indeed as electrodes with partially blocked surface (PBE); the nanodisks electrodes are the unblocked surface and the template membrane is the blocking material. According to the pioneering model elaborated by Amatore et al. [118], the current response at this kind of electrodes is identical to that at a naked electrode of the same overall geometric area, but with a smaller apparent standard rate constant for the electron transfer which decreases as the coverage with the blocking agent increases. Such an apparent rate constant ($k°_{app}$) is related, in fact, to the true standard charge transfer rate constant (k°), by the relationship [118]:

$$k°_{app} = k°(1 - \vartheta) = k° f \quad (5)$$

where ϑ is the fraction of blocked electrode surface and f is the fraction of the electrode surface that is Au nanodisks (see eq. 4).

Such a dependence has two different practical consequences. From a mechanistic viewpoint, it is an advantage since it means that with NEEs it is easier to obtain experimentally very large k° values [126]. What is measured at NEE is indeed the smaller $k°_{app}$, which can be converted into the larger k° by means of eq. 5 [119,124].

From an analytical viewpoint, the operativeness of eq. 5 means that, at NEEs, high Faradaic current signals are obtained only for redox systems that behave “very” reversibly [99]. In cyclic voltammetry, the reversibility depends on k° and the scan rate; at a regular electrode a redox system gives a reversible voltammetric pattern when $k° > 0.3\ v^{1/2}$ cm s^{-1} [126]. At NEEs kapp substitutes k°; this means that at a NEE a redox system gives a reversible voltammetric pattern when $k° > k_{app}/f$, i.e. $k° > 3 \times 10^2\ v^{1/2}$ cm s-1 when, for instance, f is 10^{-3} [127,128].

With fixed pore density, the excessive lowering of the nanodisks diameter can increase the irreversibility problem. This is a limitation to be seriously taken into account when trying to optimize NEEs for analytical application, since it is important to consider the contrasting effect both of the increased I_F/I_C value and the apparent slowing down of the electron transfer kinetics. On the other hand, it is worth pointing out that the high sensitivity of NEEs to electron transfer kinetics can be even turned into an advantage, to avoid the effect of interfering substances when the interferences are sluggish redox couples while the analyte is an electrochemically (very) reversible redox species.

Electrodes with highly controlled surfaces

Notwithstanding their interesting behavior and related analytical advantages [129], ensembles of nanodisks electrodes can present some limitations with respect to their use as sensors when the electrode surface has to be functionalized.

In fact, when immobilizing chemical reactant on the electrode surface or when analyzing real samples one has to take into account the very low value of the active area of the ensemble, which can be 10^2-10^3 times smaller than the overall geometric area.

It was shown [113,114] that the small surface area of the nanodisk electrodes of an ensemble can be increased in a controlled way by suitable etching, in order to partially remove the upper layers of the PC template membrane. This causes the structure of the final ensemble to change from a flat 2-D surface, made of metal nanodisks embedded into the PC, to a 3-D structure made of gold nanowires partially protruding from the PC insulating layer. Such an approach is summarized in Scheme of Figure 1.9.

Figure 1.9. Schematic drawing of the effect of the etching on the NEE structure.

Martin at al. [114] first proposed O_2 plasma as a way for achieving the controlled removal of PC. This method was applied to the preparation of 3D-NEEs functionalized with ss-DNA for DNA sequencing [130,131].

1.6.3 Pyrolized photoresist derived electrodes

Carbon allotropes

Carbon exists in several allotropes, resulting in a large variety of molecular configurations for multi-atomic structures. Carbon allotropes include diamond, lonsdaleite, buckminsterfullerenes, graphene, carbine, graphite, carbon nanofoams, diamond-like carbon, amorphous carbon and those carbons derived from the pyrolysis of organic materials, also known as glass-like carbons [132-135]. These exhibit a wide range of mechanical, chemical, electrical and electrochemical properties based on the underlying microstructure [136]. Among the various carbon allotropes, graphite and glassy carbon (GC) are widely investigated for electrochemical applications [137].

Graphite is formed by stacking graphene layers parallel to each other in a threedimensional, crystalline, long-range order. There are two allotropic forms with different stacking arrangements: hexagonal and rombohedral, but the chemical bonds within the layers are covalent with sp2 hybridization in both cases. Carbon atoms in graphite, as in graphene, are bonded trigonally in a plane composed of fused hexagonal rings. The resulting network is 2-dimensional and the resulting flat sheets are stacked and loosely bound through weak Van derWaals forces. Because of the delocalization of one of the outer electrons of each atom to form a π-cloud, graphite conducts electricity preferentially in the plane parallel to the covalently bonded sheets.

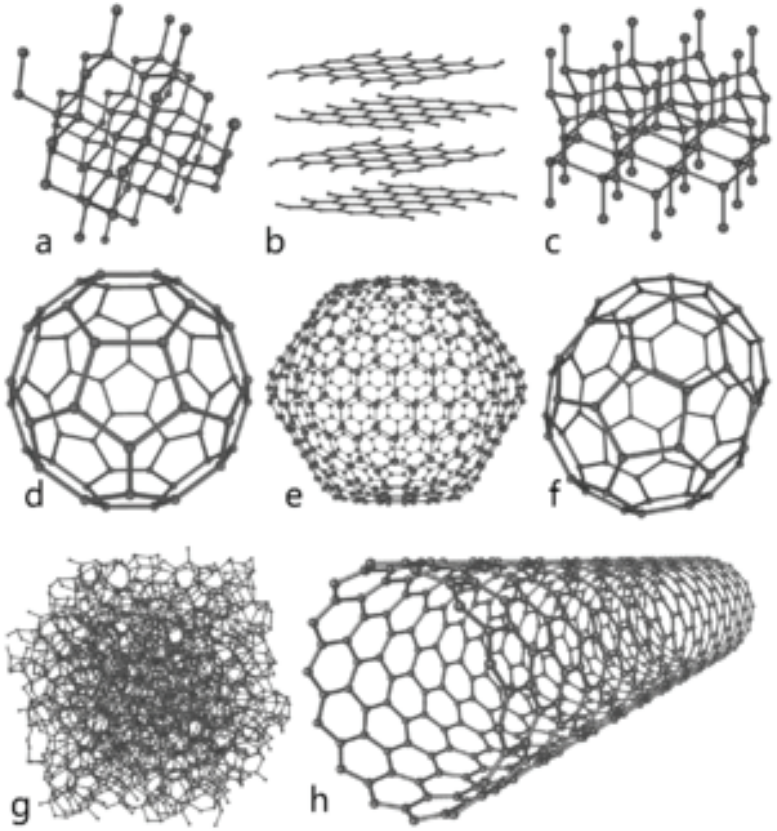

Figure 1.10. Some Carbon Allotropes: a) Diamond, b) Graphite and c) Lonsdaleite. Examples of Buckminsterfullerenes: d) C60 (buckyball), e) C540, f) C70 and h) single-walled carbon nanotube. g) Amorphous carbon.

Glass-like carbon

Glass-like carbons are derived through the carbonization, or thermal degradation, of organic polymers in inert atmospheres. The resultant carbon has a glass-like appearance in the sense that is smooth, shiny and exhibits a conchoidal fracture [138]. Because of its appearance, glass-like carbon has also been referred historically as *vitreous carbon* or *glassy carbon*. It is impermeable to gases and extremely inert, with a remarkable resistance to chemical attack from strong acids such as nitric, sulfuric, hydrofluoric or chromic and other corrosive agents such as bromine. Even when it does react with oxygen it only does so at high temperatures. Its rates of oxidation in oxygen, carbon dioxide or water vapor are lower than those of any other carbon. It has a hardness of 6 to 7 on Mohs scale, a value comparable to that of quartz. X-ray diffraction studies have shown that glass-like carbon presents an extremely small pore size of a closed nature and an amorphous structure [139,140].

Glass-like carbon also has a wider electrochemical stability window than platinum and gold, which makes it ideal in electrochemistry experiments [136]. Even when the overall properties

of the resulting carbon depend on the nature of the precursor used, they do not change very significantly [141] and the above values could be employed as an initial reference.

A consensus on the crystalline structure of glass-like carbon has not been reached jet. The most widely accepted model is the one that considers this type of carbon as made up of tangled and wrinkled aromatic ribbon molecules that are randomly cross-linked by carbon-carbon covalent bonds. The ribbon molecules form a networked structure, the unit of which is a stack of high strained aromatic ribbon molecules. Such structure of crystallites reflects the features of thermosetting resins structure which are commonly used as precursors for glass-like carbons. This model explains the high variety of experimental results obtained so far on glass-like carbons including its impermeability, brittleness and conductivity [141].

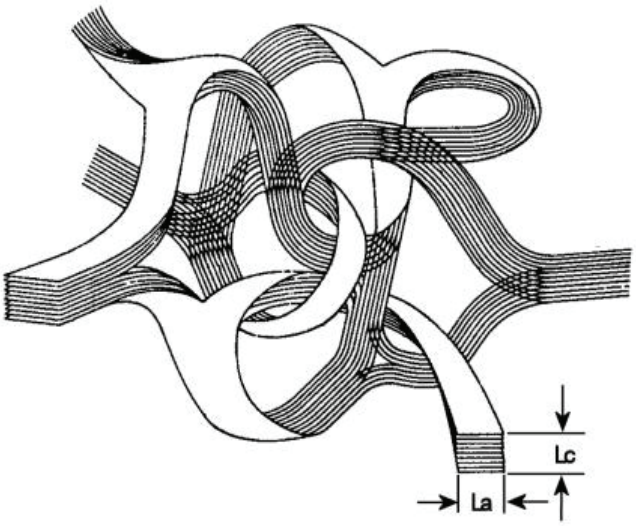

Figure 1.11. Structural model of glass-like carbon as proposed by Jenkins in 1971. This model is able to explain most of the properties exhibit by glass-like carbon up to this day. From [141].

Carbon Micro-Electro-Mechanical Systems

Carbon Micro-Electro-Mechanical Systems, also referred to as Carbon-MEMS or CMEMS, are carbon-based micro- or nano-devices whose fabrication is based on obtaining glass-like carbon micro-structures from pre-patterned organic polymers. Fabrication techniques that can be used include stamping, casting, machining and lithography, among others. The selection of each technique is dictated by the quality, complexity and final dimensions of the desired carbon part. Currently, the fabrication of Carbon-MEMS devices is principally based on the use of photolithography as the main tool to pattern the polymeric precursors, due to the existence of commercial high-quality precursors and standardized photolithograpic tools that make the fabrication process and the dimensional control highly reproducible.

During the 90's, initial work emerged regarding the derivation of carbon from photoresists in the quest for alternatives to carbon films produced by physical deposition techniques. The interest was driven by the use of pyrolyzed photoresists in batteries, electrochemical sensors, capacitors and Micro-Electro-Mechanical Systems (MEMS). Electrochemical studies of carbon films derived from positive photoresists were conducted in 1998 by Kim et al. [142] and later by Ranganathan et al. [61]

By 2000, Kostecki, Song and Kinoshita patterned these carbon films as microelectrodes and studied the influence of the geometry in their electrochemical response [143].

The resulting carbon showed an electrochemical behavior similar to glass-like carbon although with decreased surface roughness. In 2002 the derivation of carbon from negative photoresists (SU-8) was reported by Singh et al [144].

Photolitography

Photolithography relies on light to pattern substrates. In the Integrated Circuits (IC) industry, pattern transfer from masks onto thin films is accomplished almost exclusively via photolithography. This essentially two-dimensional process has a limited tolerance for non-planar topographies and creates a major constraint for building non-IC miniaturized systems, such as microfluidic devices and polymer precursors for C-MEMS. Fortunately, research over the last ten years in high-aspect-ratio resists is finally improving dramatically photolithography's capabilities, allowing for it to cover wider ranges of topographies and to resolve ever-smaller features.

Photolithography generally involves a set of basic processing steps: photoresist deposition, soft bake, exposure, post-exposure treatment and developing. De-scumming and post-baking might also be part of the process. Each one of these steps is detailed below, together with their related topics.

Substrate cleaning

Substrate cleaning is the first and important step in any lithographic process, as the adhesion of the resist to the substrate could be severely compromised by the presence of impurities and residual coatings if it is not carried out properly. Contaminants include solvent stains and airborne dust particles from operators, equipment, smoke, etc.

Depending on the substrate and the type of contaminants, several cleaning techniques can be used: wet immersion cleaning might be carried out using diluted hydrofluoric acid, piranha or milder, but not as effective, procedures such as DI water rinsing followed by solvent rinse.

Dry methods include vapor cleaning; thermal treatments, for example baking the substrate at 1000°C in vacuum or in oxygen; and plasma or glow discharge techniques, for example in Freons with or without oxygen. In general, vapor phase cleaning methods use significantly less chemicals than wet immersion cleaning. In the case of wet immersion cleaning, dehydration prior to resist deposition is recommended.

Photoresist deposition

To deposit photosensitive materials for MEMS, spin coating is the most common method for thicknesses smaller than 500 μm. Other coating techniques are also available, such as roller, curtain or extrusion coating, although they are not as efficient when depositing layers thicker than 200 μm. For very thick resist coats (> 1 mm), techniques such as casting and the use of thick sheets of dry photoresists replace the use of resist spinners.

In spin coating, centrifugal forces cause the resist to flow to the edges, where it builds up until expelled when its surface tension is exceeded. The resulting polymer thickness, T, is a function of spin speed, solution concentration, and molecular weight (measured by intrinsic viscosity). Generally, the photoresist is dispensed onto the substrate, which is held in place by a vacuum-actuated chuck in a resist spinner.

A rotating speed of about 500 rpm is commonly used during the dispensing step to spread the fluid over the substrate. After the dispensing step, it is common to accelerate to a higher speed to thin down the fluid near to its final desired thickness. Typical spin speeds for this step range from 1500 to 4000 rpm, depending on the properties of the fluid as well as the substrate. This step can usually takes less than 1 minute. The combination of spinning speed and time will generally define the final film thickness.

Resists

In order to understand the photolithographic process better it is necessary to study in detail its basic element: the photoresist. The principal components of a photoresist are the polymer (base resin), a sensitizer, and a casting solvent. The polymer changes its structure when is exposed to electromagnetic radiation; the solvent allows for spin application and the formation of thin layers over the wafer; sensitizers control the chemical reactions in the polymeric phase. Resists without sensitizers are single-component systems, whereas sensitizer-based resists are two-component systems. Solvents and other potential additives do not directly relate to the photoactivity of the resist. Photoresists must meet several rigorous requirements: good adhesion, high sensitivity, high contrast, good etching resistance (wet or dry etching), good resolution, easy processing, high purity, long shelf life, minimal solvent use, low cost, and a high glass transition temperature (T*g*). Most resins used as base for photoresists, such as novolacs, are amorphous polymers that exhibit viscous flow with considerable molecular motion of the polymer chain segments at temperatures above the glass transition.

The most common photoresist of use in the Carbon-MEMS process is SU-8. SU-8 is an acid-catalyzed negative photoresist, made by dissolving EPON-SU-8 resin (a registered trademark of Shell Chemical Company) in an organic solvent such as cyclopentanone or GBL (gamma-butyloractone) and adding a photoinitiator. The viscosity and hence the range of thicknesses accessible, is determined by the ratio of solvent to resin. The EPON resist is a multifunctional, highly-branched epoxy derivative that consists of bisphenol-a novolac glycidyl ether (see Figure 1.9).

SU-8 resist, patented by IBM in 1992, was originally developed for e-beam lithography and became commercially available in 1996. Because of its aromatic functionality and highly cross-linked matrix, the SU-8 resist is thermally stable (a fundamental feature to develop Carbon-MEMS devices) and chemically very inert. After a hard bake, it withstands nitric acid, acetone, and even NaOH at 90°C.

The main issue to be resolved with this resist is the thermal mismatch of SU-8 on a Si substrate (the thermal expansion coefficient for Si is 2.361 ppm/°K versus 21-52 ppm/°K for SU-8) which produces stress and may cause film cracking. Moreover, the absorption spectrum of SU-8 shows much higher absorption coefficients at shorter wavelengths. As a result lithography using a broadband light source tends to result in over-exposure at the surface of the resist layer and under-exposure at the bottom.

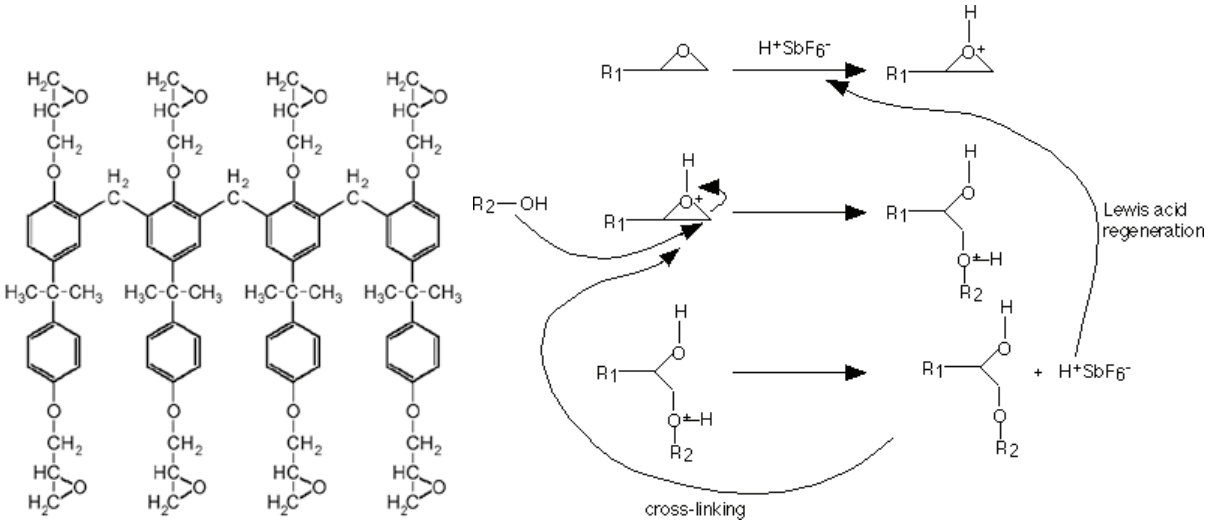

Figure 1.12. (a) The basic SU8 molecule (from *http://www2.mic.dtu.dk*). (b) The photopolymerization process. The Lewis acid is generated during UV illumination. The polymerization is done by the ring-opening of the 1,2-epoxy (from *www.geocities.com/guerinlj*)

Soft baking or prebaking

After resist coating, the resist still contains up to 15% solvent and may have built-in stresses. The photoresist is therefore soft baked for a given time in a hotplate at temperatures ranging from 70 to 100 °C to remove solvents and stress and to promote adhesion of the resist layer to the substrate. This is a critical step: failure to sufficiently remove the solvent will affect the resist profile.

Hot plating the resist is faster, more controllable, and does not trap solvent like convection oven baking does. In convection ovens the solvent at the surface of the resist is evaporated first, and this can cause an impermeable resist skin, trapping the remaining solvent inside. Commercially, microwave heating or IR lamps are also used in production lines.

Exposure

After soft baking, the resist-coated substrates are transferred to an illumination or exposure system where they are aligned with the features on a mask. In the simplest case, an exposure system consists of a UV lamp illuminating the resist-coated substrate through a mask without any lenses between the two. The purpose of the illumination systems is to deliver light with the proper intensity, directionality, spectral characteristics, and uniformity across the wafer, allowing a nearly perfect transfer or printing of the mask image onto the resist in the form of a latent image. The incident light intensity (in mW/cm^2) multiplied by the exposure time (in

seconds) gives the incident energy (mJ/cm2) or dose, D, across the surface of the resist film. Radiation induces polymerization in the exposed areas of the photoresist, altering the solubility of the resist in a solvent either directly or indirectly via a sensitizer. The absolute size of a minimum feature in an IC or a miniature device, whether it involves a line-width, spacing, or contact dimension, is called the critical dimension (CD). The overall resolution of a process describes the consistent ability to print a minimum size image, a critical dimension, under conditions of reasonable manufacturing variation.

Post-exposure treatments

A post-exposure treatment of the exposed photoresist is often desired because the reactions initiated during exposure might not have run to completion. To halt the reactions or to induce new ones, several post-exposure treatments are common: post- exposure baking (PEB), flood exposure with other types of radiation, treatment with a reactive gas, and vacuum treatment. Post-exposure baking (sometimes in vacuum) and treatment with reactive gas are used in image reversal and dry resist development. In the case of a chemically amplified resist, such as SU-8, the post-exposure bake is most critical. Although reactions induced by the catalyst that forms during exposure take place at room temperature, their rate is greatly increased by baking at 60-100 °C. The precise control of PEB times and temperatures critically determines the subsequent development and the quality of the final features. Extended PEB times will introduce significant amounts of stress in the polymer that will most likely cause structure bending and peeling from the substrate; especially in extended, large surface area features. Reduced times will yield structures that are not completely cross-linked and can be attacked by the developer. This causes extremely high surface roughness or even complete dissolution.

Development

Development is the dissolution of un-polymerized resist that transforms the latent resist image, formed during exposure, into a relief image that will serve as a mask for further subtractive and additive steps, as a permanent structural element, or as a precursor for carbonization as in the case of C-MEMS. During the development of an exposed resist, selective dissolving takes place. Two main technologies are available for development: wet development, which is widely used in circuit and miniaturization manufacture in general, and dry development, which is starting to replace wet development for some of the ultimate line-width resolution applications.

Positive resists are typically developed in aqueous alkaline solutions, and negative resists in organic ones. Each developer has a different dilution, and some require longer development times than others. They are generally matched to a type of photoresist. Though they may be interchangeable to some extent, changing the type of developer used in a process will usually change the development time necessary to resolve the pattern. The use of organic solvents leads to some swelling of the resist (especially for negative resists) and loss of adhesion of the resist to the substrate. Dry development overcomes these problems, as it is based either on a vapor phase process or plasma [145].

Carbonization

Carbonization is the process by which solid residues with a high content of carbon are obtained from organic materials, usually by pyrolysis in an inert atmosphere [86]. Different degrees of shrinkage and carbon yield (the ratio of the weight of carbon to the weight of the original polymer sample) are obtained during carbonization depending on the precursor used.
Novolac-epoxy resins, or acid-catalyzed phenol formaldehyde resins, present a volume shrinkage which varies from 50 to 90% [61,144,146,147]. As with all pyrolytic reactions, carbonization is a complex process with many reactions taking place concurrently, including dehydrogenation, condensation, hydrogen transfer and isomerization [148-150].
The pyrolysis process of organic compounds can be divided into three major steps: pre-carbonization, carbonization and annealing. During pre-carbonization ($T < 300$ °C) molecules of solvent and leftover monomer are eliminated from the polymeric precursor. The carbonization step can be further divided into two stages. From 300 to 500 °C, heteroatoms such as oxygen and halogens are eliminated causing a rapid loss of mass while a network of conjugated carbon systems is formed. Hydrogen atoms start being eliminated towards the end of this stage. The second stage of carbonization, from 500 to 1200 °C, completely eliminates hydrogen, oxygen and nitrogen atoms and forces the aromatic network to become interconnected. At this point, permeability decreases and density, hardness and electrical conductivity increase.
The final pyrolysis temperature determines the degree of carbonization and the residual content of foreign elements. For instance, at $T \approx 1200$ K the carbon content of the residue exceeds a mass fraction of 90% in weight, whereas at $T \approx 1600$ K more than 99% wt. of carbon is found [150,151].

1.7 References

[1] J. Heyrovsky, F. Kůta, *Principles of polarography,* Academic Press, 1966, USA.

[2] M. Kalousek, *Chem. Listy*, 40 (1946) 149-157.

[3] G.C. Barker, I.L. Jenkins, Analyst, 77 (1952) 685-696.

[4] S. Bruckenstein, I.W. Bixler, *Anal. Chem.*, 37 (1965) 786.

[5] D. Jagner, *Analyst*, 107 (1982) 593-599.

[6] J. Růžička, E.H. Hansen, *Flow injection analysis*, 2nd Ed. Wiley, 1988, New York, USA.

[7] I.M. Kolthoff, N.H. Furman, *Potentiometric titrations*, Wiley & Sons, 1931, New York (USA) and Chapmann & Hall, 1931, London (UK).

[8] M.E. Orazem, B. Tribollet, *Electrochemical impedance spectroscopy (EIS)*, Wiley, 2011, New York, USA.

[9] A.W. Knight, *Trends Anal Chem.*, 18 (1999) 47-62.

[10] A.J. Bard, M.V. Mirkin, *Scanning Electrochemical Microscopy*, Markel Dekker, New York, 2001

[11] S. Daniele, C. Bragato, I. Ciani, M.A. Baldo, *Electroanalysis*, 15 (2003) 621-628.

[12] G. Lindsey, G. Denuault, S. Daniele, E. De Faveri, *Anal. Chem.*, 79 (2007) 2952-2956.

[13] J. Wang, *Analytical Electrochemistry*, Wiley, VCH, USA, 2006**.**

[14] M.G. Paneli, A. Voulgaropoulos, *Electroanalysis*, 5 (1993) 355-373.

[15] C.M.A. Brett, A.M.C.F. Oliveira Brett, J.L.C. Pereira, *Electroanalysis,* 3 (1991) 683-689.

[16] H. Li, R.B. Smart, *Anal. Chim. Acta,* 333 (1996) 131-138.

[17] O. Domínguez and M. J. Arcos, *Anal. Chim. Acta*, 470 (2002) 241-252.

[18] B. Baś, *Anal. Chim. Acta,* 570 (2006) 195-201.

[19] R. Piech, B. Baś, W.W. Kubiak, *Talanta,* 76 (2008) 295-300.

[20] V. Arancibia, C. Muñoz, *Talanta,* 73 (2007) 546-552.

[21] P. Kapturski, A. Bobrowski, *J. Electroanal. Chem.,* 617 (2008) 1-6.

[22] F. Ma, D. Jagner, L. Renman, *Anal. Chem.,* 69 (1997) 1782-1784.

[23] K. Rajeshwar, J.G. Ibanez, G.M. Swain, *J Appl Electrochem.*, 24 (1994) 1077-1091.

[24] J. Wang, *Analyst*, 119 (1994) 763-766.

[25] M. Esteban, E. Casassas, *Trends Anal. Chem.*, 13 (1994) 110-117.

[26] J. Wang, *Trends Anal Chem.*, 21 (2002) 226-232.

[27] J. A. Rodrigues, C. M. Rodrigues, P. J. Almeida, I. M. Valente, L. M. Gonçalves, R. G. Compton, A. A. Barros, *Anal. Chim. Acta*, 701 (2011) 152-156.

[28] E. Fischer, C. M.G Van den Berg, *Anal. Chim. Acta*, 385 (1999) 273-280.

[29] K. Brainina, E. Neyman, *Electrochemical Stripping Methods*, Wiley, VCH, USA, 1993.

[30] S. Daniele, M.A. Baldo, P. Ugo, G.A. Mazzocchin, *Anal. Chim. Acta*, 219 (1989) 19-26.

[31] M.A. Baldo, S. Daniele, I. Ciani, C. Bragato, J. Wang, *Electroanalysis*, 16 (2004) 360-336.

[32] M.E. Abdelsalam, G. Denauault, S. Daniele, *Anal. Chim. Acta*, 452 (2002) 65.

[33] J. Barek, A.G. Fogg, A. Muck, J. Zima, *Crit. Rev. Anal. Che.m*, 31 (2001) 291-309.

[34] P. Ostapczuk, *Anal. Chim. Acta*, 273 (1993) 35-40.

[35] A. Economou A, P. R. Fielden, *Analyst*, 128 (2003) 205-212.

[36] J. Wang, J. Lu, S.B. Hocevar, P.A.M. Farias, B. Ogorevc, *Anal. Chem.*, 72 (2000) 3218-3222.

[37] A. Economou, TrAC *Trends in Anal. Chem.*, 24 (2005) 334-340.

[38] F. Arduini, J.Q. Calvo, A. Amine, G. Palleschi, and D. Moscone, TrAC *Trends in Anal. Chem.*, 29 (2010) 1295-1304.

[39] S.B. Hocevar, I. Svancara, B. Ogorevc, K. Vytras, *Anal. chem.,* 79 (2007) 8639-8643.

[40] S. Dal Borgo, V. Jovanovsky, S.B. Hocevar, *Electrochim. Acta*, 2013 (88) 713-717.

[41] O. Mikkelsen, S.M. Skogvold, K.H. Schroder, M.I. Gjerde, T.A. Aarhaug, *Anal. Bioanal. Chem.*, 377 (2003) 322-326

[42] B. Yosypchuk, L. Novotný, *Crit. Rev. Anal. Chem.*, 32 (2002) 141-151.

[43] O. Mikkelsen, K.H. Schrøder KH, *Electroanalysis*, 15 (2003) 679-687.

[44] A.L. Beilby, W. Brooks, G.L. Lawrence, *Anal. Chem.*, 36 (1964) 22-26.

[45] I. Švancara, K. Kalcher, A. Walcarius, K. Vytřas, *Electroanalysis with carbon paste electrodes*, CRC Press, 2012, Boca Raton (FL, USA).

[46] R.G. Compton, J.S. Foord, F. Marken, *Electroanalysis*, 15 (2003) 1349-1363.

[47] J.P. Hart, S.A. Wring, *Trends Anal. Chem.*, 16 (1997) 89-103.

[48] G.A. Rivas, *Carbon nanotubes: A new alternative for electrochemical sensors*, Nova Science Publishers, 2009, Hauppauge (NY, USA).

[49] G. Liu, Y. Lin, Y. Tu, Z. Ren, *Analyst*, 130 (2005) 1098-1101.

[50] S. Banerjee, P. Sarkar, *Sensor Letters*, 9 (2011) 1370-1375.

[51] V. Pifferi, F. Spadavecchia, G. Cappelletti, E.A. Paoli, C.L. Bianchi, L. Falciola, *Catal. Today*, 209 (2013) 8-12.

[52] N. Serrano, J. Díaz-Cruz, C. Ariño, M. Esteban, *Anal. Bioanal. Chem.*, 396 (2010) 1365-1369.

[53] N.A. Malakhova, N.Y. Stojko, K.Z. Brainina, *Electrochem. Commun.*, 9 (2007) 221-227.

[54] N. Lezi, A. Economou, P.A. Dimovasilis, P.N. Trikalitis, M.I. Prodromidis, *Anal. Chim. Acta*, 728 (2012) 1-8.

[55] M. Khairy, R.O. Kadara, D.K. Kampouris, C.E. Banks, *Electroanalysis*, 22 (2010) 1455-1459.

[56] X. Niu, H. Zhao, M. Lan, *Anal. Sci.*, 27 (2011) 1237-1241.

[57] C. Kokkinos, A. Economou, I. Raptis, T. Speliotis, *Anal. Chim. Acta*, 622 (2008) 111-118.

[58] C. Kokkinos, A. Economou, M. Koupparis, *Talanta*, 77 (2009) 1137-1142.

[59] M. Khairy, D.K. Kampouris, R.O. Kadara, C.E. Banks, *Electroanalysis*, 22 (2010) 2496-2501.

[60] Q. He, Z. Yin, H. Zhang, *Chem. Sci.*, 3 (2012) 1764-1772.

[61] S. Ranganathan, R. L. McCreery, S. M. Majji, M. Madou, *J. Electrochem. Soc.*, 147 (2000) 277-282.

[62] A. Mardegan, R. Kamath, S. Sharma, P. Scopece, P. Ugo, M. Madou, *J. Electrochem. Soc.*, 160 (2013) B132-B137.

[63] Y. Liu, D.-W. Wang, J.-S. Huang, H.-Q. Hou, and T.-Y. You, *Electrochem. Commun*., 12 (2010) 1108–1111.

[64] N. Pentland, J. O. M. Bockris, E. Sheldon, *J. Electrochem. Soc.*, 104 (1957) 182-194.

[65] R. Feeney, S. P. Kounaves, *Anal. Chem.,* 72 (2000) 2222-2228.

[66] I. Svancara, K. Vytras, A. Bobrowsky, K. Kalcher, *Talanta*, 58 (2002) 45-55.

[67] Y.-C. Sun, J. Mierzwa, M.-H. Yang, *Talanta*, 44 (1997) 1379-1387.

[68] Z. Bi, P. Salaun, C. Van den Berg, *Electroanalysis*, 25 (2013) 357-366.

[69] E. Chow, D.B. Hibbert, J.J. Gooding, *Analyst*, 130 (2005) 831-837.

[70] C. Chunguo, *Talanta*, 31 (1984) 221-223.

[71] Y. Bonfil, M. Brand, E. Kirova-Eisner, *Anal. Chim. Acta*, 387 (1999) 85-95.

[72] F. Rueda-Holgado, E. Bernalte, M. R., L., F. Cereceda-Balic, E. Pinilla-Gil, *Talanta*, 101 (2012) 435-439.

[73] P. Ugo, S. Zampieri, L.M. Moretto and D. Paolucci, *Anal. Chim. Acta*, 434 (2001) 291-300.

[74] R.D. Riso, M. Waeles, P. Monbet, C.J. Chaumery, *Anal. Chim. Acta*, 410 (2000) 97-105.

[75] Y. Bonfil, M. Brand, E. Kirowa-Eisner, *Anal. Chim. Acta*, 424 (2000) 65-76.

[76] A. Giacomino, O. Abollino, M. Malandrino, E. Mentasti, *Talanta*, 75 (2008) 266-273.

[77] R. Murray, *Molecular design of electrode surfaces*, John Wiley, 1992, New York, USA.

[78] M.I. Montenegro, M.I. Queiros, J.L. Daschbach, *Microelectrodes: Theory and Applications*, NATO ASI Series, Kluwer Academic Publishers, Dordrecht, 1991.

[79] M. Fleischmann, S. Pons, D.R. Rolison, P.P. Schmidt, *Ultramicroelectrodes*, Datatech Systems Inc., Morganton, NC, 1987.

[80] R.G. Compton, G.G. Wildgoose, N.V. Rees, I. Streeter, R. Baron, *Chem. Phys. Lett.*, 459 (2008) 1-17.

[81] R.M. Penner, C.R. Martin, *Anal. Chem.*, 59 (1987) 2625-2630.

[82] L.X. Cao, P.S.Yan, K. Sun, D.W. Kirk, *Electroanalysis,* 21 (2009) 1183–1188.

[83] P. Wu, *Anal. Chem.*, 65 (1993) 1643-1646.

[84] C.Y. Lee, Y.J. Tan, A.M. Bond, *Anal. Chem.*, 80 (2008) 3873-3881.

[85] V.B. Nascimento, M.A. Augelli, J.J. Pedrotti, I.G.R. Gutz, L. Angnes, *Electroanalysis*, 9 (1997) 335-339.

[86] S. Szunerits, P. Garrigue, J.-L. Bruneel, L. Servant, N. Sojic, *Electroanalysis*, 15 (2003) 548-555.

[87] I.F. Cheng, C.R. Martin, *Anal. Chem.*, 60 (1988) 2163-2165.

[88] I.F. Cheng, L.D. Whiteley, C.R. Martin, *Anal. Chem.*, 61 (1989) 762-766.

[89] M.J. Madou, *Fundamentals of Microfabrications*, CRC Press, 2002, Boca Radon FL (USA)

[90] D. Lowinsohn, H.E.M. Peres, L. Kosminsky, T.R.L.C. Paixao, T.L. Ferreira, F.-J. Ramirez-Fernandez, M. Bertotti, *Sensor Actuat. B-Chem.*, 113 (2006) 80-87.

[91] F.A. Aguiar, A.J. Gallant, M.C. Rosamond, A. Rhodes, D. Wood, R. Kataky, *Electrochem. Commun.*, 9 (2007) 879-885.

[92] O. Ordeig, N. Godino, J. Del Campo, F.X. Munoz, F. Nikolajeff, L. Nyholm, *Anal. Chem*., 80 (2008) 3622-3632.

[93] M. Varshney, Y. Li, *Talanta*, 74 (2008) 518-525.

[94] A. Berduque, Y.H. Lanyon, V. Beni, G. Herzog, Y.E. Watson, K. Rodgers, F. Stam, J. Alderman, D.W.M. Arrigan, *Talanta*, 71 (2007) 1022-1030.

[95] M.A. Nolan, S.P. Kouvanes, *Anal. Chem.*, 71 (1999) 3567-3573.

[96] J.I. Heo, D.S. Shim, G.T. Teixidor, S. Oh, M.J. Madou, H. Shin, *J. Electrochem. Soc.*, 158 (2011) J76-J80.

[97] G.E. Possin, *Rev. Sci. Instrum.*, 41 (1970) 772-774.

[98] W.D. Williams, N. Giordano, *Rev. Sci. Instrum.*, 55 (1984) 410-412.

[99] V.P. Menon, C.R. Martin, *Anal. Chem.*, 67 (1995) 1920-1928.

[100] D. Routkevitch, T. Bigioni, M. Moskovits, J.-M. Xu, *J. Phys. Chem.*, 100 (1996) 14037–14047.

[101] C. Schoenberger, B.M.I van der Zande, L.G.J. Fokkink, M. Henny, C. Schmid, M. Kruger, A. Bachtold, R. Huber, H. Birk, U. Staufer, *J Phys Chem B*, 101 (1997) 5497-5505.

[102] Martin CR, In: A.J. Bard, I. Rubinstein I, *Electroanalytical chemistry*, Marcel Dekker, 1999, New York.

[103] M. De Leo, F. C. Pereira, L. M. Moretto, P. Scopece, S. Polizzi, P. Ugo, *Chem. Mater.*, 2007, 19, 5955-5964.

[104] R.J. Gilliam, S.J. Thorpe, D.J.W. Kirk, *Appl. Electrochem.*, 37 (2006) 233-239.

[105] L.D.-D. Pra, E. Ferain, R. Legras, S. Demoustier-Champagne, *Nucl. Instrum. Methods Phys. Res. B*, 196 (2002) 81-88.

[106] P.Apel, *Radiat. Meas*., 34 (2001) 559-556

[107] N. Li, S. Yun, C.C. Harrel, C.R. Martin, *Anal. Chem.*, 76 (2004) 2025-2030.

[108] Z. Siwy, A. Fulinsky, *Phys. Rev. Lett.*, 198 (2002) 103

[109] Z. Siwy, D. Dobrev, R. Naumann, C. Trautmann, K. Voss, *Appl. Phys. A*, 76 (2003) 781-785.

[110] R.V. Parthasarathy and C.R. Martin, *Nature*, 369 (1994) 298-301.

[111] P. Ugo, L. M. Moretto, *Handbook of Electrochemistry* (Ed: C. Zoski), Elsevier, Amsterdam 2007, ch. 16.2.

[112] M. Silvestrini, P. Schiavuta, P. Scopece, G. Pecchielan, L. M. Moretto, P. Ugo, *Electrochim. Acta*, 2011, 56, 7718-7724.

[113] M. De Leo, A. Kuhn, P. Ugo, *Electroanalysis*, 19 (2007) 227-236.

[114] S. Yu, N. Li, J. Wharton, C.R. Martin, *Nano Letters*, 3 (2003) 813-818.

[115] C.R. Martin and D.T. Mitchell, in *Electroanalytical Chemistry*, a Series of Advances, edited A.J. Bard, I. Rubinstein, Marcel Dekker, New York 1999, vol. 21, p.1

[116] M. Wirtz, C.R. Martin, *Adv. Mater*, 15 (2003) 455-458.

[117] P. Ugo, L.M. Moretto, S. Bellomi, V.P. Menon, C.R. Martin, *Anal. Chem.*, 68 (1996) 4160-4165.

[118] C. Amatore, J.M. Saveant, D. Tessier, *J. Electroanal. Chem.*, 147 (1983) 39-51.

[119] E. Sabatani, J. Rubinstein, *J. Phys. Chem.*, 91 (1987) 6663-6669.

[120] L.M. Moretto, N. Pepe, P. Ugo, *Talanta*, 62 (2004) 1055-1060.

[121] H.J. Lee, C. Beriet, R. Ferrigno, H.H. Girault, *J. Electroanal. Chem.*, 502 (2001) 138-145.

[122] J.C. Hulteen, V.P. Menon, C.R. Martin, *J. Chem. Soc. Faraday Trans*., 92 (1996) 4029-4032.

[123] J.F. Cheng, L.D. Whiteley, C.R. Martin, *Anal. Chem*., 61 (1989) 762-766.

[124] B. Brunetti, P. Ugo, L.M. Moretto, C.R. Martin, *J. Electroanal. Chem.*, 491 (2000) 166-174.

[125] P. Ugo, N. Pepe, L.M. Moretto, M. Battagliarin, *J. Electroanal. Chem.*, 560 (2003) 51-58.

[126] A.J. Bard, L. Faulkner, *Electrochemical Methods*, Wiley, New York (2000)

[127] P. Ugo, L.M. Moretto, F. Vezzà, *ChemPhysChem,* 3 (2002) 917.

[128] P. Ugo, L.M. Moretto, F. Vezzà, in *Sensors Update*, edited by H. Baltes, G.K. Fedder, J.G. Korvink, , Wiley-VCH, Weinheim 12 (2003) 121.

[129] M. Ongaro, P. Ugo, *Anal. Bioanal. Chem.*, 405 (2013) 3715-3729.

[130] R. Gasparac, B.J. Taft, M.A. Lapierre-Devlin, A.D. Lazareck, J.M. Xu, S.O. Kelly, *J. Am. Chem. Soc*., 126 (2004) 12270-12271.

[131] M.A. Lapierre-Devlin, C.L. Asher, B.J. Taft, R. Gasparac, M.A. Roberts, S.O. Kelly, *Nano Letters*, 5 (2005) 1051-1055.

[132] A. M. Sladkov, V. I. Kasatochkin, Yu P. Kudryavstev, and V. V. Korshak., *Rus. Chem. Bul.*, 17 (1968) 2560-2566.

[133] I. P. Sergushin, Y. P. Kudryavstev, V. M. Elizen, A. P. Sadovskii, A. M. Sladkov, V. I. Nefedov, and V. V. Korshak., *J. Structural Chem.*, 18 (1977) 698-700.

[134] R. J. Lagow, J. J. Kampa, H-C Wei, S. L. Battle, J. W. Genge, D. A. Laude, C. J. Harper, R. Bau, R. C. Stevens, J. F. Haw, E. Munson, *Science*, 267 (1995) 362-367.

[135] R. H. Baughman, *Science*, 312 (2006) 1009-1010.

[136] K. Kinoshita, *Carbon Electrochemical and Physico-chemical Properties*, John Wiley & Sons, New York (1988).

[137] R. J. Taylor, and A. A. Humffray, *J. Electroanal. Chem. and lnterfacial Electrochem.*, 42 (1973) 347-354.

[138] H. S. Dobbs. *J. Physics D: Applied Physics*, 7 (1974) 24-34.

[139] N. Iwashita, C. R. Park, H. Fujimoto, M. Shiraishi, M. Inagaki, *Carbon*, 42 (2004) 701-714.

[140] A. Dekanski, J. Stevanovic, R. Stevanovic, B. Z. Nikolic, V.M. Jovanovic. *Carbon*, 39 (2001) 1195-1205.

[141] G. M. Jenkins, K. Kawamura, L.L. Ban, *Proceedings of the Royal Society of London, Series A, Mathematical and Physical Sciences*, 327 (1972) 501-517.

[142] J. Kim, X. Song, K. Kinoshita, M. Madou, R. White, *J. Electrochem. Soc.*, 145 (1998) 2314-2319.

[143] R. Kostecki, X. Song, and K. Kinoshita. *J. Electrochem. Soc.*, 147 (2000) 1878–1881.

[144] A. Singh, J. Jayaram, M. Madou, and S. Akbara, *Journal of the Electrochemical Society*, 149 (2002) E78–E83.

[145] W. M. Moreau. *Semiconductor Lithography: Principles, Practices and Materials*. Springer, New York, 1987.

[146] E. Fitzer, K. H. Kochling, H. P. Boehm, H. Marsh, *Pure and Applied Chemistry*, 67 (1995) 473-506.

[147] Ch. Wang, G. Jia, L. H. Taherabadi, and M. J. Madou, *J. of Microelectromechanical Systems*, 14 (2005) 348-358.

[148] E. Fitzer, W. Schafer, *Carbon*, 8 (1970) 353-364.

[149] A. M. Lyons, C. W. Wilkins, M. Robbins, *Thin Solid Films*, 103 (1983) 333-341.

[150] H. Nakagawa and S. Tsuge, *Journal of Analytic and Applied Pyrolysis*, 12 (1987) 97-113.

[151] K. Nishikawa, K. Fukuyama, T. Nishizawa, *Japan J. Appl. Physics*, 37 (1998) 6486-6491.

Chapter 2: Electroanalysis of Trace Inorganic Arsenic with Gold Nanoelectrode Ensemble

2.1 Introduction

The control of arsenic concentration in drinking water is an actual challenge because of the toxicity of this element and its widespread presence in the environment [1]. The origin of this presence can be found both in the natural composition of rocks and soils (As is the 20th element in the earth's crust in abundance), and as a consequence of human activity. In 1993, the World Health Organization (WHO) set to 10 μg/L the maximum limit for As concentration in drinking water, value adopted also by the European legislation. As a consequence, there is a real need for simple and reliable analytical methods able to reach this low detection limit, being, at the same time, suitable for decentralized analysis even in remote areas. Arsenic toxicity is function of its speciation; as far as the oxidation state is concerned, it is known that As(V) is 100 times less toxic than As(III) [2].

Hydride generation followed by atomic absorption spectroscopy is, perhaps, the most widely used method for inorganic arsenic detection, after Holak's [3] first report in 1969. Considering that As can be present both in the 3+ and 5+ oxidation state, a preliminary reduction step is required since only As(III) reacts with $NaBH_4$ [4]. Inductively coupled plasma (ICP) techniques are also used as analytical tools for arsenic analysis [5]. The most important advantage (but also limit [6]) of this technique is that the high temperature of the plasma atomizes and ionizes all forms of arsenic so that the response does not depend on the molecular speciation of As in the sample. Another possible drawback of ICP-MS is the possible interference from high levels of chloride which generates argon chloride ($^{40}Ar^{35}Cl$) in the plasma which interferes with (^{75}As) [7].

Among the others, electrochemical methods of analysis are employed for As determination with the advantage of requiring less expensive instrumentation and being suitable for on-site control and decentralized monitoring. Both cathodic and anodic stripping voltammetry are used for the electrochemical determination of trace As using the hanging mercury electrode [8-10], or gold electrodes [11] as the working electrode. The reactions involved in the ASV of

As(III) at gold electrodes are the electrochemical reduction (deposition) of As^{3+} to As^0 (2.1) and the oxidation (stripping) where an anodic current is detected at the electrode (2.2):

$$As^{3+} + 3e- + Au \rightarrow As(Au) \quad (2.1)$$

$$As(Au) \rightarrow As^{3+} + 3e- + Au \quad (2.2)$$

Recent papers [12,13] showed that the stripping voltammetric (ASV) determination of arsenic can be improved by nanostructuring the electrode surface. In particular, several papers described the successful use of carbon electrodes modified with gold nanoparticles (Au-Nps) for trace arsenic analysis. The Au-Nps can be deposited by mean of electroless [14] or electrochemical methods [15,16]. The so prepared modified electrodes showed detection limit (DL) of 0.01 μg L^{-1} [12]. Trace As(III) has been successfully detected also using gold microelectrode array in which the electrode surface is coated by a thin Nafion film [13].

Different approaches for the speciation of As(III) and As(V) have been described, after the first reported by Nurnberg and coworkers [17]. In most cases, the speciation analysis is performed by quantifying the difference between As(III), originally present in the sample, and total inorganic arsenic determined after reduction of As(V) to As(III). The latter process can be performed by using chemical or electrochemical reduction [18], but the former method is the most widely applied. For this purpose, various chemical reducing agents have been used such as potassium iodide and ascorbic acid [19], sodium sulfite [20], gaseous SO_2 [17], cuprous chloride [21,22] and a-cysteine [11,23]. However, some of them are not suitable for combination with ASV (KI) or require complex setup (SO_2 and Cu_2Cl_2). In the present work we choose to use solid a-cysteine as the reducing agent, which acts easily and efficiently on As(V) reduction, according to the reaction shown in Scheme 1:

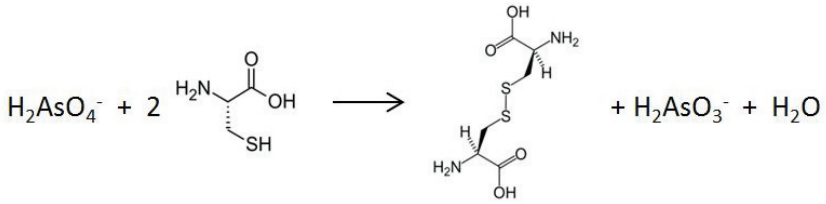

In order to try to further improve the reliability and analytical performances of the ASV determination of trace arsenic, in this chapter we examine the possibility to exploit the improved electroanalytical performances of the so called nanoelectrode ensembles (NEEs). It was indeed demonstrated that, thanks to dramatically improved signal to background current ratio and enhanced diffusion [24,25], NEEs can be successfully applied to trace analysis of a variety of redox analytes ranging from small organics [26,27] to large redox proteins and

antigens [28,29], from antibiotics [30] to iodide [31,32]. In the present chapter we examine the use of NEEs for the anodic stripping analysis of inorganic arsenic focusing, in particular, on the optimization of the analytical conditions in order to lower the DL and improve the analytical performance. Note that, up to know, NEEs were used for the direct determination of analytes and this is the first paper showing that such nanostructured electrodes can be applied to ASV analysis. With respect to the so-called GNEEs grown from seeded Au-Nps in thiol functionalized silicate network [33], the membrane template NEEs used here allow a better control of the nanoelectrode density. The improved ratio between the active and geometric area of the NEEs used here with respect to the GNEE in ref [33], should improve the signal/background current ratio, further lowering detection limits [25,34].

Particular attention has been addressed to the optimization of the analytical parameters in order to improve the reproducibility of the analysis. In order to widen the dynamic range, the controlled etching of the polycarbonate template was also tested. By this method, the nanofibers are partially exposed increasing the gold surface area and obtaining 3D-NEEs. As a consequence, the saturation of the Au-nanoelectrodes is expected to be observed at higher As concentration, so allowing the widening of the linearity range. This is particularly attractive for analysis in real samples where As concentration can range from few ng/L to more than 10 μg/L.

Water samples from rivers in the lagoon of Venice basin were analyzed both with 3D-NEEs and the results compared with those determined by ICP-MS. Advantages and limits of the field analysis of inorganic arsenic with NEEs are presented and discussed.

2.2 Experimental

2.2.1 Materials

Polycarbonate filtration membranes (SPI-Pore, 47 mm filter diameter, 6 mm filter thickness, $6x10^8$ pores/cm^2) with a nominal pore diameter of 30 nm and coated with the wetting agent polyvinylpyrrolidone were used as the templates to prepare the NEEs. As(III) stock solutions (100 mg/L) were prepared by dilution of a 0.05 mol/L standard $NaAsO_2$ solution (Carlo Erba). As(V) stock solutions (1000 mg/L) were prepared from a 1000 mg/L standard commercial solution of As_2O_5 (tritisol, Merck). All other solutions were prepared with ACS grade reagents. Purified water (18.3 MW) was obtained using a Human UP 900 water purification system. CASS-4 certified reference standard was provided by the Canadian National Research Council. It consists of sea water (Nearshore seawater), acidified with

HNO_3, with mass fractions and mass concentrations assigned for 12 elements. The certified concentration of As is 1.11 ± 0.16 μg/L and of Cu is 0.592 ± 0.055 μg/L.

2.2.2 Apparatus

All electroanalytical measurements were carried out at room temperature (22°C) using a three-electrodes single compartment cell equipped with a platinum wire counter electrode and an Ag/AgCl (KCl saturated) reference electrode. All potential values are referred to this reference electrode. A CHI440 apparatus controlled via PC by its own software, was used for voltammetric measurements.

2.2.3 Electrodes Preparation

The nanoelectrode ensembles were prepared using the electroless plating procedure and assembled using the procedure described in Chapter 1, based on literature report [25, 35-37]. Briefly, after wetting for 2 h in methanol, the track-etched polycarbonate membrane was sensitized into 0.026 M $SnCl_2$, 0.07 M trifluoroacetic acid in 50% methanol in water, for 45 min. After rinsing in methanol, the membrane was dipped in 0.029 M $Ag[(NH_3)_2]NO_3$ for 10 min. The membrane was rinsed in methanol and then in water and successively was immersed into the Au plating bath containing $7.9x10^{-3}$M $Na_3Au(SO_3)_2$ in 0.127 M Na_2SO_3, at 0°C. After 30 min, 0.625 M formaldehyde was added to the bath. Electroless deposition was allowed to proceed for 15 h, after which additional 0.625 M formaldehyde was added.

After a total of 24 h of plating, the golden membrane was rinsed with water and dipped for 6 h in 10% HNO_3, then rinsed again with water and dried. Handy NEEs were assembled as previously described [25]. A small piece (approximately 8 mm x 8 mm) of golden membrane was attached to a suitable conductive substrate; the gold layer on the outer face of the membrane was removed by peeling with scotch tape (so that only the head of the gold nanowires inside the pores will be exposed to the sample solution); all the surface of the NEE, apart a hole of 3 mm diameter (which defines the geometric area of the ensemble, A_{geom} = 0.07 cm^2), was insulated with a film of plastics (Monokote by Topflite). The estimated active area (A_{act}), i.e. the area of the Au nanodisks exposed is $3*10^{-4}$ cm^2 [37]. Good sealing between the nanoelectrodes and the polycarbonate was assured by heating the NEE at 150°C for 15 min.

Conventional "macro" gold electrodes, hereafter named "Au_{macro}", were prepared via sputtering deposition (roughness Ra=15 nm) into a spirally tracked polycarbonate (PC) slide

(a support for CDs). This kind of material allows the deposition of gold without any interlayer and therefore the preparation of the electrode became easier. The gilded plate was cut into slides (ca. 2.5 cm x 1.0 cm) and the geometric area of the electrodes (0.07 cm^2) was defined, as for the NEE, by the diameter of a hole punched in a strip of insulating tape. The electrical contact was made with a copper tape before placing the insulating tape.

3D-NEEs preparation

Ensembles of gold nanowires were produced with two etching procedures, i.e. oxygen plasma [38,39] vs chemical etching [39,40]. Three etching times has been used for each etching strategy, namely 1, 5, 10 min of oxygen plasma and 5, 10, 30 seconds of chemical etching.

2.2.4 Procedures

Determination of As(III)

0.33 mL of 6 M HCl + 65 mg hydrazine dihydrochloride were added to 10 mL of water (or to 10 mL of diluted certified reference solution). ASV measurements were performed as follows: i) accumulation at -0.4 V performed for the desired time under continuous stirring; ii) 15 s equilibration in quiet solution; iii) SWV stripping from -0.4 to 0.45 Vat 250 Hz frequency, square wave amplitude 75 mV, scan increment 12 mV. Every determination is an average of three successive ASV.

Determination of As(V)

50 mL of As(V) solution, 314 mL of 0.78 M hydrazine (final concentration1.9 mM) and 30 mg of solid cysteine (4.9 mM) were heated at 80°C in a water bath for 30 min under continuous stirring. After cooling to room temperature the solution was brought to 50 mL in a volumetric flask and analyzed with the same procedure used for As(III).

Sampling of river water

Real samples were collected in a river (Naviglio – Brenta) of the Venice lagoon basin, in Malcontenta. After sampling, the water was filtered (0.45 μm) in order to remove sand and other suspended solids and acidified with nitric acid (reaching pH 2.0), following the standard procedure used for heavy metal analysis in water [41]. Before the analysis the sample was stored at 4°C.

2.3 Results and Discussion

2.3.1 Morphological characterization of the 2D-NEEs and 3D-NEEs

Figure 2.1 show the SEM images of the NEEs treated with oxygen plasma namely for 0 (Fig. 2.1A), 1 (Fig. 2.1B), 5 (Fig. 2.1C) and 10 min (Fig. 2.1D).

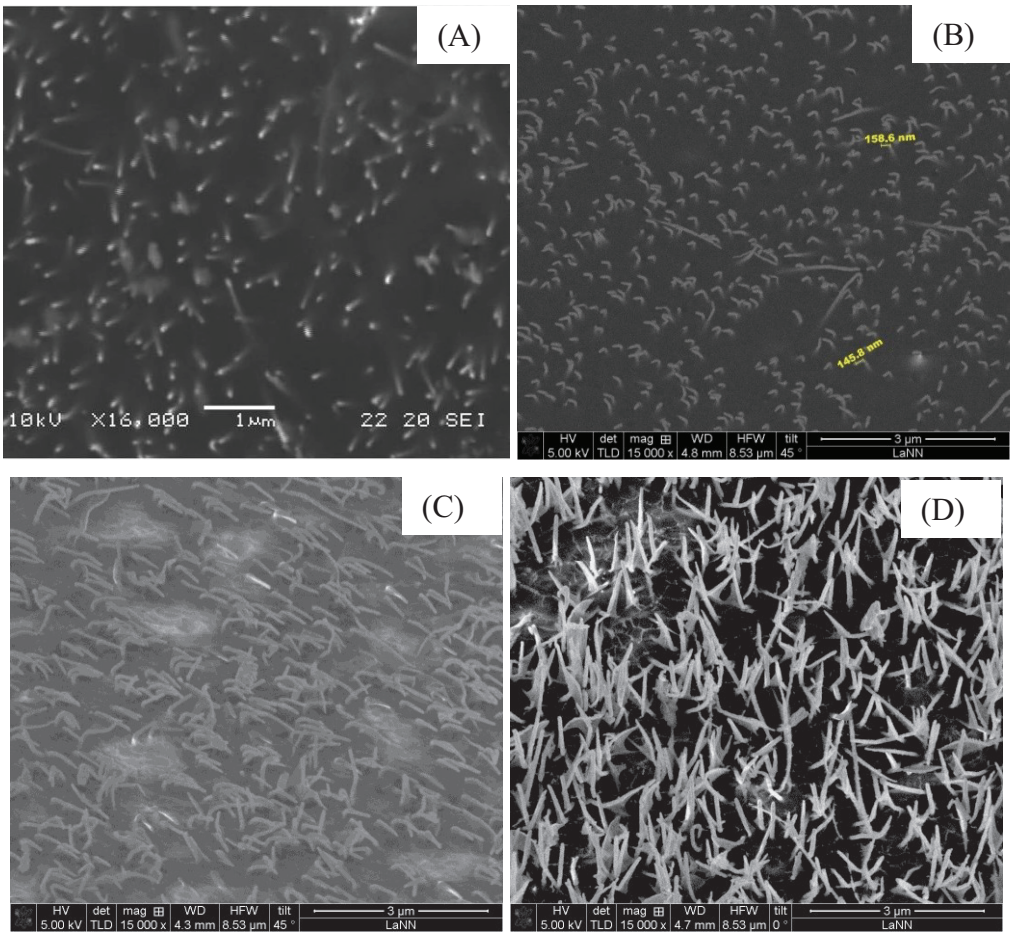

Figure 2.1. FE-SEM images of NEEs after etching with O_2/Ar plasma for A) 0 min; B) 1 min; C) 5 min; D) 10 min.

Table 2.1 summarizes the data obtained from the SEM images presented in Figure 2.1. The nanofibers length was measured directly on the scanning electron microscope images and is an average of at least 10 measurements. Once obtained the nanofibers length, it was possible to calculate the average increase in area ($A_{(3D\text{-}NEE)}$ / $A_{(2D\text{-}NEE)}$) and the ratio between the active area of the ensemble and the active area of a flat gold electrode of the same geometric area ($A_{(ACTIVE)}$ / $A_{(GEOMETRIC)}$).

Treatment duration (min)	Nanofiber lenght (μm)	$A_{(3D\text{-}NEE)}$ / $A_{(2D\text{-}NEE)}$	$A_{(ACTIVE)}$ / $A_{(GEOMETRIC)}$
0	0	1	0.004
1	0.15	20	0.089
5	0.5	67	0.287
10	1	133	0.569

Table 2.1. Data obtained from the FE-SEM images for the 3D-NEEs.

For the set of electrodes etched chemically, it was not possible to calculate the nanofiber length since the rate of etching is slower and they are not enough exposed from the polycarbonate template. By the way, De Leo et al. calculated the increase in capacitive current for these kind of electrodes [39]. An FE-SEM image of a NEE after chemical etching with 1:9 CH_2Cl_2 / C_2H_5OH for 10 seconds is presented in Figure 2.2.

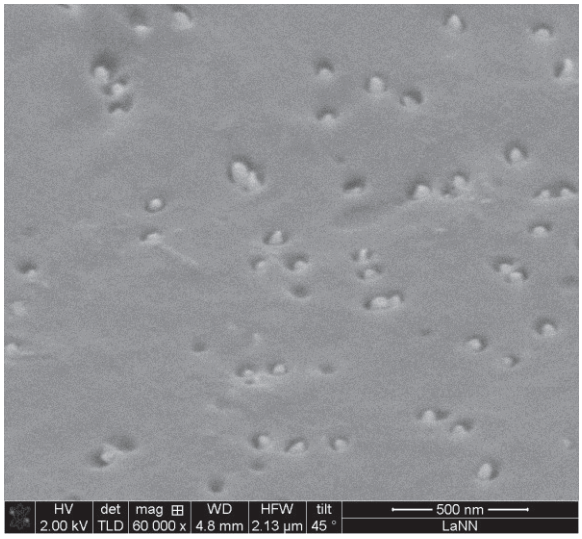

Figure 2.2. FE-SEM images of NEEs after etching with 1:9 CH_2Cl_2 / C_2H_5OH for 10 seconds.

2.3.2 Selection of the Electrolyte

According to previous literature [18,42], at first we examined the electrochemical behavior of NEEs in 1 M HCl, 62 mM hydrazine [18,42–46]. Hydrazine chloride was added to each sample to prevent the oxidation of As(III) to As(V). Figure 2.3a shows the square wave voltammograms recorded at NEE in 1 M HCl. One can note that the background current in the blank electrolyte increases in subsequent scans, displaying a drift. At the seventh scan the drift was approximately 500 nA. This effect suggests the deterioration of the NEE surface with progressive exposure of the gold of the nanofibers and consequent increase of the double-layer charging current [39].

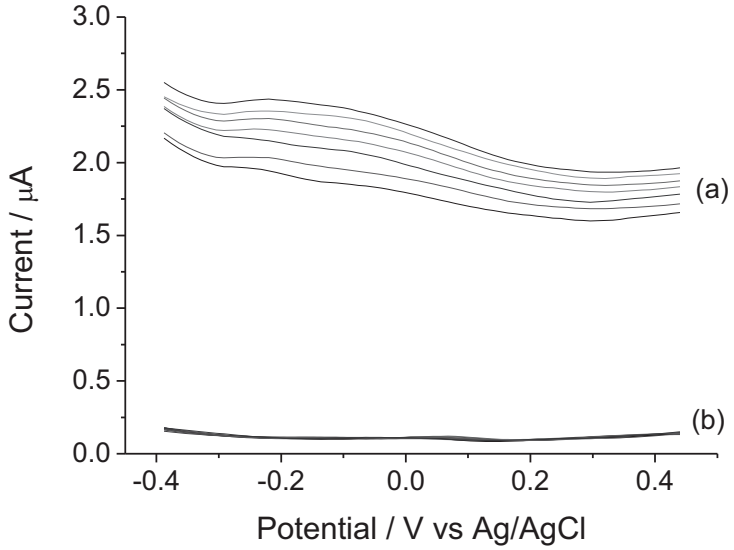

Figure 2.3. Square wave voltammograms recorded at NEE in 1 M HCl (a) or 0.2 M HCl (b) and 62 mM hydrazine. SW parameters: scan increment 12 mV; amplitude 75 mV; frequency 250 Hz; initial potential -0.4 V.

In order to investigate such a possibility, the AFM characterization before and after the exposure of the NEEs to 1 M HCl was performed. It was recently shown that AFM can furnish useful information on the morphology of NEEs [37]. Note that, in the present case, we are interested more in the general behavior of all the assembly rather than on the destiny of the individual nanoelectrodes. Therefore, the AFM scans were performed on a relatively large spatial scale, examining areas 50x50 μm wide. At variance with the previous paper [37], working with such a wide spatial scale, the single nanoelectrodes are only scarcely distinguished from the surrounding polycarbonate. Relevant AFM topographies are shown in Figure 2.4, where Figure 2.4A refers to a brand new NEE and Figure 2.4B shows the topography of a NEE after being used in 1 M HCl. One can note that the brand new NEE presents a low surface roughness, which is quite homogeneously distributed all over the examined area. On the contrary, the NEE used in 1 M HCl shows a much rougher surface, with deep “canyons and valleys” running diagonally all through the surface. Figure 2.5 shows relevant profilometric patterns run in correspondence of the white lines in Figure 2.4A and 2.4B and for a NEE after use in 0.2 M HCl (see below). The comparison between the broken line (brand new NEE) and gray line (1 M HCl treated NEE) profiles confirms the dramatic increase in roughness caused by the 1 M HCl electrolyte. These evidences suggest that in 1 M HCl the surface of the PC is partially etched, probably because of hydrolysis of the polymer by the concentrated acid. This behavior suggested us to test the effect of a decrease of the HCl concentration to 0.2 M (always keeping hydrazine to 62 mM). Figure 2.3B shows an overlay

of ten voltammograms recorded in this medium and demonstrates that now the background current values stay rather constant for many consecutive scans, moreover the average SWV background current is much lower, setting around a value of 0.1 μA. The comparison of the AFM profilometric sections recorded for the NEE after use in 0.2 M HCl (Figure 4, black line) indicates that the more diluted acid doesn't damage the NEE surface. Diluted HCl (with hydrazine) could potentially be the electrolyte of choice. To test such possibility, in the following section we will examine the cyclic voltammetric behavior of As(III) at NEEs in such a medium.

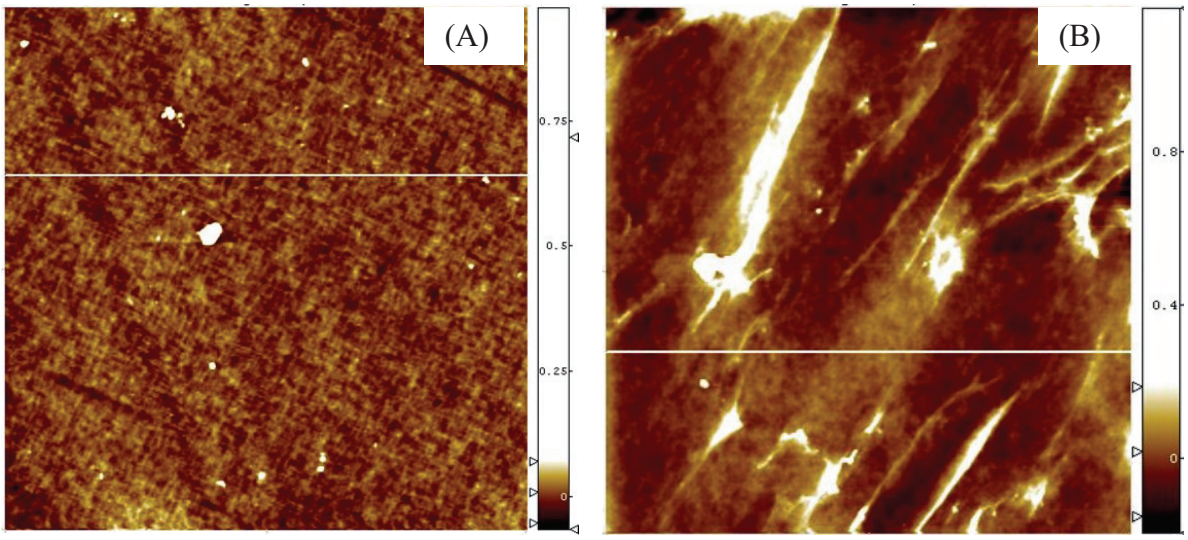

Figure 2.4. AFM topographic images of the surface: (A) of brand new NEE, (B) a NEE after use in 1 M HCl.

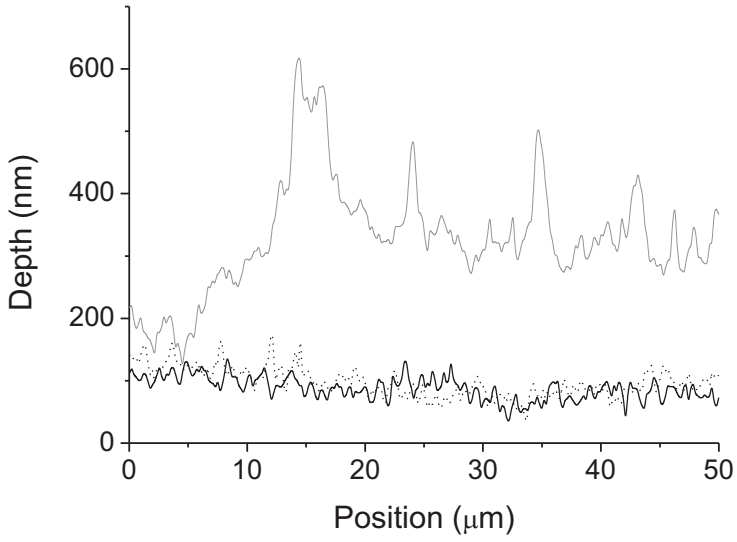

Figure 2.5. Profilometric patterns recorded for a brand new NEE (dotted black line), for a NEE used in 0.2 M HCl (full black line) and of a NEE used in 1 M HCl (full grey line).

2.3.3 CV of As(III) at NEE

Figure 2.6A shows the CVs recorded at 200 mV/s in 40 mg/ L As(III) (in 0.2 M HCl, 62 mM hydrazine, full line) vs. the background signal recorded in aerated pure supporting electrolyte (dotted line). The forward scan of the CV recorded in the presence of As(III), is characterized by a cathodic peak at -0.400 V. CVs recorded at different scan rates (not shown) indicate that the potential of the cathodic peak shifts from -0.350 V (at 50 mV/s) to -0.450 V (at 500 mV/s). The peak current scales linearly with $v^{1/2}$ (see Figure 2.6A, Inset), indicating a diffusion controlled process. In the backward scan an anodic peak is detected at about 0.220 V, whose peak height scales linearly with the scan rate (not shown). Note that in the reoxidation scan a crossover in the voltammogram is observed, indicating a process involving the deposition of a metal on electrodes having a different chemical nature from the deposit itself [47,48]. All these evidences agree with the reduction of dissolved As(III) in the forward scan, according to:

$$As(III) + 3e^- \rightarrow As(0) \qquad (2.3)$$

The quite large value of E_p-$E_{p/2}$, which is 100 mV at v = 200 mV/s, indicates that the reduction is not fully reversible. In the backward scan the reverse reaction occurs which corresponds to the anodic stripping of deposited As(0). Figure 2.6B shows the CV recorded in the same solution than in Figure 2.6A, but at a Au_{macro} electrode. In this case, the reduction process takes place at less negative potential values (approximately at -0.245 V) than at the NEE, with the peak current still linearly dependent on $v^{1/2}$ (see Figure 2.6B, Inset). The oxidation peak current recorded is much higher than at the NEE, but still depends linearly on v. This behavior indicates that the electrochemical process occurring at the NEE and the Au_{macro} is the same. The large cathodic shift in the peak potential relevant to As(III) reduction at the NEE with respect to the Au_{macro}, agrees with a slow electron transfer kinetics. It is indeed known that NEEs behave like electrodes with partially blocked surface [25,26], therefore they are more sensitive to electron transfer kinetics than electrodes with continuous surface, this reflecting in an increase in the electrochemical overpotential which influences the electrochemical behavior for redox couples with slow electron transfer kinetics. For a reduction process this reflects in a cathodic shift of the peak potential as observed by us for arsenic. Also the lower current for the As(0) stripping peak at the NEE vs. the Au_{macro} agrees with the microscopic morphology of the NEE. Since the gold active area is much smaller at the NEE, a lower amount of elemental arsenic can be deposited and, consequently, a much lower reoxidation stripping peak is recorded. Note that the stripping peak describes a surface

controlled process (i_p proportional to v), while the reduction process is diffusion controlled (i_p proportional to $v^{1/2}$) and that at NEEs, even under total overlap diffusion conditions, diffusional fluxes at the nanoelectrodes are dramatically enhanced [25]. Such a different dependence on mass fluxes can explain the large difference in peak current observed at the NEE for the reduction versus reoxidation process.

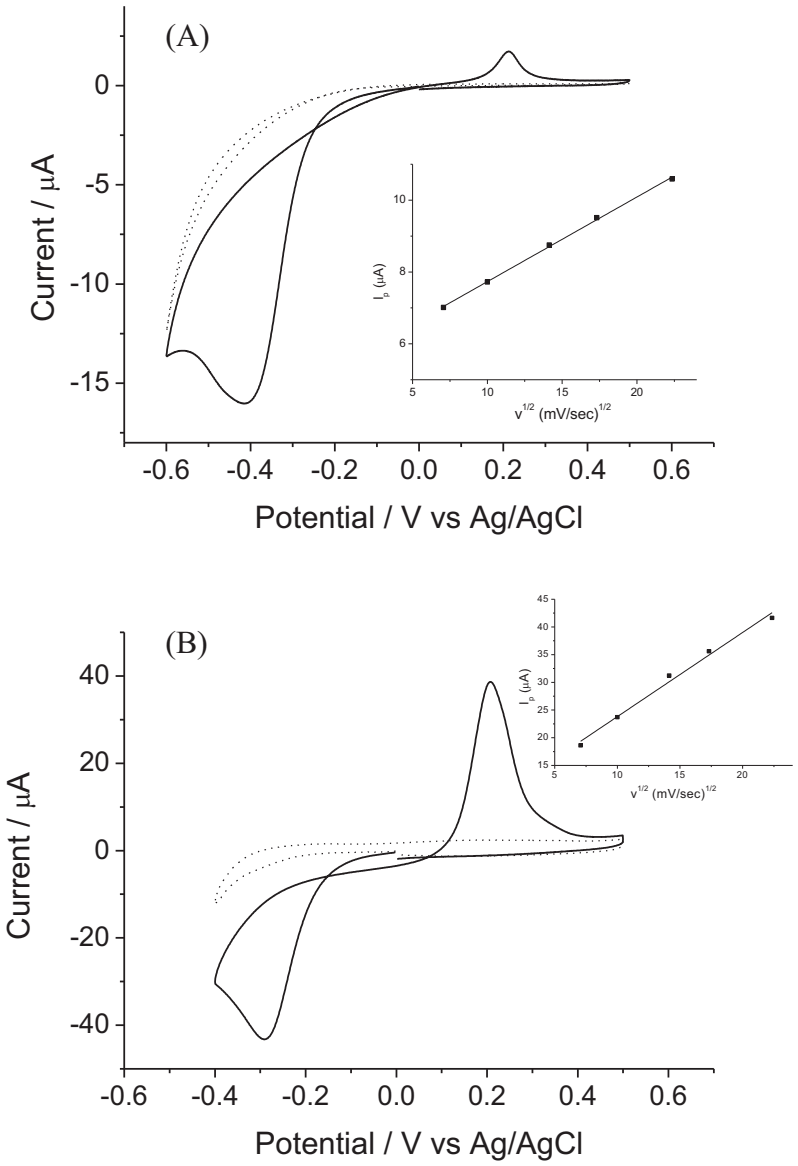

Figure 2.6. Cyclic voltammograms recorded at 0.2 V/s at a NEE (A) and at an Au_{macro} electrode (B) in solution of 40 mg/L As(III) in HCl 0.2 M, 62 mM hydrazine. Forward scan: cathodic. Insets: dependence of i_p cathodic on the square root of the scan rate.

2.3.4 AS-SWV of As(III) at NEE

For the determination of trace concentration levels of arsenic, we chose to operate with NEE using anodic stripping-square wave voltammetry, AS-SWV. Preliminary experiments indicated that a deposition time between 120 s and 180 s gives good results, the final choice depending on the concentration of the analyte. At longer deposition time we observed a decrease in the reproducibility of the stripping peak current and a shorter linear range (see below). This fact is explained taking into account a saturation effect of the available Au surface of the nano-sites of the NEE, in agreement with the above cyclic voltammetric observations. Figure 2.7 shows the AS-SWVs recorded at a NEE in 0.2 M HCl, 62 mM hydrazine, spiked with increasing amounts of As(III). A very sharp stripping peak is recorded at 0.0 V, with peak current which scales linearly for concentrations between 0.2 and 3.0 μg/L (see Inset). The evidence that in Figure 2.7 the oxidation of As takes place at less positive potential values could be due to the fact that at nanoelectrodes in diluted solutions, only small nuclei of elementary As are formed, whose oxidation is energetically easier than that of a bulk deposit.

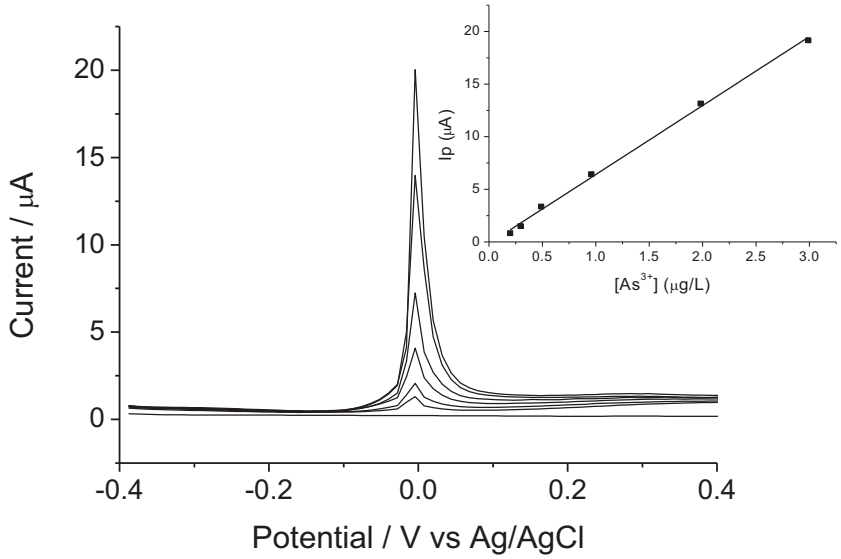

Figure 2.7. AS-SWVs at NEE in 0.2 M HCl at different As(III) concentrations (from 0 to 3.0 μg/L). Inset: Relevant calibration plot. Deposition at -0.4 V for 180 s. Other parameters as in Figure 2.3.

As shown in Figure 2.8 (triangles) the increase of As(III) concentration above 8–10 μg/L causes the progressive lowering of the sensitivity up to a saturation effect. The effect of decreasing the deposition time to 120 s is shown in Figure 2.8 (squares). As expected, the sensitivity at low concentrations decrease, but the linear range increases.

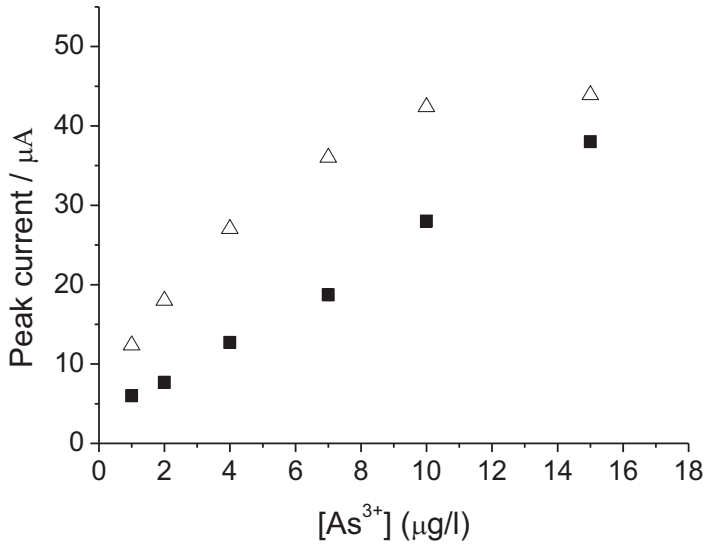

Figure 2.8. I_p vs. As(III) plot for continuous additions of As(III) at deposition time of 180 s (triangles) and 120 s (squares).

For comparison, Figure 2.9 shows the AS-SWVs at a Au_{macro} electrode recorded at As(III) concentrations from 20 to 150 μg/L, which shows that the stripping peak shifts to slightly more positive potential values, with much larger half-peak width (approximately 120 mV).

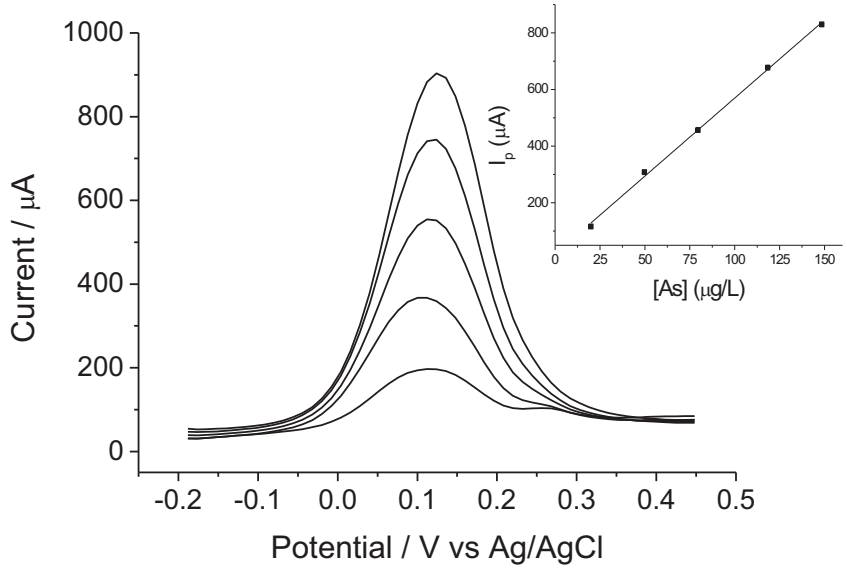

Figure 2.9. AS-SWVs recorded at Au_{macro} electrode at increasing concentration of As(III): 20, 50, 75, 125 and 150 μg/L. Inset: Relevant calibration plot. Other parameters as in Figure 2.3.

Table 2.2 compares the analytical parameters obtained with a NEE and a Au_{macro}. The NEE furnishes a detection limit roughly 2 order of magnitude lower, however the linearity range at the NEE is shorter, in agreement with the hypothesis of the saturation of the gold nano-sites that occurs for the NEE: the larger is the available gold surface, the wider is the linear range. In comparison with other nanostructured electrodes, DL at our NEEs compares or is even slightly lower than previous achievements [12–16].

	NEE	**Au_{macro}**
DL (mgL^{-1})	0.005	0.75
LR (mgL^{-1})	0.2 – 6	20 – 150
Sensitivity (mA L mg^{-1})	6.6	5.5
σ_b (mA)	0.11	1.38

Table 2.2. Comparison of the AS-SWV performances of NEE and Aumacro electrode for the As(III) determination (deposition time 180 s). DL: Detection limit calculated as DL=3sb/m, where σ_b is the standard deviation of the blank; LR=Linear range.

2.3.5 As(III) at 3D-NEE

Since the active area of the NEE is very small, the linearity range of the analytical response of these kind of electrode is very narrow (see Section 2.3.4) and the main disadvantage of this electrodes is a saturation effect. This can be a limit, especially in the analysis of real samples. We indeed decided to perform a controlled increase of the active area of the nanoelectrode ensemble, through the etching of the polycarbonate membrane and the partial exposure of the nanofibers.

Chemical etching

Three different set of ensemble of nanowires (3D-NEE) were prepared with different etching times and the electroanalytical performance of the so-prepared electrodes were studied while increasing the concentration of As(III), as shown in Figure 2.10 and 2.11 and relative insets.
In order to compare the results obtained with the un-etched NEEs, it was decided to keep the As deposition time constant at 180s to study the change of the linearity range of the different set of electrodes. The electrodes revealed a good linear behavior and, as we expected, the linear range becomes wider as the active area accessible to As accumulation increases (see also Table 2.3). As drawback, also the double layer charging current increased with the active area therefore a compromise between a wide linear range and a small limit of quantification must be found.

As it is shown in Figure 2.11, when the electrode is etched for more than 30s an anodic shift in the stripping peak potential (around 100 mV) occurs, as explained in the previous section. This confirm that at electrodes with very small area only As nuclei are formed, while at larger electrodes (flat gold or heavily etched NEEs) bulk As is deposited.

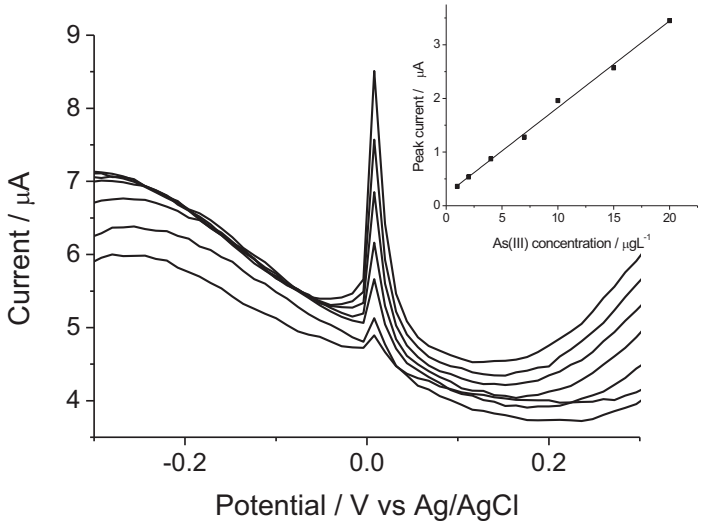

Figure 2.10. AS-SWVs at 3D-NEE etched for 20s in 0.2 M HCl at different As(III) concentrations (from 1 to 20.0 μg/L). Inset: Relevant calibration plot. Deposition at -0.4 V for 180 s. Other parameters as in Figure 2.3.

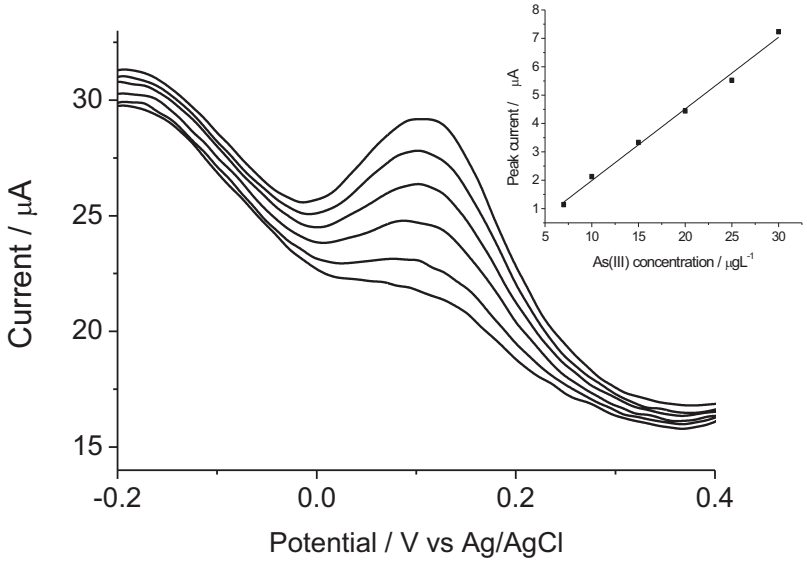

Figure 2.11. AS-SWVs at 3D-NEE etched for 30s in 0.2 M HCl at different As(III) concentrations (from 7 to 30.0 μg/L). Inset: Relevant calibration plot. Deposition at -0.4 V for 180 s. Other parameters as in Figure 2.3.

$t_{etching}$ (sec)	t_{dep} (sec)	LR (µg/L)
5	180	1-5
20	180	1-20
30	180	7-30

Table 2.3. Comparison of the AS-SWV performances of 3D-NEEs the As(III) determination. LR: Linear range.

Plasma etching

Also the 3D-NEEs prepared with plasma etching were tested in the ASV of As(III). The results, summarized in Table 2.4, are similar to those obtained with the chemical etching. The linear range becomes wider as the active area accessible to As accumulation increases, that means, as the etching time increases.

$t_{etching}$ (min)	t_{dep} (sec)	LR (µg/L)
1	180	1-20
5	180	2-30
10	180	5-40

Table 2.4. Comparison of the AS-SWV performances of 3D-NEEs the As(III) determination. LR: Linear range.

In spite of that, for further applications the chemical etching method has been preferred for the electrodes preparation: it doesn't require particular and expensive instrumentation which is not present in all the research laboratories; can avoid possible contaminations (either metallic and not) coming from the plasma chamber if it isn't perfectly clean, or if the instrument is used also for other purposes.

2.3.6 Redox state speciation and Cu interference

Preliminary experiments performed with Au_{macro} electrode confirmed the completion of the reduction of As(V) to As(III) using cysteine as the reducing agent, under the conditions described in the experimental section. It was observed indeed that AS-SWVs performed on equimolar concentration of As(III) generated by in situ chemical reduction of As(V), and As(III) added directly as $NaAsO_2$ give exactly the same voltammetric peaks, with calibration plots displaying the same sensitivity. Figure 2.12 shows the AS-SWVs of As(III) produced by chemical reduction of As(V) with cysteine (SWVs A and B), together with the voltammogram

recorded after standard addition of As(III) (signal C in Fig. 2.12). These signals scale linearly with the total content of As, indicating that the possible presence of a cysteine excess and of generated cystine do not interfere.

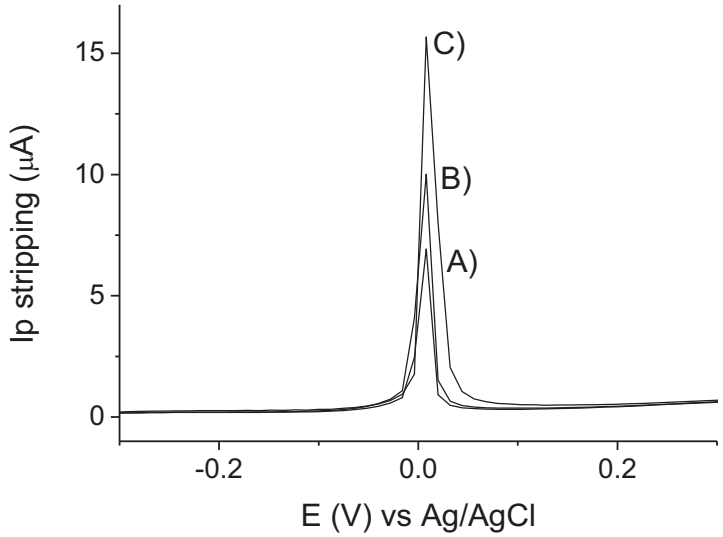

Figure 2.12. AS-SWVs recorded at a NEE in 0.2 M HCl and subsequent additions of As(V) chemically reduced by cysteine (A and B) and of As(III) added as As^{3+} salt (C).

Since it is known that copper(II) can interfere with As(III) ASV determination [49], we performed a series of experiments adding increasing concentrations of Cu(II) to a constant As(III) concentration (namely 2 μg/ L). It was observed that the stripping peak current of As(III) is practically unaffected by the addition up to a 5- fold copper excess. Two stripping peaks for Cu are indeed observed at approximately -0.150 V vs. Ag/AgCl ($Cu(0) \rightarrow Cu(I)+e^-$) and at +0.350 V ($Cu(I) \rightarrow Cu(II)+e^-$), but they are separated enough from the As peak to cause only a minor interference (see Figure 2.13).

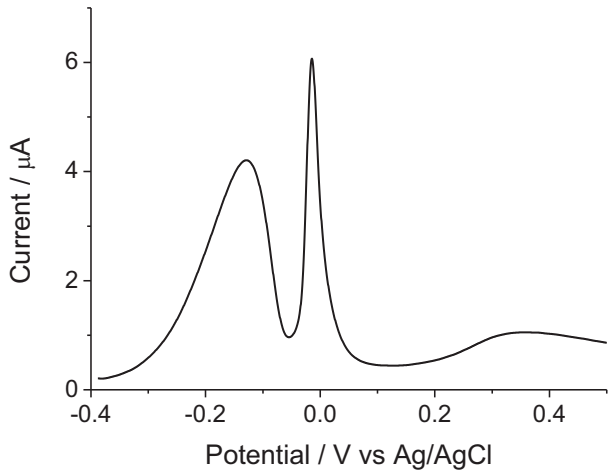

Figure 2.13. AS-SWVs recorded at a NEE in 0.2 M HCl solution spiked with 2 μg/L As(III) and 10 μg/L Cu(II).

2.3.7 Electroanalysis of Certified Samples with NEEs

The above-developed method was tested for the determination of As in a certified sample (CASS-4) which consists of Nearshore seawater. After reduction with cysteine (see Section 2.2.4), 5 mL of CASS-4 were diluted 1 : 1 with HCl (final concentration 0.2 M), adding hydrazine dihydrochloride (62 mM). The AS-SWV is characterized by a peak at 0.0 V vs. Ag/AgCl which increases linearly after standard addition of As(III). The sample concentration, calculated by extrapolation of the calibration plot shown in Figure 2.14 and considering the dilution factor, was 1.18 ± 0.06 μg/L (based on three replicates). This value is in satisfactory agreement with the value of 1.11 ± 0.16 μg/L certified by the National Research Council of Canada, who furnished the CASS-4 standard.

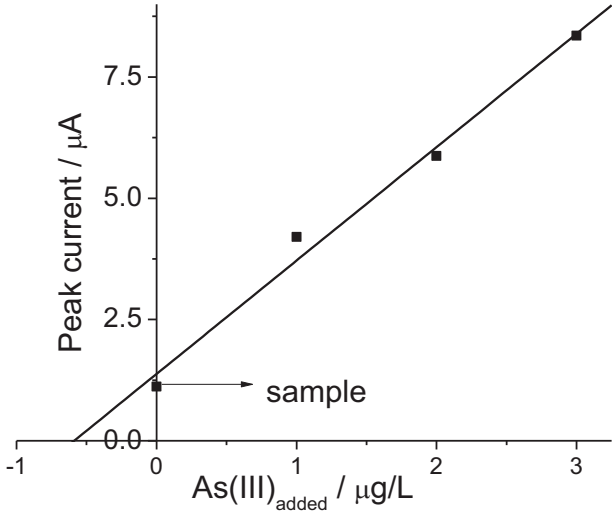

Figure 2.14. Standard addition plot obtained by AS-SWV with NEE on a CASS-4 sample diluted 1 : 1.

2.3.8 Real sample analysis with 3D-NEE

The procedure optimized in the previous paragraphs was applied to the speciation of inorganic arsenic (namely As(III) and As(V)) concentration in a river (Naviglio Brenta) of the Venice lagoon basin using 3D-NEE (chemically etched for 20seconds).

First of all, total inorganic arsenic concentration was calculated, as explained in section 2.2.4, by reduction of As(V) to As(III) with solid cysteine at 80°C. After this step, and by diluting the sample with HCl reaching the final concentration of 0.2 M, the concentration in the real sample was calculated with the standard addition method (3 additions of 1 μg L^{-1} of As(III) each). Figure 2.15 shows that a satisfactory linear response was achieved with a correlation coefficient of R^2 0.997 and the correspondingly inorganic Arsenic (iAs) concentration in the sample resulted 3.2 ± 0.2 μg L^{-1} (n=3).

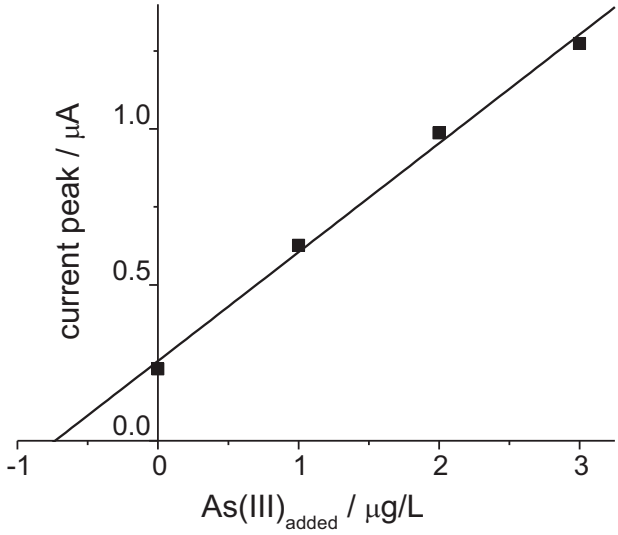

Figure 2.15. Standard addition plot obtained by AS-SWV with 3D-NEE on a sea water sample obtained in the Venice Lagoon basin (sample diluted 1:4). Deposition at -0.4 V for 180 s. Other parameters as in Figure 2.3.

The same sample was analysed with ICP-MS and a concentration of 3.2 ± 0.1 μg L^{-1} was measured, which is in very good agreement with the electrochemical analysis.

By applying ASV method without reduction with cysteine, As(III) concentration in the same sample was evaluated giving a concentration of 1.1 ± 0.1 μg L^{-1} (n=3). The concentration of As(III) was indeed the 30% of the total inorganic arsenic present in the sample.

As we stressed in the introduction, As(III) is the most toxic species of arsenic indeed it is important to develop a method capable to distinguish between the two species. This can be done with ASV method which is, in comparison with ICP-MS one, also less expensive and doesn't require special instrumentation.

2.3.9 Flow analysis of As(III)

NEEs have already been used in flow analysis by coupling them with a screen printed substrate (SPS) [50-52]. The difficulties in the assembly of this kind of electrode have been overtaken by designing a flow system where the auxiliary electrodes were placed opposite to the working electrode in the walls of a thin flow channel (see Fig 2.16 and 2.17).

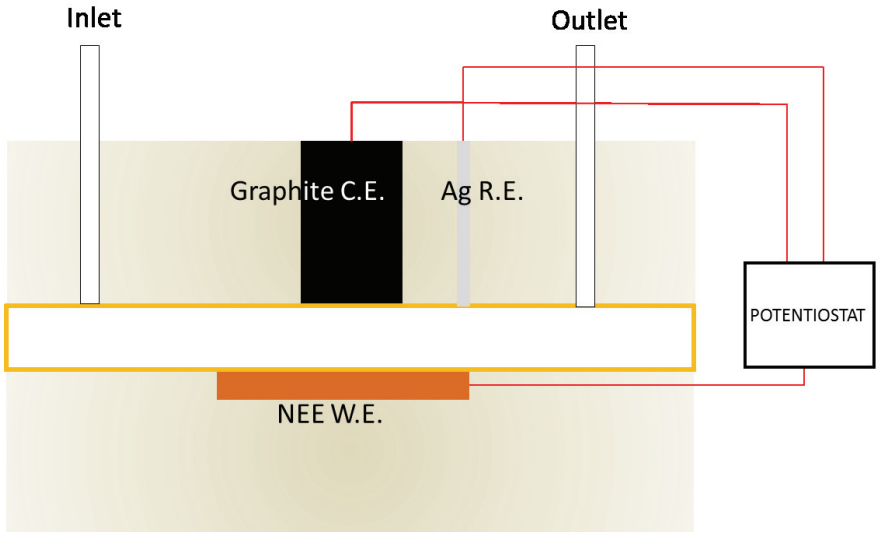

Figure 2.16. Scheme of the thin film flow cell (not in scale).

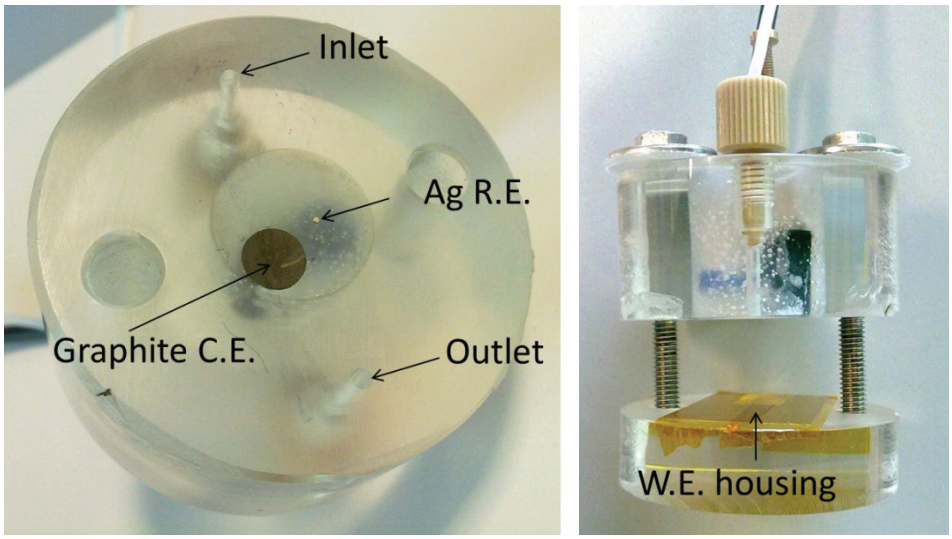

Figure 2.17. Photographs of the auxiliary electrodes (A) and of the whole flow cell (B).

Preliminary experiments were carried out in order to verify the actual behavior of this kind of configuration. In particular, ASV of As(III) has been performed by changing the deposition time and the flow rate. It is important to underline that the solution was continuously pumped

into the flow cell only during the deposition step, while the stripping step was carried out with quiet solution (after 15s of quite time).

The optimization of the analytical procedure was first performed in solution containing 1 mgL^{-1} As(III) and the stripping current was recorded at different flow rates, by keeping the deposition time constant at 180s. As shown by data in Figure 2.18, a maximum in the peak current was recorded at 0.5 mL/min. At higher rates, the flow is probably too high and As(III) is not efficiently deposited onto the working electrode.

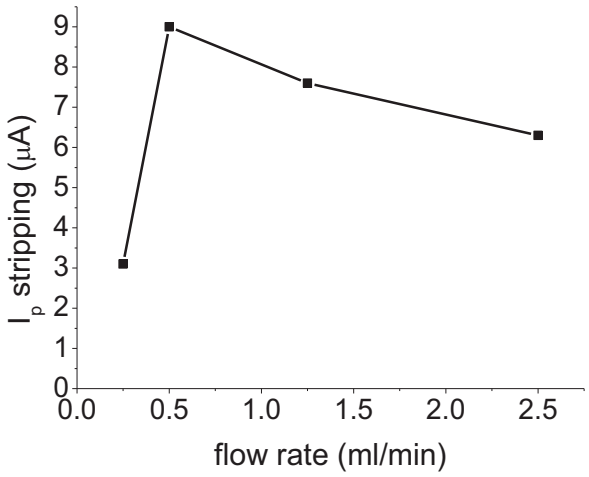

Figure 2.18. Effect of the flow rate on the stripping peak current in a solution containing 0.2 $molL^{-1}$ HCl, 62 mM hydrazine dihydrochloride and 1 mgL^{-1} of As(III). Other conditions as in Figure 2.3.

The effect of the deposition time on the peak current was also studied, while keeping fixed both flow rates (0.5 mL/min) and As(III) concentration. Data in Figure 2.19 indicate that the peak current increased with the deposition time. By the way, it is required a minimum of 2-3 minutes of deposition time to get a detectable signal.

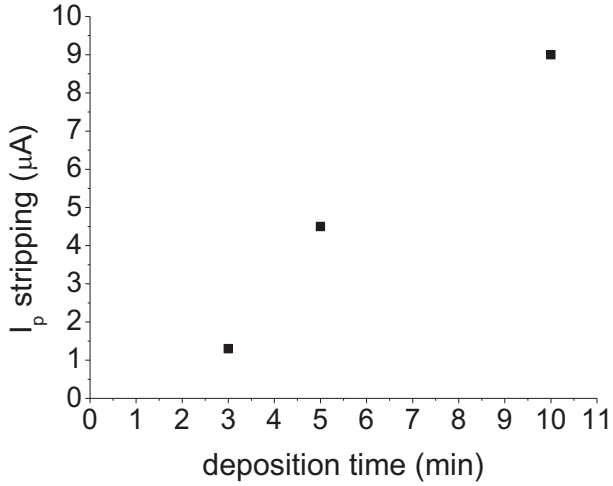

Figure 2.19. Effect of the deposition time on the stripping peak current in a solution containing 0.2 $molL^{-1}$ HCl, 62 mM hydrazine dihydrochloride and 1 mgL^{-1} of As(III). Other conditions as in Figure 2.3.

Flow cell coupled with NEEs can indeed represent a valid alternative to conventional cell configuration, displaying interesting characteristics when used for As(III) analysis, in particular with respect to the low volume required and the possibility to use the cell for on-site or even remote measurements.

By using other kind of material it would be possible to reduce the thickness of the flow cell and, indeed, the efficiency of the method. At the present state of research what is interesting is that we demonstrated the experimental possibility to exploit this kind of system for electroanalytical application; further refinements are obviously required in order to find application of the flow-analysis method.

2.4 Conclusions

In the present chapter we demonstrated that DLs for the determination of inorganic As with NEEs are significantly lower than those achieved with gold macroelectrodes and are competitive with respect to other nanostructured gold electrodes. With respect to other nanostructured gold electrodes, the surface of the NEEs is more controllable and reproducible, since the geometry of the nanoelectrodes is fully controlled by the geometry of the templating membrane. On the other hand, NEEs present a shorter dynamic range than the Au-macroelectrodes, therefore their use is advised especially for trace and ultratrace determinations, that is for concentrations < 10 μg/L. This agrees with the operativity of a surface saturation effect which is enhanced by the very small active area of the NEE. The choice of the appropriate supporting electrolyte minimizes the damage of the electrode surface and allows one to use an individual NEE for one complete analysis without suffering any deterioration problem. Anyway, considering the low cost of the electrodes (from one membrane of the cost of approximately 2 USD one can prepare 40 NEEs) their use as disposable electrodes is recommended. Experiments with NEEs in certified samples showed very good results supporting the practical applicability of these nanostructured electrodes for trace As analysis in natural water.

2.5. References

[1] B. K. Mandal, K. T. Suzuki, *Talanta*, 58 (2002) 201-235.

[2] L. Vega, M. Styblo, R. Petterson, W. Cullen, C. Wang, D. Germolec, *Toxicol. Appl. Pharmacol.*, 172 (2001) 225-232.

[3] W. Holak, *Anal. Chem.*, 41 (1969) 1712-1713.

[4] M. Belli, D. Centioli, P. d. Zorzi, U. Sansone, S. Capri, R. Pagnotta, M. Pettine , *Vol. Metodi Analitici per le Acque*, APAT & IRSA-CNR, Roma 2004, p. 3080.

[5] K. J. Stetzenbach, M. Amano, D. K. Kreamer, V. F. Hodge, *Ground Water*, 32 (1994) 976-985.

[6] E. H. Larsen, G. Pritzl, S. H. Hansen, *J. Anal. At. Spectrom.*, 8 (1993) 1075-1082.

[7] B. S. Sheppard, W. L. Shen, J. A. Caruso, D. T. Heitkemper, F. L. Fricke, *J. Anal. At. Spectrom.*, 5 (1990) 431-435.

[8] L. Meiters, *J. Am. Chem. Soc.*, 76 (1954) 5927.

[9] U. Greulach, G. Henze, *Anal. Chim. Acta*, 306 (1995) 217-223.

[10] A. Profumo, D. Merli, M. Pesavento, *Anal. Chim. Acta*, 539 (2005) 245-250.

[11] I. Svancara, K. Vytras, A. Bobrowsky, K. Kalcher, *Talanta*, 58 (2002) 45-55.

[12] X. Dai, O. Nekrassova, M. E. Hyde, R. G. Compton, *Anal. Chem.*, 76 (2004) 5924-5929.

[13] R. Feeney, S. P. Kounaves, *Anal. Chem.*, 72 (2000) 2222-2228.

[14] M. Khairy, D. K. Kampouris, R. O. Kadara, C. E. Banks, *Electroanalysis*, 22 (2010) 2496-2501.

[15] M. Hossain, M. Islam, S. Fersousi, T. Okajiama, T. Ohsaka, *Electroanalysis*, 20 (2008) 2435-2441.

[16] X. Dai, R. G. Compton, *Anal. Sci.*, 22 (2006) 567-570.

[17] F. C. Bodewig, P. Valenta, H.W. Nurnberg, *Fresenius Z. Anal. Chem.*, 331 (1982) 187-191.

[18] H. Huang, P. K. Dasgupta, *Anal. Chim. Acta*, 380 (1999) 27-37.

[19] C. M. Barra, M. M. Correia dos Santos, *Electroanalysis*, 13 (2001) 1098-1104.

[20] R. Feeney, S. P. Kounaves, *Talanta*, 58 (2002) 23-31.

[21] P. H. Davis, G. R. Dulude, R. M. Griffin, W. R. Matson, E.W. Zink, *Anal. Chem.*, 50 (1978) 137-143.

[22] S.W. Lee, J. C. Miranger, *Anal. Chem.*, 53 (1981) 130-131.

[23] R. I. Mrzljak, A. M. Bond, T. J. Cardwell, R. W. Cattrall, O. M. G. Newmann, B. R. Champion, *Analyst*, 119 (1994) 1051-1055.

[24] P. Ugo, L. M. Moretto, F. Vezzà, *ChemPhysChem*, 3 (2002) 917-925.

[25] V. P. Menon, C. R. Martin, *Anal. Chem.*, 67 (1995) 1920-1928.

[26] B. Brunetti, P. Ugo, L. M. Moretto, C. R. Martin, *J. Electroanal. Chem.*, 491 (2000) 166-174.

[27] S. Viswanathan, W.-C. Liao, C.-C. Huang, W.-L. Hsu, J. A. Ho, *Talanta*, 74 (2007) 229-234.

[28] P. Ugo, N. Pepe, L. M. Moretto, M. Battagliarin, *J. Electroanal. Chem.*, 560 (2003) 51-58.

[29] S. P. Mucelli, M. Zamuner, M. Tormen, G. Stanta, P. Ugo, *Biosens. Bioelectron.*, 23 (2008) 1900-1903.

[30] L. Cao, P. Yan, K. Sun, D. W. Kirk, *Electroanalysis*, 21 (2009) 1183-1188.

[31] F. C. Pereira, L. M. Moretto, M. D. Leo, M. V. B. Zanoni, P. Ugo, *Anal. Chim. Acta*, 575 (2006) 16-24.

[32] P. Ugo, L. M. Moretto, M. Silvestrini, F. C. Pereira, *Intern. J. Environ. Anal. Chem.*, 90 (2010) 747-759.

[33] B. K. Jena, C. R. Ray, *Anal. Chem.*, 80 (2008) 4836-4844.

[34] L. M. Moretto, N. Pepe, P. Ugo, *Talanta*, 62 (2003) 1055-1060.

[35] M. D. Leo, F. C. Pereira, L. M. Moretto, P. Scopece, S. Polizzi, P. Ugo, *Chem. Mater.*, 19 (2007) 5955-5964.

[36] P. Ugo, L. M. Moretto , *Handbook of Electrochemistry* (Ed: C. Zoski), Elsevier, Amsterdam 2007, ch. 16.2.

[37] M. Silvestrini, P. Schiavuta, P. Scopece, G. Pecchielan, L. M. Moretto, P. Ugo, *Electrochim. Acta*, 56 (2011) 7718-7724.

[38] S. Yu, N. Li, J. Wharton, C.R. Martin, *Nano Letters*, 3 (2003) 815-818.

[39] M. D. Leo, A. Kuhn, P. Ugo, *Electroanalysis*, 19 (2007) 227-236.

[40] K. Krishnamoorthy, C.G. Zosky, *Anal. Chem.*, 77 (2005) 5068-5071.

[41] M. Belli, D. Centioli, P. De Zorzi, U. Sansone, S. Capri, R. Pagnotta, M. Pettine, *Metodi Analitici per le acque*, APAT, Roma, 2004, pg 202.

[42] Y.-C. Sun, J. Mierzwa, M.-H. Yang, *Talanta*, 44 (1997) 1379-1387.

[43] G. Dugo, L. L. Pera, V. L. Turco, G. D. Bella, *Chemosphere*, 61 (2005) 1093-1101.

[44] M. Kopanica, L. Novotny, *Anal. Chim. Acta*, 368 (1998) 211-218.

[45] R. S. Sadana, *Anal. Chem.*, 55 (1983) 304-307.

[46] H. Li, R. B. Smart, *Anal. Chim. Acta*, 325 (1996) 25-32.

[47] R. Greef, R. Peat, L. M. Peter, D. Pletcher, J. Robinson, in *Instrumental Methods in Electrochemistry*, Ellis Horwood, Chichester 1985, ch. 6.

[48] K. Brainina, E. Neyman, in *Electroanalytical Stripping Methods*, Wiley, New York 1993, Ch. 1 and 2.

[49] X. Dai, R. G. Compton, *Electroanalysis*, 17 (2005) 1325-1330.

[50] S. Timur, L. Della Seta, N. Pazarlioglu, R. Pilloton, A. Telefoncu, *Proc. Biochem*., 29 (2004) 1325-1329

[51] MR. Montereali, W. Vastarella, L. Della Seta, R. Pilloton, *Int. J. Env. Anal. Chem.*, 85 (2005) 795-806.

[52] M. De Leo, *Nanoelectrode Ensemble for Electrochemical Sensing Purposes*, PhD Thesis, 2007, University of Venice.

Chapter 3:
Bismuth Modified NEE for the electroanalysis of Pb(II)

3.1 Introduction

Since lead is a toxic element whose maximum acceptable concentration in drinkable water was set by the World Health Organization to 10 μg L^{-1}, there is an increasing interest for novel, simple and reliable protocols and sensors for its determination. Among a variety of spectroscopic methods suitable for measuring trace concentrations of lead, electrochemical methods distinguish themselves for their high sensitivity and selectivity, low cost, applicability in colored, turbid as well as in high salinity water samples; moreover they are particularly suitable for on-site and decentralized analyses [1].

Concerning electrode materials, mercury has been widely used for stripping detection of trace heavy metal ions in general and for lead [2], in particular. However, due to the well-known toxicity of mercury, several alternative materials have been examined such as gold, silver, iridium, alloys, amalgams and various forms of carbon [3-5]. However, none of the above mentioned materials approached the attractive electroanalytical behavior of mercury, particularly with respect to its wide operational potential window and high overpotential for hydrogen evolution reaction. At the beginning of 2000, bismuth film electrodes (BiFEs) were introduced as an efficient replacement for mercury counterparts [6]. Bismuth electrode exhibits a cathodic part of the operational potential window very similar to that of mercury, with even superior performance in the presence of dissolved oxygen. Due to its non-toxic character and excellent electroanalytical performance, bismuth electrodes have been exploited for various electroanalytical applications [7-10].

Here, we combined the advantages of NEEs (which were discussed in Chapter 1 and 2) with those of bismuth film electrodes through modification of NEEs with bismuth films (Bi-NEE) prepared either via in-situ or ex-situ deposition protocol. These nanostructured bismuth modified electrodes were applied for the anodic stripping voltammetry of trace lead and their characteristics compared with those of bare gold NEEs and conventional Au-electrodes modified with bismuth film.

3.2. Experimental

3.2.1 Materials

NEEs were prepared using an electroless plating protocol and assembled using the procedure described in section 2.2.3.

. Standard solutions of Bi(III) and Pb(II) (1000 mg L^{-1}) were from Merck, and diluted as required with 0.01 M HCl.

3.2.2 Apparatus

All electrochemical measurements were carried out at room temperature (22°C) using a three electrodes single compartment electrochemical cell equipped with a platinum wire as the counter electrode and Ag/AgCl (KCl saturated) as the reference electrode. A CHI440 electrochemical workstation controlled via PC was used for all anodic stripping voltammetric (ASV) measurements.

3.2.3Procedures

ASV measurements were performed with both in-situ and ex-situ prepared Bi-NEEs in the absence of dissolved oxygen. For the in-situ protocol, the three electrodes were immersed into a 10 mL electrochemical cell containing 0.01 M HCl and, usually, 100 μg L^{-1} Bi(III). The accumulation potential of -1.1 V was applied to the working electrode in stirred solution for 120 s. The anodic stripping voltammogram was recorded by applying a positive-going square-wave voltammetric (SWV) scan up to +0.3 V with a frequency of 25 Hz, an amplitude of 50 mV and a potential step of 5 mV. Prior to the next measurement, a 90 s conditioning step at +0.5 V (while stirring) was employed to clean the substrate electrode surface.

The ex-situ preparation of bismuth film on the NEEs was carried out in 0.01 M HCl containing 1 mg L^{-1} Bi(III) at -1.1 V for 30 s, followed by ASV measurement in 0.01 M HCl solution containing the analyte. The anodic stripping voltammogram was recorded as for the in-situ procedure. Before each measurement, a cleaning step at -0.3 V for 60 s was performed.

3.3 Results and discussion

3.3.1 Optimization of the analytical parameters

After a set of preliminary experiments corroborating the successful deposition of Bi-films onto NEEs, we investigated the effect of Bi deposition on the AS-SWV detection of Pb with NEEs. These tests showed that, even if the reverse component of the SWV is almost flat, there is still advantage in using SWV instead of linear sweep voltammetry, thanks to the capability of the former to lower the background current, even with NEEs [11]. A frequency of 25 Hz gave a sufficiently high peak current, resolved well enough from the Bi stripping peak. Figure 3.1 compares the ASV signals after 15 s accumulation at -1.0 V at gold NEE in the absence (dashed line) and presence (solid line) of 1.0 mg L^{-1} Bi(III) in the solution. The dashed line in Fig. 3.1 shows that in the absence of Bi(III), the hydrogen evolution reaction results in a large increase of the background current at potential values more negative than -0.6 V. On the other hand, in the presence of Bi(III), the hydrogen evolution was shifted significantly towards more negative potential values, thus considerably widening the potential window accessible with NEEs. In the anodic region, a sharp oxidation peak is observed at -0.09 V that proves the extensive deposition of bismuth during the accumulation step [6]. This characteristic is similar to that observed under the same experimental conditions at the Au-macro electrode (not shown) with the main difference being the bismuth stripping peak, which was roughly one order of magnitude higher, as a consequence of a significantly larger surface of the Au-macro electrode.

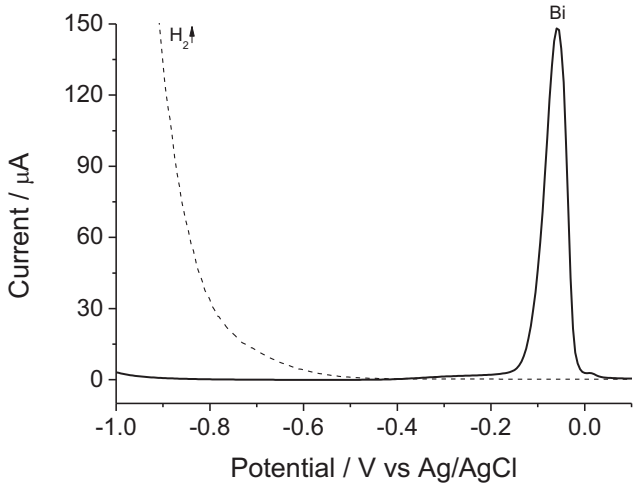

Figure 3.1. ASV at Au-NEEs with (solid line) and without (dashed line) 1 mg L^{-1} Bi(III) in 0.01 M HCl after deposition for 15 s.

Fig. 3.2 depicts ASVs recorded at the NEE, in the absence (dashed line) and presence (solid line) of 100 μg L^{-1} Bi(III) in 0.01 M HCl solution containing 20 μg L^{-1} Pb(II). Under these conditions, a well-defined stripping peak at -0.47 V can be observed for Pb(II) only when Bi(III) is present in the solution. When similar measurements were performed at the Au-macro electrode (Fig. 3.2, dotted line) in solution containing both Bi(III) and the analyte, significantly lower Pb responses were detected, confirming the effect of the nanoelectrode ensembles upon the signal enhancement.

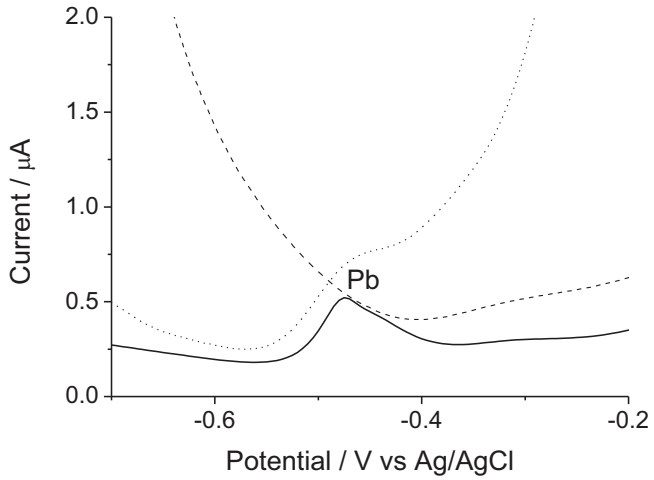

Figure 3.2. ASVs in 0.01 M HCl, 20 μg L^{-1} Pb(II) at the Au-macro with 1 mg L^{-1} Bi(III) (dotted line), at bare NEE (dashed line) and at the NEE with 100 μg L^{-1} Bi(III) (solid line) after deposition for 120 s. Accumulation potential: -1.0 V, frequency 25 Hz, amplitude 50 mV, potential step of 5 mV.

After these preliminary measurements, we examined several operational parameters affecting the performance of Bi-NEEs. The study was focused on the use of acidic media, in order to prevent the formation of insoluble metal hydroxides [12]. Different media such as nitric, perchloric, hydrochloric acid and acetate buffer solution (pH 4.5) were investigated. HCl solution provided the highest Pb stripping peak current and best reproducibility. Additional experiments performed in HCl in the concentration range of 0.001 - 0.1 M indicated that 0.01 M HCl exhibited the most favorable compromise between the acidity required for metal ions analysis and the interference caused by the hydrogen evolution reaction.

Because of their small active area, the surface of NEEs can be relatively quickly saturated, therefore the optimization of bismuth concentration in the measurement solution was of crucial importance. The highest stripping signal was observed with 0.1 mg L^{-1} bismuth, that is a bismuth concentration from one to two orders of magnitude lower than the concentration used in combination with classical GC electrodes [6]; this observation matches with the hypothesis of the saturation effect.

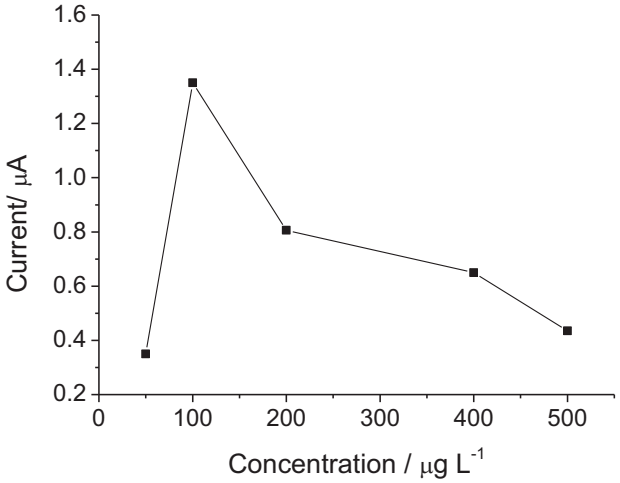

Figure 3.3. Effect of Bi(III) on the Pb(II) stripping peak. Deposition potential -1.0 V, deposition time 180 s, frequency 25 Hz, amplitude 50 mV, step potential 5 mV. Different bismuth concentration from 0.05 to 0.5 mg L^{-1} of Bi(III). Fix concentration of Pb(II) equals to 50 μg L^{-1}.

The optimization of the accumulation potential in the range from -1.3 to -0.8 V indicated that the optimal analytical response is recorded at -1.1 V, whereas at more negative potentials, the attenuation of the stripping signals could be observed as a consequence of the hydrogen evolution reaction.

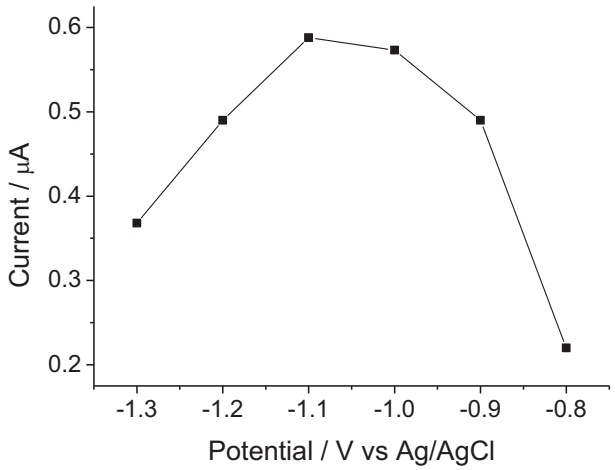

Figure 3.4. Effect of Deposition potential on the Pb(II) stripping peak. Deposition time 120 s, frequency 25 Hz, amplitude 50 mV, step potential 5 mV. Bismuth concentration equal to 0.1 mg L^{-1}. Fix concentration of Pb(II) equal to 40 μg L^{-1}.

3.3.2 Calibration plots

To provide more information on the electroanalytical performance of the Bi-NEEs, the in-situ and ex-situ Bi-film preparation protocols were compared. As shown in Fig. 3.5, the in-situ prepared Bi- NEE exhibits a good linear response with R^2 of 0.997 in the concentration range of 1-14 μg L^{-1} with 180 s accumulation. The calculated detection limit (3σ) was 0.06 μg L^{-1}, whereas repetitive measurements yielded a relative standard deviation of 7.10 % (30 μg L^{-1}, n = 8).

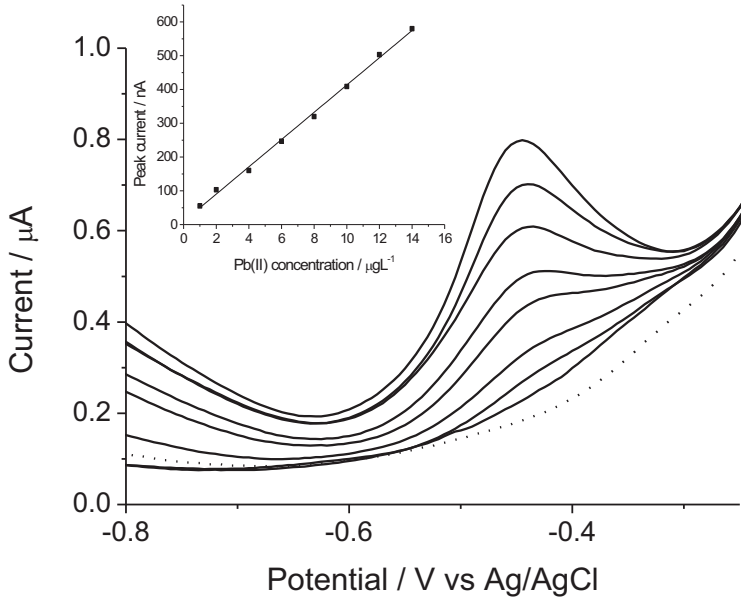

Figure 3.5. ASV recorded at the in-situ prepared Bi-NEE in 0.01 M HCl , 0.1 mg L^{-1} Bi(III) in the absence (dotted line) and presence of increasing concentrations of Pb(II), from 1 to 14 μg L^{-1} (full lines).(

Fig. 3.6 shows the ASVs (and corresponding calibration plot) for the ex-situ prepared Bi-NEE. This configuration unveiled electrochemical stripping characteristics similar to those of its in-situ counterpart, particularly concerning the stripping peak potential of Pb(II) and the hydrogen evolution overpotential. However, the electroanalytical performance of the ex-situ prepared Bi-NEE was markedly improved (R^2=0.999), in the concentration range 1-8 μg L^{-1} with a 180 s accumulation step. The calculated detection limit (3σ) was 0.03 μg L^{-1}, which is 4-times lower than the best limit previously achieved with Bi-films carbon electrodes [13].

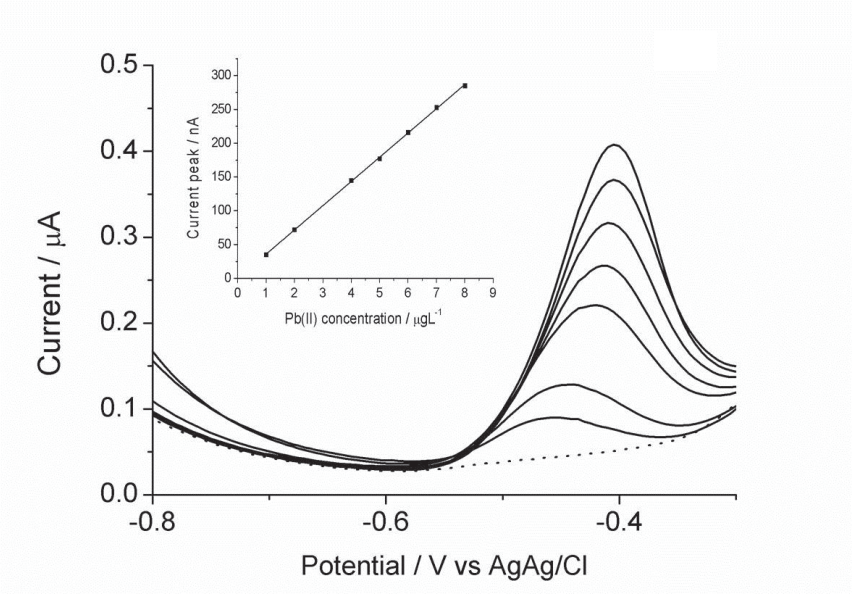

Figure 3.6. ASVs recorded at the ex-situ prepared Bi-NEE in 0.01 M HCl, in the absence (dotted line) and in the presence of increasing concentrations of Pb(II), from 1 to 8 μg L^{-1} (full lines). Deposition of Bi at -1.0V for 30 s. Insets: corresponding calibration plots. Other conditions as in Fig. 1.

A detailed analysis of the ASV revealed an interesting difference between the stripping patterns of the in-situ and ex-situ electrode configurations. For the ex-situ prepared Bi-NEE, the stripping peak potentials were shifted towards less negative potential values with increasing Pb(II) concentration; on the contrary, when employing the in-situ prepared configuration, the signal shifted towards more negative potentials when Pb(II) concentration was consecutively increased. This phenomenon can be explained with recently presented theoretical model suggesting different electrode mechanisms during the anodic stripping process, i.e. attractive forces between the deposited metal particles results in a positive shift of the stripping signal, whereas the opposite trend being observed in the case of repulsive forces [14]. The application of this model to the NEEs suggests that for the in-situ prepared Bi-NEE, i.e. when Bi and Pb are deposited together, repulsive forces are operative, while attractive forces rule the behavior of the ex-situ prepared Bi-NEE, i.e. when Pb is deposited over Bi.

3.4 Conclusion

We demonstrated that bismuth films can be readily deposited on the surface of gold NEEs, thus beneficially exploiting the inherent characteristics of NEEs and favorable stripping performance of bismuth film electrode. This modification allows sensitive detection of trace Pb(II) in combination with relatively short accumulation times. Preliminary studies based on the comparison between the in-situ and ex-situ preparation of the Bi- NEEs indicated that the latter approach yielded improved electroanalytical performances. The observed shifts of the stripping peaks associated with increasing the concentration of the analyte agrees with a theoretical model taking into account the role of interaction forces between the deposited metals.

3.5 References

[1] J. Wang, *Analytical Electrochemistry*, John Wiley & Sons, Inc., 2006.

[2] T.M. Florence, *J. Electroanal. Chem.*, 27 (1970) 273-281.

[3] M.A. Nolan, S.P. Kounaves, *Anal. Chem.*, 71 (1999) 3567-3573.

[4] Ø. Mikkelsen, S. M. Skogvold, K. H. Schrøder, M. I. Gjerde, T. A. Aarhaug, *Anal. Bioanal. Chem.*, 377 (2003) 322-326.

[5] I. Švancara, M. Matoušek, E. Sikora, K. Schachl, K. Kalcher, K. Vytřas, *Electroanalysis*, 9 (1997) 827-833.

[6] J. Wang, J. Lu, S.B. Hocevar, P.A.M. Farias and B. Ogorevc, *Anal. Chem.*, 72 (2000) 3218-3222.

[7] E.A. Hutton, S.B. Hočevar, L. Mauko and B. Ogorevc, *Anal. Chim. Acta*, 580 (2006) 244-250.

[8] E.A. Hutton, S.B. Hočevar, B. Ogorevc and M.R. Smyth, *Electrochem. Commun.*, 5 (2003) 765-769.

[9] A. Krolicka, A. Bobrowski, *Electrochem. Commun.*, 6 (2004) 99-104.

[10] A. Krolicka, R. Pauliukaite, I. Svancara, R. Metelka, A. Bobrowski, E. Norkus, K.

[11] L. M. Moretto, N. Pepe and P. Ugo, *Talanta*, 62 (2004) 1055-1060.

[12] A. Economou, *TrAC Trends Anal. Chem.*, 24 (2005) 334-340.

[13] G.-H. Hwang, W.-K. Han, S.-J. Hong, J.-S. Park and S.-G. Kang, *Talanta*, 77 (2009) 1432-1436.

[14] V. Mirceski, S.B. Hocevar, B. Ogorevc, R. Gulaboski and I. Drangov, *Anal. Chem.*, 84 (2012) 4429-4436.

Chapter 4:
Simultaneous cathodic stripping determination of Nickel(II) and Cobalt(II) at in-situ prepared bismuth modified gold electrodes

4.1 Introduction

The power and scope of electrochemical stripping analysis have been greatly enhanced during the past decades owing to the introduction of novel electrode materials and associated procedures [1]. The unique accumulation of the metal analytes relies on the efficient formation of the amalgams/alloys in/on the surface of the working electrode. When the analyte reacts irreversibly or forms intermetallic compounds or cannot form an amalgam/alloy, the adsorptive stripping protocols can be an interesting approach [2,3]. The adsorptive stripping procedures commonly rely on the interfacial accumulation of target metal complexes onto a mercury drop or mercury film electrode, thus a large variety of metal analytes such as vanadium [4], chromium [5,6], molybdenum [7], aluminum [8], nickel, cobalt [9], etc. can be successfully determined. Despite mercury's attractive electroanalytical performance, there is a growing demand to replace mercury with alternative, non-toxic and "environmentally friendly" electrode materials. As we discussed in Chapter 3, this alternative can be represented by bismuth film electrodes.

Electrochemical methods for measuring nickel(II) and cobalt(II) with bismuth-modified electrodes have been proposed in the last decade [10,11]. The majority of these studies were performed using the ex-situ prepared bismuth film electrode with the bismuth deposited usually onto different carbon substrates [12-14]. Alves et al. proposed a solid bismuth vibrating electrode for the determination of Ni(II) and Co(II) [15].

Only few papers report on the application of bismuth-modified gold electrodes for anodic (or adsorptive / cathodic) stripping voltammetry / potentiometry [16-21].

With the goal of developing electrodes suitable for multiple analysis of water pollutants, we focus here on gold substrate as a widespread material which display valuable performances both for the anodic stripping analysis of toxic metal ions such as arsenic (III) [22-24], copper [23] and mercury (II) [25] and for the cathodic stripping determination of other water pollutants such as nickel (II) and cobalt (II). In principle, the same gold substrate could be

used as a bare electrode for the anodic determination of the first three above analytes, while after the modification of Au with bismuth, one could perform the simultaneous determination also of Ni(II) and Co(II).

Recently, M. Korolczuk et al. [26,27], and Sopha et al. [28] proposed the use of in-situ prepared BiFE and antimony film electrode (SbFE) for measuring solely nickel ions. The only example of simultaneous determination of nickel and cobalt was reported by Korolczuk et al. using an in-situ prepared lead film electrode (PbFE) [29], but also lead is toxic.

The above considerations prompted us to study and apply to water analyses an electrochemical method suitable for the simultaneous determination of nickel(II) and cobalt(II), using the in-situ prepared bismuth-modified gold electrode (Bi-AuE) as a substitute for the Hg electrode used previously for similar purposes [30]. Compared to the ex-situ preparation procedure, the proposed in-situ strategy provides simplified, faster and yet sensitive and reliable operation together with fresh electrode surface for each consecutive measurement. This protocol also obviates the need of using bromide, which is in certain cases necessary to stabilize the ex-situ prepared bismuth film [31]. The very sensitive method developed was successfully validated also in real samples, namely water samples from the lagoon of Venice, by comparing the results obtained electrochemically with the Bi-AuE with those obtained by ICP-MS and ICP-OES analyses, which require more expensive instrumentation and are not suitable for direct on-field testing or decentralized monitoring.

4.2. Experimental

4.2.1. Reagents and materials

The working electrode was a conventional Au-disc electrode embedded in Teflon with geometric area of 0.07 cm^2. Standard solutions of Bi(III), Ni(II) and Co(II) (1000 mg L^{-1}) were provided by Merck and diluted as required with 0.01 mol L^{-1} HCl. Other standard solutions (ICP-MS standards of Zn(II), Al(II), Cr(III), Fe(III), Cu(II)) were also purchased from Merck and diluted with HCl to pH 2. 0.1 mol L^{-1} ammonia buffer (pH 9.0) was prepared from analytical grade reagents, Sigma Aldrich. 1 mol L^{-1} potassium sodium tartrate and 0.01 mol L^{-1} DMG were prepared from the reagents obtained from Sigma.

NIST 1640a certified reference standard was provided by the National Institute of Standards & Technology of United States. It consists of spring water acidified with 2% HNO_3 with mass fractions and mass concentrations assigned for 22 elements. The certified concentration of Ni(II) is 27.4 ± 0.8 μg L^{-1} and of Co(II) is 20.1 ± 0.3 μg L^{-1}.

4.2.2. Apparatus

All adsorptive cathodic stripping voltammetric (AdCSV) measurements were carried out using a CHI440 electrochemical workstation at room temperature (22°C). A classical 20 mL 3-electrodes single compartment electrochemical cell equipped with a bismuth-modified gold electrode as the working electrode, a platinum wire as the counter electrode and an Ag/AgCl (KCl sat.) reference electrode was used. The gold electrode was polished daily using 0.3 μm alumina slurry. Morphological information of the electrode surface were achieved with a VEGA TS 5130 LM (Tescan) Scanning Electron Microscope. For comparison, real sample investigations were carried out using a quadrupole ICP-MS instrument Agilent 7500ce (Agilent Technologies) and an Optima 2100 DV (Perkin Elmer) ICP-OES.

4.2.3. Procedures

The working electrode was dipped into a 0.1 mol L^{-1} ammonium buffer solution containing 10 mg L^{-1} Bi(III) in the form of its complex with tartrate and 1 x 10^{-5} mol L^{-1} dimethylglyoxyme (DMG) as complexing agent. Tartrate was selected in order to avoid the precipitation of bismuth at the pH value necessary for Ni(II) and Co(II) determination [27]. A two-step accumulation protocol, i.e. (i) -1.1 V for 60 s (in-situ deposition of bismuth) followed by (ii) -0.8 V for 120 s (accumulation of Ni-DMG and/or Co-DMG complexes), was applied under stirring conditions. After the accumulation step, stirring was stopped and following a 15 s equilibration period, a stripping square-wave voltammogram was recorded from -0.8 V to -1.3 V, with a frequency of 25 Hz, a potential step of 5 mV and amplitude of 50 mV. After each measurement a cleaning step was applied by holding the potential at +0.3 V for 60 s.

4.3 Results and discussion

4.3.1 Morphological characterization of the in-situ prepared bismuth-modified gold electrode

Aimed at obtaining insights into the morphology of bismuth deposits on a gold substrate, scanning electron microscopy (SEM) study was carried out before and after the electrochemical deposition of bismuth. Figures 4.1A and 4.1B show SEM images of a bare gold electrode surface after its immersion for 5 minutes in 0.1 mol L^{-1} ammonium buffer

solution containing 0.01 mol L^{-1} tartrate ions. The star-like structures visible on the gold electrode surface with a regular distribution are consistent with tartrate crystals, as confirmed also by the literature [32]. Figures 4.1C and 4.1D show the same gold electrode surface after 60 s electrochemical deposition of bismuth at -1.1 V from a 0.1 mol L^{-1} ammonium buffer solution containing 0.01 mol L^{-1} tartrate and 10 mg L^{-1} Bi(III). The images clearly depict the formation of bismuth micro-crystals aggregated in rosettes indicating that these micro-crystals are formed on the surface of the gold electrode instead of a bulk deposit. These results are similar to those obtained with a deposition from an acidic solution using carbon substrate [33,34]. Note that the structure of the tartrate crystals is still detectable in Figures 4.1C and 4.1D, although with a lower contrast.

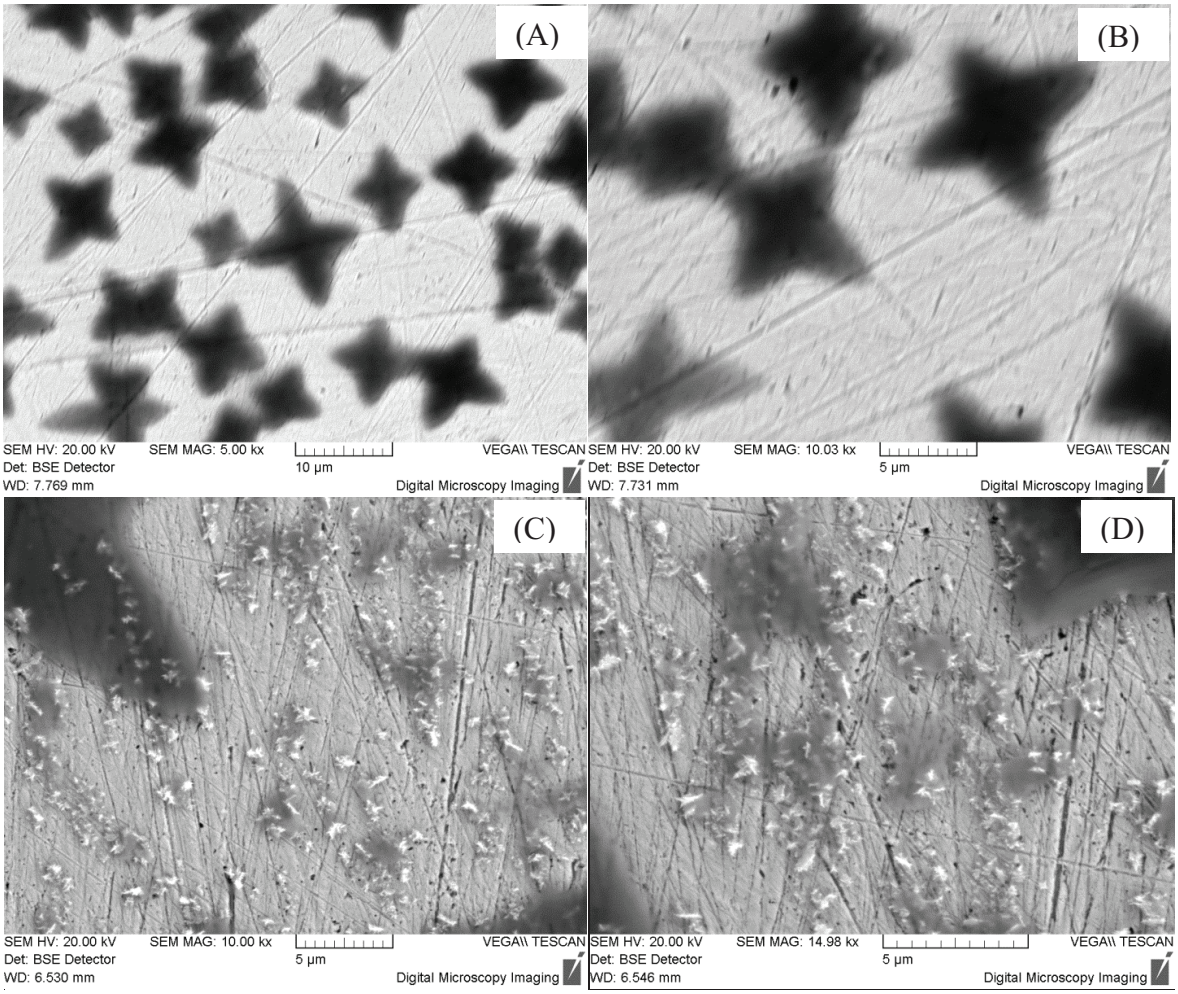

Figure 4.1. A and B: SEM images of the gold elecrode surface after 5 minutes dipping in 0.1 mol L^{-1} ammonium buffer and 0.01 mol L^{-1} tartrate solution. C and D: the same gold electrode surface after 60 s electro-deposition of bismuth from the 0.1 mol L^{-1} ammonium buffer solution containing 0.01 mol L^{-1} tartrate and 10 mg L^{-1} Bi(III) applying a negative potential of -1.1V.

4.3.2 Optimization of the experimental procedure

As proposed by F. Ma et al. [35], the mechanism for the adsorption and cathodic stripping voltammetry of M(II)-DMG_2 (M^{2+} is either Ni^{2+} or Co^{2+}) complexes can be explained as:

$$M(II)\text{-}DMG_2\ (solution) \rightarrow M(II)\text{-}DMG_2\ (ads) \qquad (4.1)$$

After adsorption on the electrode surface

the application of cathodic potential scan brings to the reduction of the metal complex schematically represented by the equation (4.2):

$$M(II)\text{-}DMG_2\ (ads) + ne^- \rightarrow M(II)\text{-}DMG_2^{n-} \qquad (4.2)$$

In reaction (4.2), both the metal ion and complex are reduced. The first step is the reduction of the central metal

$$M(II)\text{-}DMG_2(ads) + 2e^- \rightarrow M(0) + 2\ DMG^-\ (ads) \qquad (4.3)$$

followed by a four electron reduction of the glyoximate ligand:

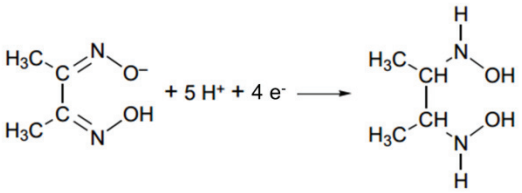

(4.4)

The resulting reduction peak, which describes both the cathodic reactions (4.3) and (4.4), gives a 10 electron transfer: 2 electrons for the metal ion and 4 electrons for each one of the two ligands. The typical AdCSV for the Ni complex is shown in Figure 4.2, that is characterized by a sharp peak at – 0.950 V.

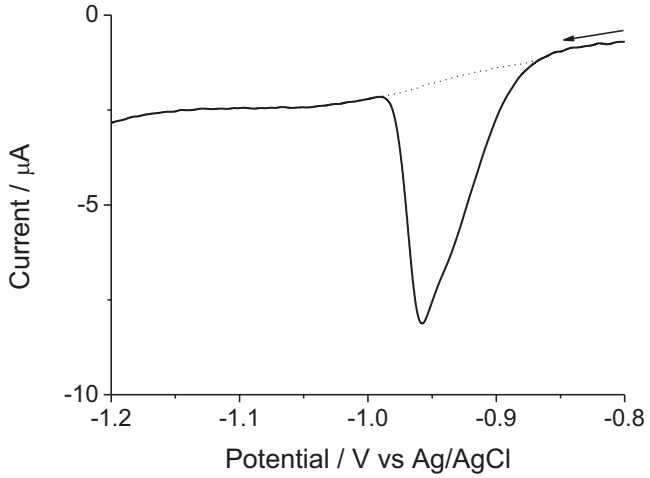

Figure 4.2. AdSV of the in-situ prepared Bi-AuE in 0.1 mol L^{-1} ammonia buffer solution (pH = 9.0) containing 10 mg L^{-1} Bi(III), 1×10^{-5} mol L^{-1} DMG and 0.01 mol L^{-1} potassium sodium tartrate in the presence (solid line) and absence (dotted line) of 50 μg L^{-1} Ni(II). Deposition at −1.1 V for 60 s followed by accumulation at −0.8 V for 60 s; equilibration time of 15 s; SWV parameters: frequency 25 Hz, potential step 5 mV and amplitude 50 mV.

To optimize the electroanalytical performance of the proposed sensor, the operational parameters such as the in-situ bismuth deposition (the first step), the accumulation time (the second step) and the accumulation potential (the second step), were examined.

The optimization of the first step was carried out at fixed deposition time of 60 s and deposition potential of -1.1 V. During this step Bi was deposited on the gold electrode surface, whereas Ni(II)-DMG complex, which was also present in the solution, was not adsorbed, since the adsorption occurs at potentials between ca. -0.8 and -0.6 V and the adsorbed complex is reduced at ca. -0.95 V. The concentration of Bi(III) in the measurement solution was changed in the range of 1 to 20 mg L^{-1}, and its effect upon the Ni(II) stripping signal is shown in Figure 4.3. Evidently, the stripping peak current increased by increasing the concentration of Bi(III) from 5 mg L^{-1} and reached a constant value when the Bi(III) concentration was ≥ 10 μg L^{-1}. The increase of the signal can be attributed to the higher bismuth film surface area accessible for electrochemical adsorption of Ni(II)-DMG complex, until reaching a plateau, which indicates the achievement of the maximum surface coverage by the adsorbed nickel complex. It is important to note that at Bi(III) concentrations lower than 5 mg L^{-1} no Ni(II) signal was recorded; this fact can be explained also by considering the enhanced hydrogen evolution reaction at the surface of a gold substrate electrode. Indeed, it has been already demonstrated that the hydrogen evolution contributes to a large increase of the background current in the case of gold electrodes at potential values more negative than -

0.6 V [18]. Finally, by performing 20 independent determinations with Bi(III) concentrations of 10, 15, and 20 mg L^{-1}, the relative standard deviation (RSD) values were 2.2, 5.5 and 6.0 %, respectively. This prompted us to use 10 mg L^{-1} Bi(III), as the most suitable concentration in all further experiments.

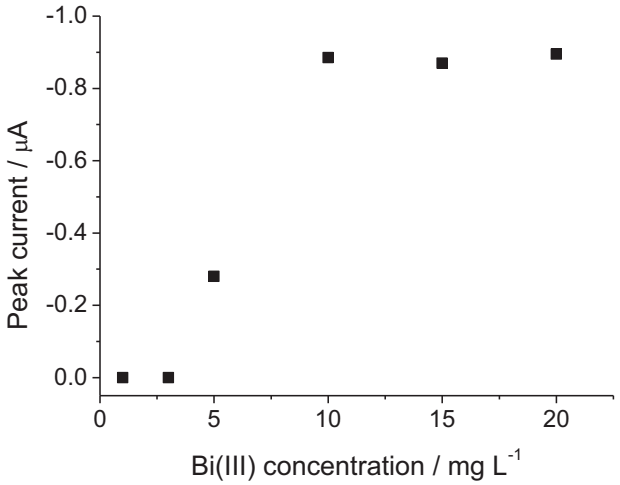

Figure 4.3. Effect of Bi(III) concentration on the Ni(II) peak current. Concentration of Ni(II): 5 μg L^{-1}, accumulation time: 60 s. Other conditions as in Figure 4.2.

Figure 4.4 shows the effect of the accumulation potential of Ni-DMG on the Ni(II) stripping peak between -0.5 and -0.85 V. From the analysis of this figure it is evident that the highest signal is observed between -0.7 and -0.8 V. At more negative accumulation potential the signal decreased due to reduction of the Ni(II)-DMG complex. For all further studies the accumulation potential of -0.8 V was chosen.

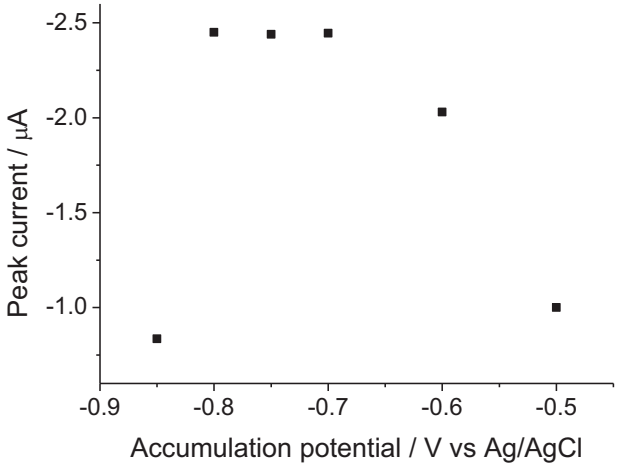

Figure 4.4. Effect of the accumulation potential on Ni(II) peak current. Concentration of Ni(II) and Bi(III): 10 μg L^{-1} and 10 mg L^{-1}, respectively and accumulation time: 60 s. Other conditions as in Figure 4.2.

Figure 4.5 depicts the dependence of the Ni(II) peak current upon the accumulation time for two concentrations of Ni(II), i.e. for 5 (full circles) and 50 (hollow circles) μg L^{-1} in the range of 30 to 450 s. In the case of 5 μg L^{-1} the signal increased linearly with the accumulation time and no saturation effect was observed. When Ni(II) concentration was 50 μg L^{-1} the stripping signal increased linearly up to 300 s and then it leveled off. Accordingly, an accumulation time of 120 s was selected as the optimal compromise between high sensitivity and short analysis time. However, for measuring more concentrated samples it is obvious that shorter accumulation times could be used.

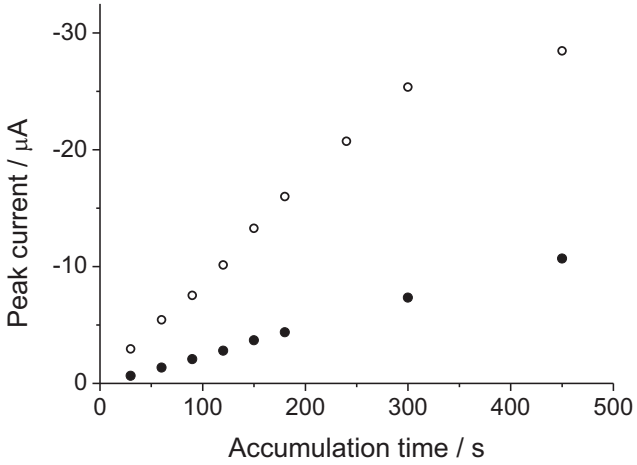

Figure 4.5. Effect of the accumulation time on Ni(II) peak current. Concentration of Ni(II): 5 μg L^{-1} (full circles) and 50 μg L^{-1} (hollow circles), Bi(III) concentration: 10 mgL^{-1}, deposition time 60 s and potential -1.1 V. Other conditions as in Figure 4.2.

4.3.3 Calibration

The electroanalytical performance of the bismuth modified gold electrode was further studied while increasing the concentration of Ni(II) in the range of 0.5 to 15.0 μg L^{-1}, as shown in Figure 4.6 and in the inset. The optimized concentration of Bi(III), as describred in the previous paragraph, was 10 mg L^{-1}. The electrode revealed a good linear behavior in the examined concentration range in combination with 120 s accumulation time, being the stripping signals surrounded by low background contribution. The detection limit (DL) was calculated by using the 3σ/m criterion; the σ value was calculated with two methods: (i) by using the standard deviation of the calibration plot, and (ii) by obtaining it from the standard

deviation of repeated measurements performed at low Ni(II) concentration, namely, 10 measurements at 0.5 μg L^{-1}, with 120 s accumulation time. In both cases the DL of 40 ng L^{-1} was calculated which is the lowest value compared with other electroanalytical methods reported in the literature [10-14]. This very favourable sensing capability, attributed also to a 10-electron transfer process [35], is associated with excellent reproducibility with relative standard deviation (RSD) of 2.2 % based on 20 consecutive measurements of 0.5 μg L^{-1} Ni(II).

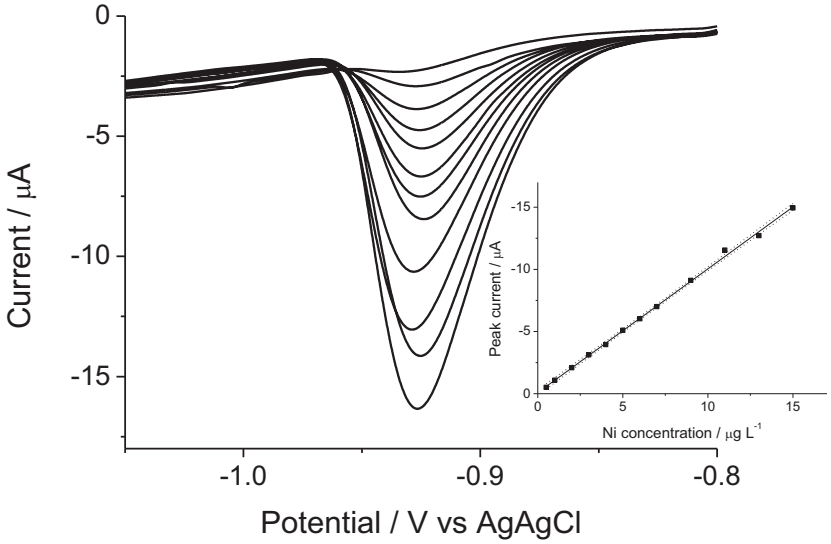

Figure 4.6. AdSVs of the in-situ prepared Bi-AuE for increasing concentration of Ni(II) in the range of 0.5 – 15 μg L^{-1} in 0.1 mol L^{-1} ammonia buffer solution (pH = 9.0) containing 10 mg L^{-1} Bi(III), 1×10^{-5} mol L^{-1} DMG and 0.01 mol L^{-1} potassium sodium tartrate. Deposition at −1.1 V for 60 s followed by accumulation at −0.8 V for 120 s; equilibration time of 15 s; SWV parameters: frequency 25 Hz, potential step 5 mV and amplitude 50 mV. Inset: corresponding calibration plot with relevant confidence band (95%).

4.3.4 Simultaneous analysis of Ni(II) and Co(II)

A common problem associated with the electrochemical determination of Ni(II) is the partial overlap of the Ni(II) peak with that of Co(II), which is also complexed by DMG [10,11]. In the literature, several papers report on the analysis of Ni(II) with bismuth-based electrodes, but only few of them describe the simultaneous determination of both trace Ni(II) and Co(II) [9-11]. Figure 4.7 shows the AdCSVs recorded at the Bi-AuE in 0.1 mol L^{-1} ammonia buffer solution containing 0.01 mol L^{-1} sodium potassium tartrate, 10 mg L^{-1} Bi(III) and 1 x 10^{-5} mol L^{-1} DMG spiked with increasing amounts of Ni(II) and Co(II). As can be seen in this figure, the stripping signals of both the analytes furnish two well-resolved stripping peaks centered around -0.940 V and -1.030 V for Ni and Co, respectivelly. The peak at -0.950 V increased linearly when the concentration of Ni(II) was increased from 5 to 35.0 μg L^{-1} while the peak at -1.030 V scaled with Co(II) concentration in the range 10 - 55 μgL^{-1} (see the corresponding inset). The calculated DLs (3σ/m) were 97 and 58 ng L^{-1} for Ni(II) and Co(II), respectively.
These results are also reported in Table 4.1 in order to compare the performances here obtained with the ones obtained in other previous works with bismuth modified electrodes. The comparison highlights that the proposed methodology give one of the best results in the simplest way.

Table 4.1. Adsorptive stripping voltammetric (AdSV) determination of Ni and Co at various bismuth electrodes with related LoD and type of samples analysed.

Working Electrode	Surface modification strategy	LoDNi(II) (μg/L)	LoD Co(II) (μg/L)	Deposition Time (s)	Real samples	Ref.
solid bismuth vibrating electrode	No modification	0.6	1.0	30	Certified surface water	[15]
BiF on GC microelectrode	Ex-situ with NaBr usage	0.06	0.07	60	Body fluid samples	[10]
BiF on GC microelectrode	Ex-situ with NaBr usage	0.09	0.07	120	No real samples	[31]
BiF on rotating GC electrode	Ex-situ	0.1	0.07	300	River water and iron ore	[36]
BiF on GC electrode	Ex-situ	0.26	0.08	60	No real samples	[11]
Bi microparticles on gold electrode	In situ	0.06	0.1	120	Certified spring water and lagoon water	Present work

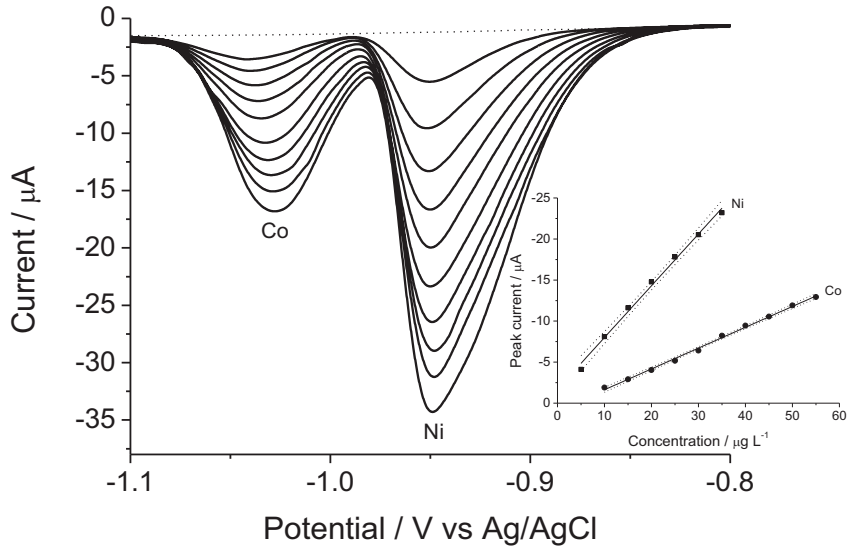

Figure 4.7. AdSVs obtained at the in-situ prepared Bi-AuE for increasing concentrations of Ni(II) and Co(II). Bi deposition at −1.1 V for 60 s followed by complex accumulation for 120 s at −0.8 V; equilibration time of 15 s. Inset shows corresponding calibration plots with relevant confidence bands (95%). Other conditions as in Fig. 4.2.

Nickel was also successfully measured in a solution containing fixed amount of Co(II) as a possible interference. Figure 4.8 shows the AdCSVs recorded in solution spiked with increasing amounts of Ni(II), whereas the concentration of Co(II) was kept unchanged, i.e. 20 μg L^{-1}. The obtained stripping voltammograms indicate that Co(II) does not interfere with neighboring signal of Ni(II), thus it was possible to measure trace concentrations of Ni(II) also in the presence of a 20 fold excess of Co(II), i.e. from 1 to 6 μg L^{-1} the Ni(II) peak current increased linearly with increasing nickel concentration. In this case, the calculated DL for Ni(II) ($3\sigma/m$) was 77 ng L^{-1}.

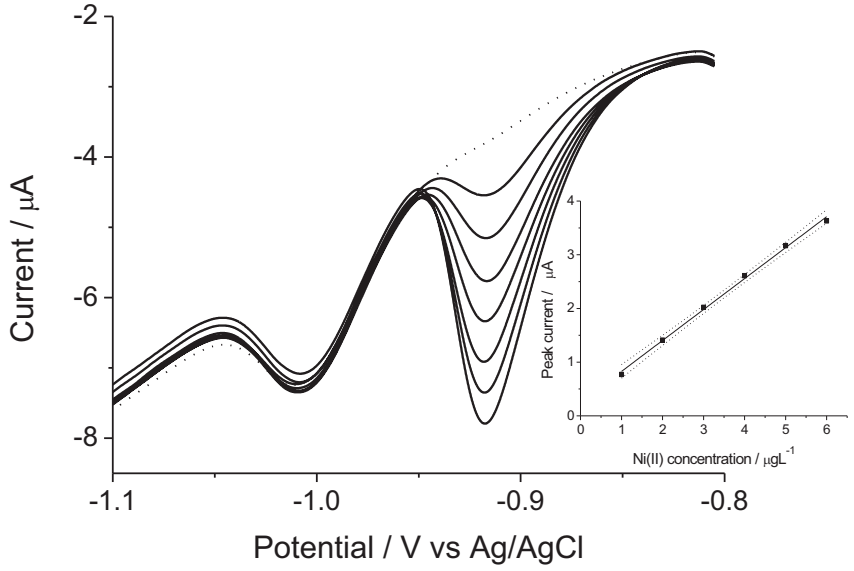

Figure 4.8. AdSVs obtained at the in-situ prepared Bi-AuE for increasing concentrations of Ni(II) from 0 (dotted line) to 6 μg L^{-1} (full lines) in 0.1 mol L^{-1} ammonia buffer solution (pH = 9.0) containing 0.01 mol L^{-1} sodium potassium tartrate, 1×10^{-5} mol L^{-1} DMG, 10 mg L^{-1} Bi(III), and 20 μg L^{-1} Co(II). Deposition of Bi at −1.1 V for 60 s followed by accumulation at −0.8 V for 120 s; equilibration time of 15 s. Inset shows calibration plot and relevant confidence band (95%). Other conditions as in Fig. 4.2.

4.3.5 Interferences on Ni determination

The possible effect of selected metal ions in solution containing 4 μgL^{-1} Ni(II) in combination with 60 s accumulation time was studied and the influence upon the Ni(II) peak current is presented in Table 4.2. The results indicate that Zn and Cr excess cause negligible effects and that Fe, Al and Cu cause an approximately 20% change in the Ni stripping current only when present in 500-fold excess. As far as Co(II) is concerned, a 10 fold excess is un-influent while a 50-fold excess reflects in a 50 % decrease in sensitivity. Note that the main reason behind this decrease in sensitivity for Ni(II) is related to a partial overlap of the two adsorptive stripping peaks; however, the quantitative determination of nickel can be anyhow performed by using the standard additions method. Finally, also the effect of the surfactant Triton-X on the Ni(II) stripping signal was examined; it was observed that the peak of Ni(II) decreased to 26 % of its original value when 1 mg L^{-1} of surfactant was present in the measurement solution.

Interferent	Weight excess	Relative signal*
Zn(II)	100	1.00
	500	1.02
Fe(III)	100	1.11
	500	1.22
Al(III)	100	0.89
	500	0.79
Cu(II)	100	0.99
	500	0.77
Cr(III)	100	1.09
	500	1.03
Co(II)	10	1.00
	50	0.49
Triton X-100	25	1.07
	250	0.26

*Relative signal is the ratio between the Ni peak before and after the addition of the foreign ion.

Table 4.2. The relative signals obtained for 4 μgL^{-1} Ni(II) in the presence of interfering ions or molecule. Deposition of Bi at −1.1 V for 60 s followed by accumulation at −0.8 V for 60 s; equilibration time of 15 s. Other conditions as in Figure 3.2.

4.3.6 Analysis of certified reference material

The proposed Bi-AuE was tested for measuring Ni(II) and Co(II) in NIST 1640a certified reference material. 1 mL of NIST 1640a was diluted 1 : 10 with 0.1 mol L^{-1} ammonium buffer solution, containing 0.01 mol L^{-1} sodium potassium tartrate, 1 x 10^{-5} mol L^{-1} DMG, and 10 mg L^{-1} Bi(III). The AdCSVs were characterized by two stripping signals with peak potentials at ca. -0.9 and -1.0 V, which increased linearly with the additions of both Ni(II) and Co(II). The sample concentrations calculated by extrapolation of the calibration plots is shown in Figure 4.9 and considering the dilution factor were 27.4 ± 0.5 μg L^{-1} for Ni(II) and 18.1 ± 0.6 μg L^{-1} for Co(II). These values are in satisfactory agreement with the values of 27.4 ± 0.8 μg L^{-1} and 20.3 ± 0.3 μg L^{-1} certified for this reference material.

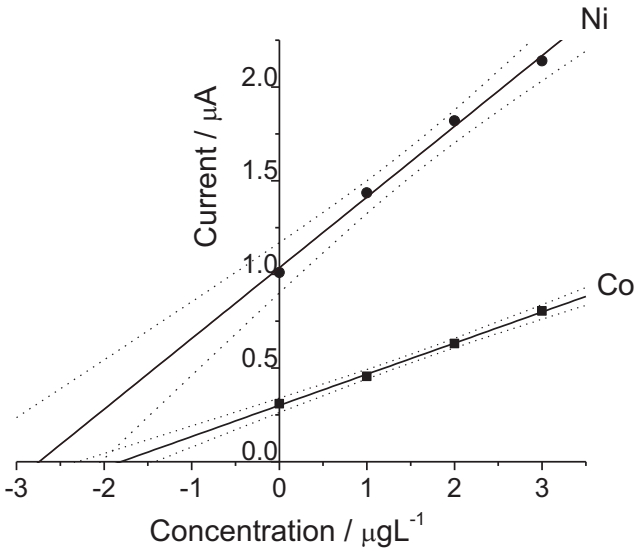

Figure 4.9. Standard addition plots and relevant confidence bands (95%) obtained at Bi-AuE for NIST 1640a certified reference sample diluted 1 : 10. Other conditions as in Figure 4.2.

4.3.7 Real samples analysis.

Sea water sample

The procedure optimized in the previous paragraphs, was applied to the measurement of Ni(II) concentration in lagoon water sample. The sample was collected in the Venice lagoon basin, in the area close to the Murano island. After sampling, the water was filtered (0.45 μm) and acidified with nitric acid (pH 2.0), following the standard procedure used for heavy metal analysis in water [37]. Before the analysis the sample was stored at 4°C. The baseline (dashed line in Figure 3.10) was recorded in order to verify the cleaness of glassware and purity of the reagents. 5 mL of sample were diluted with 15 mL of 0.1 mol L^{-1} ammonia buffer solution pH 9.0 (this dilution is necessary to keep the analysis medium at pH 9.0) and after an accumulation time of 240 s a cathodic peak current was recorded aproximatelly at -0.94 V. The concentration in the real sample was calculated with the standard addition method (3 additions of 0.3 μg L^{-1} of Ni(II) each). The insert of Figure 4.10, shows that a satisfactory linear response was achived with a correlation coefficient of R^2 0.998 and the correspondingly Ni(II) concentration in the sample resulted 0.41 ± 0.17 μg L^{-1} (n=3).

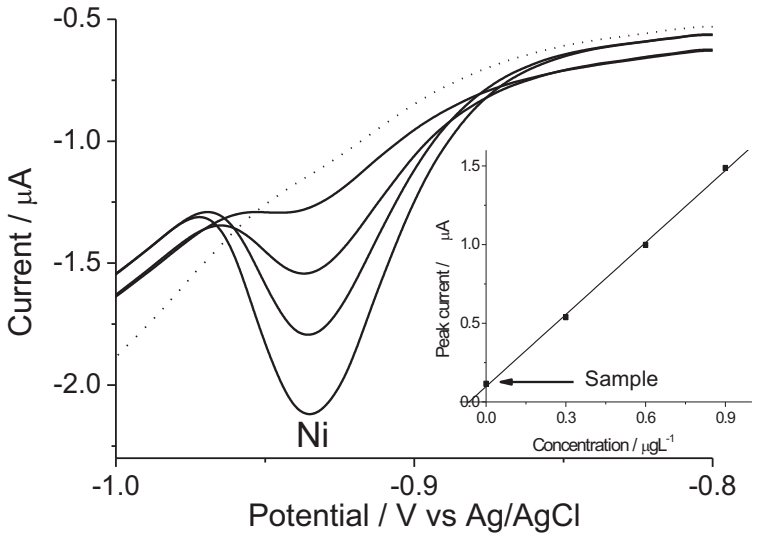

Figure 4.10. AdCSV for measuring Lagoon water sample via standard addition protocol. Conditions: -1.1 V for 60s, -0.8 V for 240 s. Other conditions as in Figure 3.2.

The same sample was analysed with both ICP-OES and ICP-MS in order to confirm the results obtained with the electrochemical method proposed, as well as to compare it with different techniques. With ICP-OES it was not possible to calculate the concentration of Ni(II) because it was lower than the detection limit achievable with the technique. With ICP-MS a Ni(II) concentration of 0.33 ± 0.01 μg L^{-1} (n=8) was measured, that is in good agreement with the electrochemical analysis. The ICP-MS yielded also a concentration of Co(II) equal to 0.63 ± 0.01 μg L^{-1} (n=8). Considering the dilution needed to the electrochemical analysis this value could not be detected with the proposed technique, since it is lower that the quantification limit.

Industrial water

The same procedure was successfully applied for the analysis of Ni(II) ions in samples coming from a galvanic industrial plant. The samples were collected at the end of the purification system (the concentration of Ni(II) has to be reduced before discharging the water in the environment). Also in this case the samples were filtered and acidified with HNO_3 following the standard protocol [37].

Ni(II) concentration was too high for a direct determination, bringing to saturation of the electrode and lack in linearity of the analytical response. Therefore the right dilution has to be found in order not to exced a Ni(II) concentration of 20 μgL^{-1} in the measuring cell. The dilution is necessary also because has been found that, in order to have reproducible results, the deposition time has to be not lower than 30s.

All the different samples were analyzed with the standard addition method (3 addition of 10 μgL^{-1} each) and the concentration of the sample is expressed as average of at least 3 different analysis.

Sample	#	Dilution factor	Dep. time (s)	Ni(II) in Cell (μgL^{-1})	Ni(II) in sample (mgL^{-1})
9441	1	1000	60	4.97	5.0
	2	1000	60	5.61	5.6
	3	800	60	6.75	5.4
				Average	**5.3 ± 0.2**
10780	1	500	60	2.80	1.40
	2	500	60	2.58	1.29
	3	1000	60	1.29	1.29
				Average	**1.33 ± 0.04**
7624	1	50	30	15.9	0.80
	2	50	30	15.4	0.77
	3	100	30	7.93	0.79
	4	100	60	8.44	0.84
				Average	**0.80±0.02**
8468	1	19	60	9.28	0.18
	2	50	60	4.39	0.22
	3	50	60	4.03	0.20
				Average	**0.20±0.01**

Table 4.3. Data obtained from the analysis of 4 different industrial water samples for Ni(II).

4.4 Conclusions

The in-situ preparation of bismuth modified gold electrodes allowed the sensitive and reliable simultaneous determination of low concentrations both of Ni(II) and Co(II). After proper optimization, the analytical procedure showed to be available as an easy method which can give analytical results characterized by very good accuracy and precision, being, at the same time, competitive with more complex and expensive analytical procedures based on ICP-MS or ICP-OES techniques. Moreover, with respect to ex-situ modification protocols, the present method can be used for in-field or on-site monitoring. The present study showed that the method can be applied successfully for trace analysis of nickel and cobalt in natural waters, but, in principle, its application can be extended to monitoring the possible contamination of drinking waters and foodstuff, fulfilling the requirements indicated by some recent recommendations and guidelines [38,39].

4.5 References

[1] J. Wang, *Analytical Electrochemistry*, Wiley, VCH, USA, 2006.

[2] M.G. Paneli, A. Voulgaropoulos, *Electroanalysis*, 5 (1993) 355-373.

[3] C.M.A. Brett, A.M.C.F. Oliveira Brett, J.L.C. Pereira, *Electroanalysis,* 3 (1991) 683-689.

[4] H. Li, R.B. Smart, *Anal. Chim. Acta,* 333 (1996) 131-138.

[5] O. Domínguez and M. J. Arcos, *Anal. Chim. Acta*, 470 (2002) 241-252.

[6] B. Baś, *Anal. Chim. Acta,* 570 (2006) 195-201.

[7] R. Piech, B. Baś, W.W. Kubiak, *Talanta,* 76 (2008) 295-300.

[8] V. Arancibia, C. Muñoz, *Talanta,* 73 (2007) 546-552.

[9] P. Kapturski, A. Bobrowski, *J. Electroanal. Chem.,* 617 (2008) 1-6.

[10] E.A. Hutton, B. Ogorevc, S.B. Hočevar, M.R. Smyth, *Anal. Chim. Acta,* 557 (2006) 57-63.

[11] E.A. Hutton, S.B. Hočevar, B. Ogorevc, M.R. Smyth, *Electrochem. Commun.,* 5 (2003) 765-769.

[12] J. Wang, J.M. Lu, *Electrochem. Commun.,* 2 (2000) 390-393.

[13] D. Ruhlig, A. Schulte, W. Schuhmann, *Electroanalysis,* 18 (2006) 53-58.

[14] L.A. Piankova, N.A. Malakhova, N.Y. Stozhko, K.Z. Brainina, A.M. Murzakaev, O.R.Timoshenkova, *Electrochem Commun.,* 13 (2011) 981-984.

[15] G.M.S. Alves, J.M.C.S. Magalhaes, H.M.V.M. Soares, *Electroanalysis,* 25 (2013) 1247-1255.

[16] L. Baldrianova, I. Svancara, A. Economou S. Sotiropoulos, *Anal. Chim. Acta,* 580 (2006) 24-31.

[17] I. Rutyna, M Korolczuk, *Electroanalysis,* 23 (2011) 637-641.

[18] A. Mardegan, S. Dal Borgo, P. Scopece, L.M. Moretto, S.B. Hočevar, P. Ugo, *Electrochem. Commun.,* 24 (2012) 28-31.

[19] X. Du, W. Gong, Y. Zhang, M. Wang, S. Wang, J.-I. Anzai, *Sensors Letters,* 5 (2007) 572-577.

[20] M. Oliveira Salles, D. Battistel, A. Silva Lima, M. Bertotti, S. Daniele, *Electroanalysis,* 23 (2011) 595-603.

[21] M. Jacobsen, H. Duwensee, F. Wachholz, M. Adamovski, G.-U. Flechsig, *Electroanalysis,* 22 (2010) 1483-1488.

[22] P. Salaün, K.B. Gibbon-Walsh, G.M.S. Alves, H.M.V.M. Soares, C.M.G. van den Berg, *Anal. Chim. Acta,* 746 (2012) 53-62.

[23] G.M.S. Alves, J.M.C.S. Magalhães, P. Salaün, C.M.G. van den Berg, H.M.V.M. Soares, *Anal. Chim. Acta*, 703 (2011) 1-7.

[24] A. Mardegan, P. Scopece, F. Lamberti, M. Meneghetti, L.M. Moretto, P. Ugo, *Electroanalysis*, 24 (2012) 798-806.

[25] P. Ugo, S. Zampieri, L.M. Moretto, D. Paolucci, *Anal. Chim. Acta,* 434 (2001) 291-300.

[26] M. Korolczuk, I. Rutyna, K. Tyszczuk, *Electroanalysis,* 22 (2010) 1494-1498.

[27] M. Korolczuk, A. Moroziewicz, M. Grabarczyk, *Anal. Bioanal. Chem.,* 382 (2005) 1678-1682.

[28] H. Sopha, V. Jovanovski, S.B. Hocevar, B. Ogorevc, *Electrochem. Commun.,* 20 (2012) 23-25.

[29] M. Korolczuk, K. Tyszczuk, M. Grabarczyk, *Electrochem. Commun.,* 7 (2005) 1185-1189.

[30] J. Pérez-Peña, J.J. Hernández-Brito, J. A. Herrera-Melián, C. Collado-Sánchez, C. M. G. van den Berg, *Electroanalysis,* 6 (1994) 1069-1076.

[31] E.A. Hutton, S.B. Hocevar, B. Ogorevc, *Anal. Chim. Acta,* 537 (2005) 285–292

[32] J.-M. Ouyang, H. Zeng, S.-P. Deng, *J. Cryst. Growth,* 293 (2006) 118-123.

[33] S.B. Hocevar, S. Daniele, C. Bragato, B. Ogorevc, *Electrochim. Acta,* 53 (2007) 555-560.

[34] Kròlicka, A. Bobrowski, *Electrochem. Commun.,* 6 (2004) 99-104.

[35] F. Ma, D. Jagner, L. Renman, *Anal. Chem.,* 69 (1997) 1782-1784.

[36] M.Morfobos, A. Economou, A. Voulgaropoulos, *Anal. Chim. Acta*, 519 (2004) 57-64.

[37] M. Belli, D. Centioli, P. De Zorzi, U. Sansone, S. Capri, R. Pagnotta, M. Pettine, *Metodi Analitici per le acque*, APAT, Roma, 2004, pg 202.

[39] C. Reilly, *Metal Contamination of Food*, 3rd Edition, Blackwell Science, 2005.

[39] WHO, *Nickel in Drinking Water*, WHO Guidelines for Drinking-water Quality, World Heath Organization, 2005.

Chapter 5:
Carbon Electrodes Derived from Epoxy-based Photoresist

5.1Introduction

Carbon is available in nature in a variety of allotropes that exhibit a wide range of mechanical, chemical, electrical and electrochemical properties based on the underlying microstructure [1]. Among the various carbon allotropes, graphite and glassy carbon (GC) are widely investigated for electrochemical applications [2]. Polymer derived carbons are mainly glassy in nature, i.e., their microstructure is a combination of graphitic and amorphous zones. The graphitic content of glassy carbon can be altered by tuning pyrolysis conditions and other fabrication parameters. GC exhibits a wide potential stability window and low background currents [1]. It features multiple electrochemically active sites due to the random orientation of the graphitic crystallites on its surface [3, 4]. Carbon's chemical inertness, stability in acidic and basic media, low cost and ease of fabrication render it an attractive material for deposition of metal thin films such as mercury [5], gold [6] and more recently bismuth and antimony [7, 8], metal nanoparticles [9, 10] and polymers [11, 12] employed for electroanalysis.

Recently, carbon research has focused on carbon nanotubes (CNTs) [13], carbon micro and nanoelectromechanical systems (C-MEMS and C-NEMS) [14, 15], carbon fibers [16], carbon nanospheres [17], carbon whiskers [18], and graphene [19, 20]. These advanced carbon materials have already found prospect applications in the field of biomedical engineering, sensor technology, electronics and electrochemical devices and miniature power sources [21-24].

In a typical C-MEMS process [14, 15] carbon electrodes are conveniently fabricated employing simple and inexpensive batch fabrication methodologies such as UV photolithography followed by pyrolysis. Pyrolysis in C-MEMS is carried out in a flow of N_2 gas with a standard temperature ramp-up of about 10°C/min and a one hour dwell time at the maximum temperature of 900°C, followed by the natural cooling down of the furnace. The pyrolysis conditions sensitively impact the microstructure of the C-MEMS electrodes and, as a consequence, they influence the chemical and electrochemical behavior; this asks for an

optimization of the entire C-MEMS process. Lithographically patterned C-MEMS electrodes pyrolyzed under standard conditions (as described above) usually generate GC, with a low graphitic content [25].

In this Chapter, we study the preparation of C-MEMS electrodes, fabricated by photopatterned SU-8, a negative tone epoxy based photoresist, and then pyrolyzed. The pyrolysis parameters, in particular pyrolysis temperatures and dwell times, were studied and optimized. Besides carrying out electrochemistry on the thus obtained electrodes we characterized them by resistivity measurements, Raman spectroscopy and X ray diffraction (XRD).

The prospect applications of pyrolyzed photoresist carbon electrodes (PPCE) go from biological applications [26, 27], to chemical sensing [28] and microbatteries [29]. In the following section we'll demonstrate for the first time the applicability of pyrolyzed photoresist electrodes for the analysis of heavy metals ions.

5.2Experimental

5.2.1 Materials and Methods

All chemicals were analytical grade. SU-8 was obteined from MicroChem Inc. MA, USA and silicon wafers were from Noel Technologies, CA, USA.

5.2.2 Electrode Preparation

A negative tone epoxy based photoresist, SU-8 was photopatterned employing standard UV photolithography. The wafers were dehydrated for 30 minutes at 120°C right before the application of the photoresist. The SU-8 patterns (Figure 5.1A) on SiO_2 were obtained by standard UV photolithography.

Briefly, the photoresist is applied manually on the wafers and then spun reaching the desired thickness according to manufacturer's specifications [30]. Layer thickness is inversely proportional to spin time, speed and acceleration. After deposition, the casting solvent is evaporated from the photoresist in the soft bake or pre-bake step. In this step, usually performed at 95°C, the use of a hot plate is recommended to avoid skin effects. Indeed, baking the photoresist layer in convection oven evaporates the solvent present on the top surface of the photoresist first, thus hindering the evaporation of the solvent from the bulk of the polymer. The resist is then exposed to UV light (360nm) which generates a low

concentration of the catalyst for the cross-linking reaction. After a post exposure bake, which is needed to fully polymerize the SU-8, the patterned features are developed. In this step, the un-polymerized SU-8 dissolves upon immersion in a developer agent.

The thus patterned structures were carbonized using a three-step pyrolysis process in an open ended quartz-tube furnace (RD Webb Red Mini #40). First, the samples were heated under N_2 (flow rate: 2000 sccm) at 300°C for 60 minutes. The temperature was ramped at a rate of 10 °C/min up to the final pyrolysis temperature (800, 900 and 1000°C). The samples were kept at the final pyrolysis temperature for the desired dwell times (1, 4 and 8 hours for both 800 and 900°C) before cooling down. One additional set of electrodes of the same dimensions was pyrolyzed at 1000°C with a dwell time of 1 hour. For prolonged dwell times, the samples used were 20 μm thick before pyrolysis. For the 900°C / 1 hour dwell time experiment, we worked with five electrodes of different thicknesses, 1, 5, 10, 20 and 30 μm before pyrolysis. Before carrying out the electrochemical measurements, the electrodes were insulated with a Monokote® (Topflite, Champaign IL) tape in order to make sure that only a defined geometric area is exposed (0.07 cm^2) to the solution during the electrochemical experiments (Figure 5.1B).

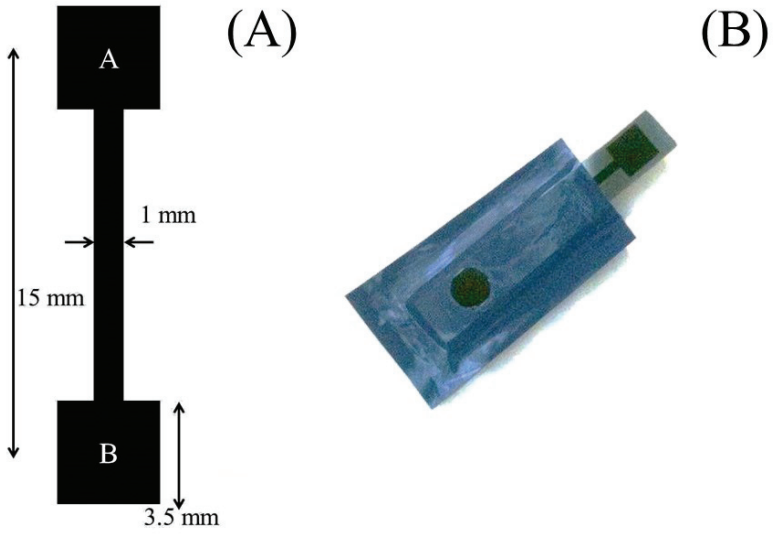

Figure 5.1. (a) Schematic diagram of the electrode design (b) photograph of an electrode on SiO_2 after pyrolysis and insulation with Monokote tape.

5.2.3 Electrode Characterization

The thickness of the films before and after pyrolysis was measured by a profilometer (Veeco Dektak3). The resistivity of the electrodes was measured using a two point probe resistance measurement unit (Keithly 2000 Sourcemeter) in a voltage range of -2.0 to +2.0 V. Raman spectroscopy was carried out on a Renishaw Raman Spectroscopy set up at 514.5 nm. Spectra in the range of 1000 - 1800 cm^{-1} were obtained for the characterization of disordered (D) and graphitic (G) bands of carbon. X Ray Diffraction experiments were carried out using a Rigaku SmartLab X-ray Diffractometer.

All voltammetric measurements were performed using a Palmsens electrochemical workstation at room temperature. A three electrode single compartment electrochemical cell was used for all experiments using the fabricated carbon electrode as the working electrode, a platinum wire as the counter electrode and an Ag/AgCl (KCl saturated) reference electrode.

5.3 Results and discussion

5.3.1 Effect of the substrate

In order to study the electrochemical response of the electrodes pyrolyzed at different conditions and fabricated on different substrates, a series of cyclic voltammetry (CV) experiments was carried out using $[Fe(CN)_6]^{4-}$ as a reversible redox probe exhibits an ideal CV behavior, characterized by a difference between anodic (E_{pa}) and cathodic (E_{pc}) peak potential ($\Delta E_p = E_{pc} - E_{pa}$) of 59 mV [31]. Another parameter taken into account to evaluate the performance of the various electrodes is peak current (I_p). According to Randles Sevcik equation [31], I_p is proportional to the electrode area, concentration and diffusion coefficient of the redox species and voltage scan rate. Electrodes with a higher I_p are considered more suitable in our experiments.

We UV photopatterned SU-8 on 4 different substrates namely bare silicon, silicon coated with silicon nitride, silicon coated with silicon oxide and sapphire. The native oxide film on the bare Silicon wafers was removed using a buffer HF etching solution. In order to test the effect of the substrate on the electrochemical behavior of the carbon electrodes on them we performed electrochemical experiments in solutions containing 1 mM $[Fe(CN)_6]^{4-}$ and 0.1 M KCl. The oxide and nitride layers offer the necessary insulation compared to bare silicon, which is a semiconductor. Silicon can act as a parallel resistance to the carbon electrodes, thereby drawing some amount of current in its path and increasing the overall resistance of the

electrode. In this case, the electrode behaves as if the reaction was quasi-irreversible (high ΔE). Having an insulating oxide or nitride layer ensures that only carbon participates in the electron transfer between electrode and $[Fe(CN)_6]^{4-}$/ $[Fe(CN)_6]^{3-}$ couple.

Out of the 4 substrates, silicon nitride gave the best results in terms of a narrow separation between anodic and cathodic peaks. This response however was only slightly better than that of Si/SiO_2 (10% higher I_p and 15% lower ΔE). For the rest of the experiments we chose oxide over nitride as we could thermally grow the oxide layer in our laboratory thus providing a cheaper alternative.

It is worth mentioning that carbon films on sapphire exhibited poor adhesion and often peeled off during pyrolysis. Hence we reduced the SU8 film thickness on sapphire to 2 μm and the ramp rate to 5 °C min^{-1} which resulted in better adhesion. Thinner films increase the resistance of the electrode which is evident, for example, from the slope of the voltammograms in Figure 5.2 (the effect of thickness is also explained in section 5.3.3).

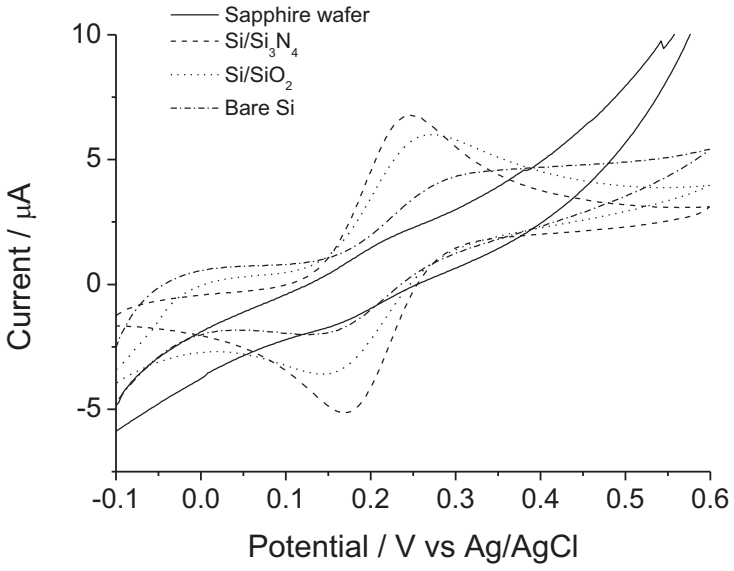

Figure 5.2. CVs recorded in 0.1 M KCl and 1 mM $[Fe(CN)_6]^{4-}$ for pyrolyzed carbon electrodes fabricated on different substrates. Scan rate 25 mV/s.

5.3.2 Effect of pyrolysis conditions on electrochemical behavior

Electrochemical and electrical characterization

Pyrolysis of a polymer for converting it into carbon encompasses a mass loss due to the release of gases such as oxygen and hydrogen, leading to an isometric shrinkage of the structure. Thermogravimetric analysis (TGA) of pyrolyzed photoresist film reported by Ranganathn et al. [32], suggests that 80% of the mass loss occurs at temperatures below 800°C. Our results indicate a further 10% shrinkage in carbon films as the dwell time is increased from 1 hour to 4 hours at 800°C as well as at 900°C.

The effect of increasing the final pyrolysis temperature on the electrochemical properties of the carbon films has been studied and reported previously [32, 33]. We demonstrate that a combined effect of temperature and dwell time leads to a much improved electrochemical performance of the SU-8 derived carbon. Figure 5.3 (A, B) illustrates that both ΔE and resistivity of our electrodes decrease on extending the dwell time from 1 to 8 hours. The curves represent ΔE and resistivity values for electrodes pyrolyzed at 800 and 900°C with dwell times 1, 4 and 8 hours. For a 1000°C pyrolysis temperature, we only carried out a one hour dwell since the ΔE values were close to 59 mV already.

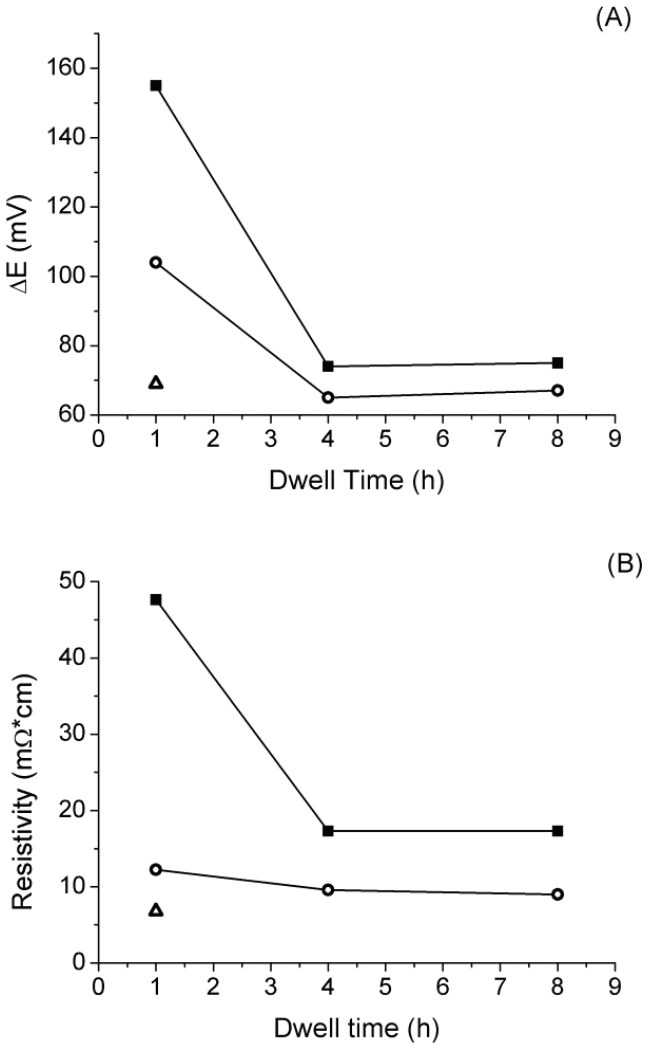

Figure 5.3. A: Effect of dwell time on the ΔE for the oxidation of $[Fe(CN)_6]^{4-}$ in 0.1M KCl at 25mV/sec. Electrodes pyrolized at 800°C (squares), 900°C (circles) and 1000°C (triangle). B: Effect of the dwell time on the resistivity. Electrodes pyrolized at 800°C (squares), 900°C (circles) and 1000°C (triangle).

Figure 5.4 presents the cyclic voltammograms of $[Fe(CN)_6]^{4-}$ for electrodes pyrolyzed at different dwell times (1hour and 4 hours) for two different temperatures (A at 800°C and B at 900°C). The role of dwell time is quite evident in the improvement of the electrochemical response (narrower ΔE and higher peak current). No further improvement in the electrochemical behavior was observed for dwell times longer than 4 hours (see also Table 1).

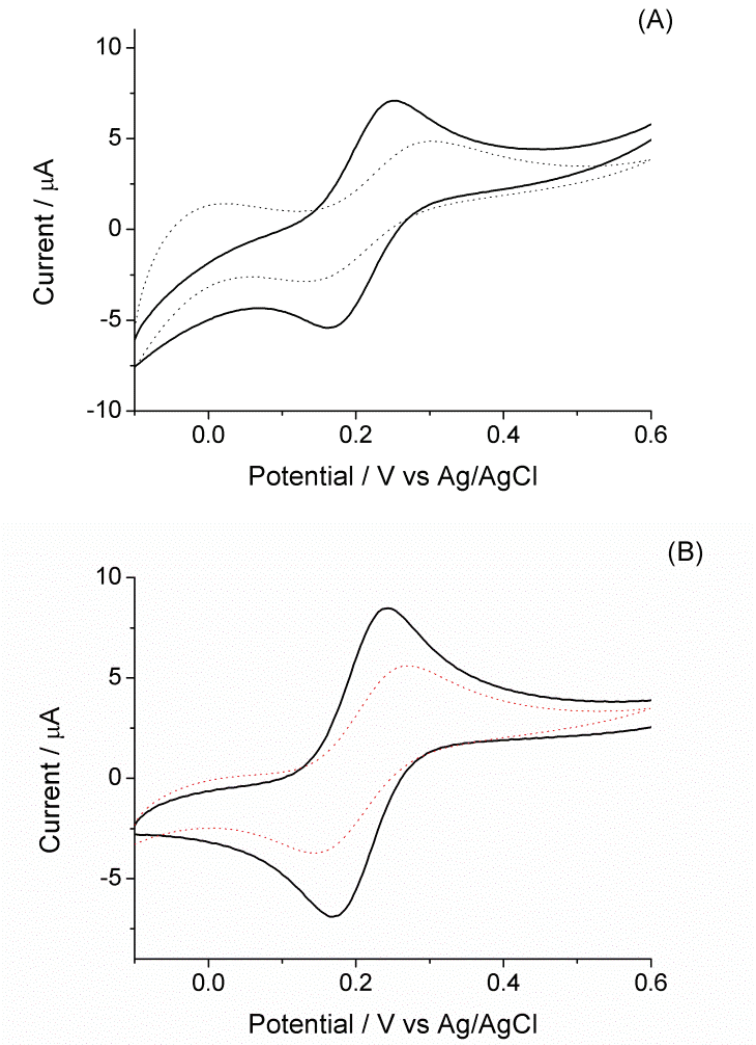

Figure 5.4. CVs recorded in 0.1 M KCl and 1 mM $[Fe(CN)_6]^{4-}$. Scan rate 25 mV/s. A) Dotted line displays an electrode pyrolyzed at 800°C for 1h; black line one treated at 800°C for 4h. B) Dotted line displays an electrode pyrolyzed at 900°C for 1h; black line one treated at 900°C for 4h.

We compared the behavior of electrodes at varying scan rates (5 to 50 mV/seconds). Figure 5.5 represents a comparison between the two limiting cases, namely 800°C pyrolyzed at 1 hour dwell (Figure 5.5A), and 900°C pyrolyzed at 4 hour dwell (Figure 5.5B). It is evident that the voltammograms in Figure 5B result in a narrower ΔE, while the voltammograms in Figure 5.5A do not. This behavior, which in principle also results from irreversibility of the redox reaction, is in this case principally attributed to high electrical resistance of the electrode material. The resistance measurements confirmed that the resistance of the GC material in these two limiting cases described here are indeed significantly different (see below).

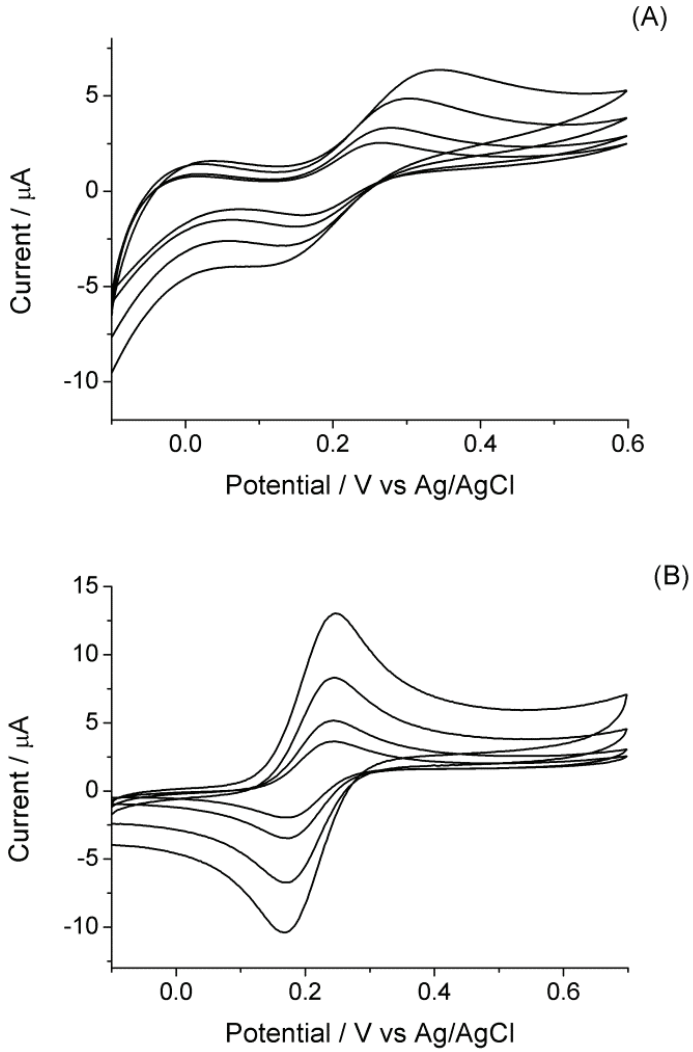

Figure 5.5. CVs recorded in 0.1 M KCl and 1 mM $[Fe(CN)_6]^{4-}$ at different scan rate (from 5 to 50 mV/s). A) Electrode pyrolyzed at 800°C for 1h. B) Electrode pyrolyzed at 900°C for 4h.

Table 5.1 summarizes the ΔE values, corrections for the uncompensated resistance (iR compensation) and calculations of the ΔE values for electrodes pyrolyzed at different temperature and dwell times. At 800°C there is approximately a 53% decrease in the ΔE value as the dwell time is increased from 1 hour to 4 hour. Similarly, at 900°C, ΔE decreases by almost 38% as the dwell time is increased from 1 hour to 4 hour, reaching closer to the theoretical value of 59 mV. Moreover, a 34% reduction in ΔE is observed when the temperature is increased from 900°C to 1000°C for 1 hour dwell time. This behavior demonstrates that prolonged heat treatment at specified temperature changes the properties of SU-8 derived carbon significantly.

Temperature and dwell time	ΔE (mV)	Resistance* (Ω)	Corrected ΔE (mV)	Resistivity (mΩ*cm)
800°C 1h	155	1743	136	47.6
800°C 4h	74	701	64	17.3
800°C 8h	75	701	66	17.3
900°C 1h	104	459	98	12.2
900°C 4h	65	389	60	9.6
900°C 8h	67	365	63	9.0
1000°C 1h	69	283	63	6.8

Table 5.1. Electrochemical and electrical data for electrodes pyrolyzed at different final temperatures and dwell times. *Resistance was measured between A and B in Fig 1A.

Spectroscopic characterization

Raman spectra and XRD patterns for the carbon electrodes were obtained to investigate the graphitic nature of the carbon pyrolyzed under different conditions. The presence and area ratio of the characteristic "D" (1360 cm^{-1}) and "G" (1582 cm^{-1}) bands in the Raman spectra have been studied extensively for determining the nature of the underlying carbon microstructures [34, 35]. A low value of the G/D ratio is an indicative of a smaller graphitic fraction, and is associated with the presence of a greater disorder. A typical spectrum is shown in Figure 5.6.

We calculated the area ratio between G/D (applying the corrections for overlapping peaks [36]) as function of pyrolysis time and temperature. Surprisingly we did not observe any significant increase in the graphitic content on dwell time extension. It is important to note that Raman spectroscopy for characterization of disordered and graphitic carbon is prone to errors as the peaks overlap partially.

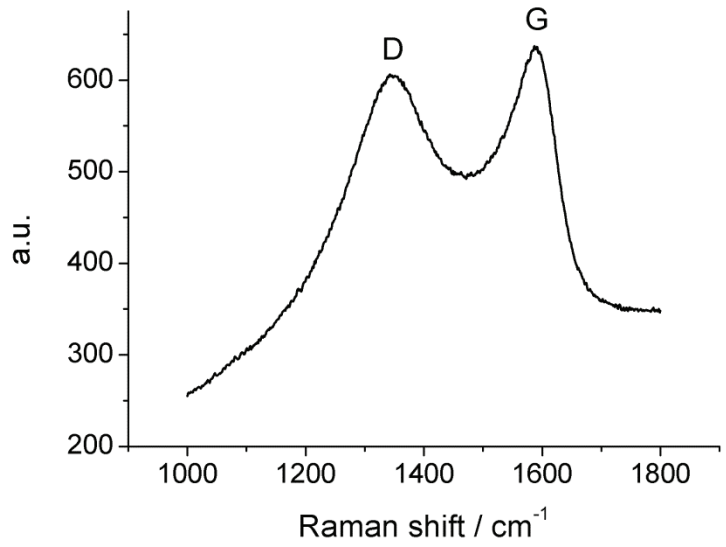

Figure 5.6. Raman spectra for SU8 derived carbon electrodes pyrolyzed at 900°C for 1h.

The XRD spectra (Figure 5.7) for all samples exhibit a peak at ~54°, characteristic of the (004) planes of graphite [37]. However, a bump extending from 10-25° indicates the presence of greater amorphous regions. It is known that GC is composed of intertwined crystalline (graphite) ribbons, filled with amorphous carbons [38]. These percolated graphite ribbons allow electron transport and make GC more suitable for electrical and electrochemical applications, unlike other amorphous materials. According to IUPAC [39] if the crystalline structure of carbon can be detected in the material by diffraction methods, independent of the volume fraction and the homogeneity of distribution of such crystalline domains, the term 'graphitic' can be used. GC is therefore considered graphitic, which explains the presence of 004 planes at 54° in our XRD spectra. The area of this peak however does not increase significantly for samples pyrolyzed at different dwell times. Figure 5.7 represents one characteristic spectrum. The additional peaks appearing at 33° can be attributed to Silicon.

The change in electrical resistance and electrochemical behavior of electrodes pyrolyzed at different conditions is generally expected to result from enhanced graphitization. However in our experiments this enhancement seems to be small, which is not detectable by Raman spectroscopy and XRD. For small sample volume, such as a thin carbon films, electrical and electrochemical measurements prove to be more sensitive compared to spectroscopic techniques. Even minor changes in the underlying carbon microstructure can lead to a much different electrical behavior due to an improved electron transport. These microstructural changes can result from an overall increase in graphitization, or from a different orientation of

graphitic planes in GC due to rearrangement of the carbon atoms during extended dwell, or both. We are currently carrying out a much detailed investigation in our group to address these questions.

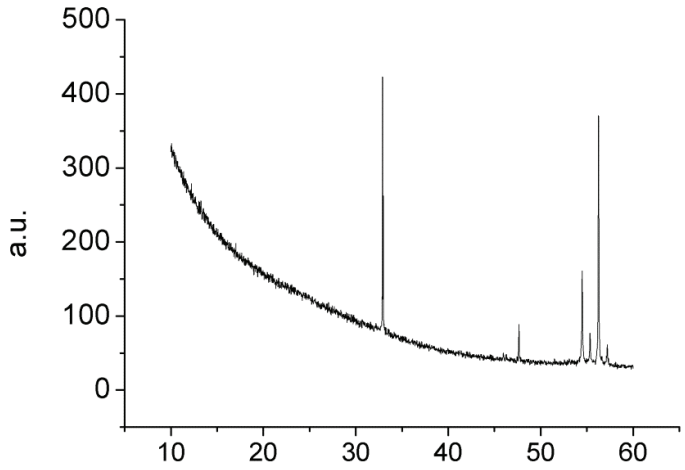

Figure 5.7. X Ray Dyffraction patterns for SU8 derived carbon electrodes pyrolyzed at 900°C for 1h.

5.3.3 Effect of film thickness on the resistance and on electrochemical behavior

To determine the effect of film thickness and the change in electrical resistance that goes with that on ΔE, we fabricated SU-8 electrodes of different thicknesses on SiO_2 wafers. In Figure 5.8 the thicknesses of the electrodes after pyrolysis at 900°C for 1 hour and their respective resistance and ΔE values are illustrated.

In this case we decided to plot resistance (instead of resistivity) because the starting material and the pyrolysis parameters are the same. Since resistivity is a property of the material (instead of geometry) this parameter is not affected by thickness. The values we found were in fact all in good agreement one with the others.

As the thickness of the carbon film decreases, the end to end resistance (between point A and B in Figure 5.1A) goes up, which in turn increases the ΔE and the electrodes are no longer ideal for electrochemical applications. We can conclude from this data (collected for 900°C, 1h) that there is a minimum required thickness (~4 μm for the given electrode dimensions, see also Figure 1) which gives a quasi-ideal response. Thicker films don't bring significant improvement of the electrochemical performances.

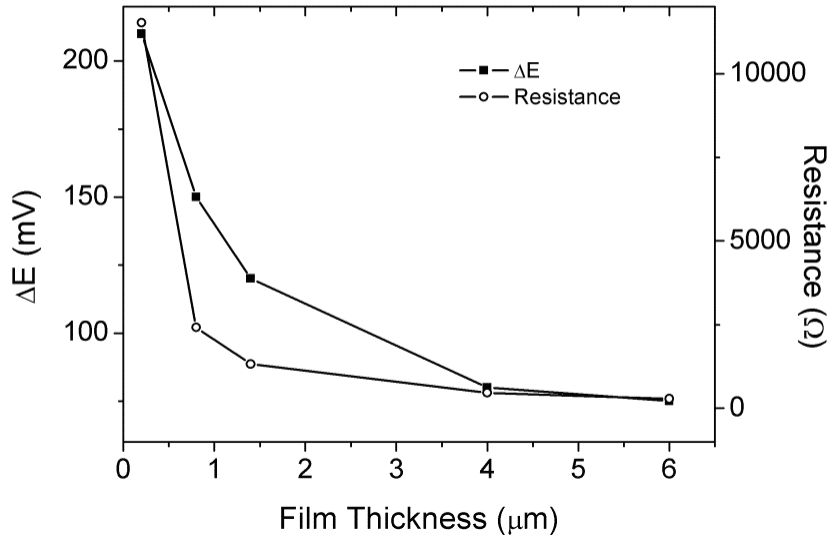

Figure 5.8. Difference in anodic and cathodic peak potential (ΔE) and resistance for different film thicknesses and keeping other dimensions constant.

5.3.4 Effect of the supporting electrolyte concentration

In order to explore the potential of these electrodes for a wide range of electrochemical applications, we studied the effect of the electrolyte concentration on the standard potential of ferro/ferrricyanide couple.

Figure 5.9 shows CVs for the 1mM $[Fe(CN)_6]^{4-}$ in solutions containing four different concentrations of KCl (from 0.05 to 1M) at 5 mVs^{-1}. It can be observed that $E_{1/2}$ changes with the electrolyte concentration. Such behavior, which was demonstrated previously for Pt microelectrodes [40], can only arise if the formal potential for the ferro/ferrricyanide depends on the concentration of KCl.

As per the Nernst equation (equation 5.1) to determine the equilibrium potential of a half cell in an electrochemical cell, the activity of the redox species is expressed as product of an activity coefficient (γ) and the concentration (C).

$$E = E^0 - (RT/nF)\ln(\gamma_r/\gamma_o) - (RT/nF)(C_r/C_o) \qquad \text{equation 5.1}$$

In the absence of supporting electrolyte $\gamma_r=\gamma_o$ but in the presence of added salt the activity coefficients for both oxidized and reduced species change [41], which in turn explains the shift.

This data demonstrates that the carbon derived from pyrolyzed photoresist can be used to study redox reaction kinetics as the electrochemical behavior of these electrodes is similar to

that of the traditionally used electrodes such as noble metals (Pt, Au) or commercially available glassy carbon.

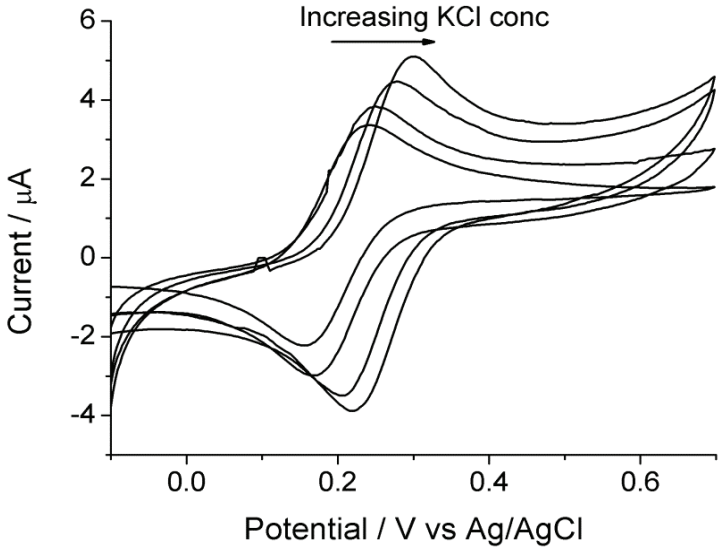

Figure 5.9. CV recorded using CMEMS electrode, at 5 mV/s, in solution of 1mM $[Fe(CN)_6]^{4-}$ and four different concentrations of KCl (from 0.05 to 1 M).

Scan rate mVs^{-1}	0.05 M KCl		0.1 M KCl		0.5 M KCl		1 M KCl	
	$E_{1/2}$ (mV)	ΔE (mV)	$E_{1/2}$ (mV)	ΔE (mV)	$E_{1/2}$ (mV)	ΔE (mV)	$E_{1/2}$ (mV)	ΔE (mV)
50	196	99	206	89	240	81	258	97
25	197	90	208	81	241	75	259	87
5	197	77	210	75	241	63	259	74

Table 5.2. Data taken from cyclic voltammograms at C-MEMS electrode, in solutions of 1 mM $[Fe(CN)_6]^{4-}$ in 4 different concentrations of aqueous KCl.

5.3.5 Accessible potential window

It is also important to explore both the accessible potential window and the electrochemical behavior of the photoresist derived carbon electrodes at negative potential values. Figure 5.10A presents a CV recorded in 0.01 M HCl (pH 2) in the absence of dissolved oxygen which shows that the potential window can go down to 1.4 V in acidic media.

Repetitive scanning to -1.3 V at C-MEMS electrode in acidic media didn't give any change in the double layer charging currents demonstrating the stability of these electrodes also in extreme pH values.

As previously demonstrated in the literature [42], the nature of the increase in the background current in the cathodic range is made clear by examining its pH dependence. The voltammograms in Fig. 5.10B clearly show that these currents are attributable to proton reduction; indeed, the potential value at which a certain reduction current is measured shifts negatively by 60 mV per unit increase in the pH of the solution.

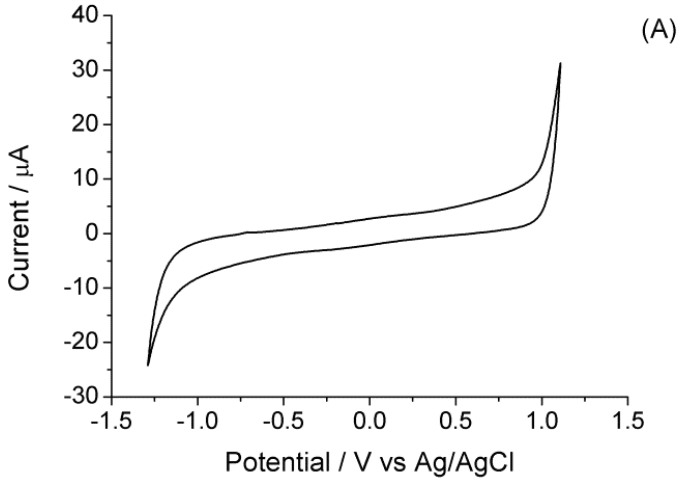

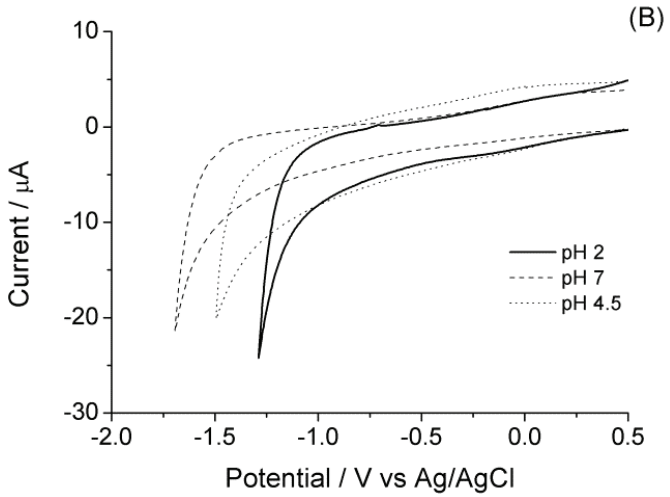

Figure 5.10. A) Background cyclic voltammogram recorded at 25 mV s^{-1} in 10^{-2} M HCl, pH 2.2. B) Background cyclic voltammograms recorded at 25 mV s^{-1} at a carbon electrode in: 10^{-2} M phosphate buffer, pH 7.0 (dashed line); 10^{-2} M acetate buffer, pH 4.5 (dotted line); (solid line).

5.3.6 Anodic stripping voltammetry of Cd(II) and Pb(II) at Bi modified PPCE

The electroanalytical performance of the previously described pyrolyzed photoresist carbon electrodes (PPCE) was first studied in the simultaneous determination of lead and cadmium through anodic stripping voltammetry (ASV). In situ surface modification of SU-8 derived carbon electrodes with bismuth was performed in order to increase the overpotential for hydrogen evolution in the cathodic range, thus, enabling detection of both analytes.

The performances of the in-situ modified carbon electrode was studied while increasing the concentration of Pb(II) and Cd(II) in the range of 5 and 30.0 μgL^{-1}, as shown in Figure 5.11A and B.

The electrode revealed a good linear behavior in the examined concentration range for both analytes in combination with 300 s accumulation time being the stripping signals well good separated and surrounded by low background contribution. The detection limit (DL) was calculated by using the $3\sigma/m$ criterion and resulted 0.8 μgL^{-1} for Pb(II) and 0.7 μgL^{-1} for Cd(II), which are close to those obtained with commercially available glassy carbon substrates [45-47].

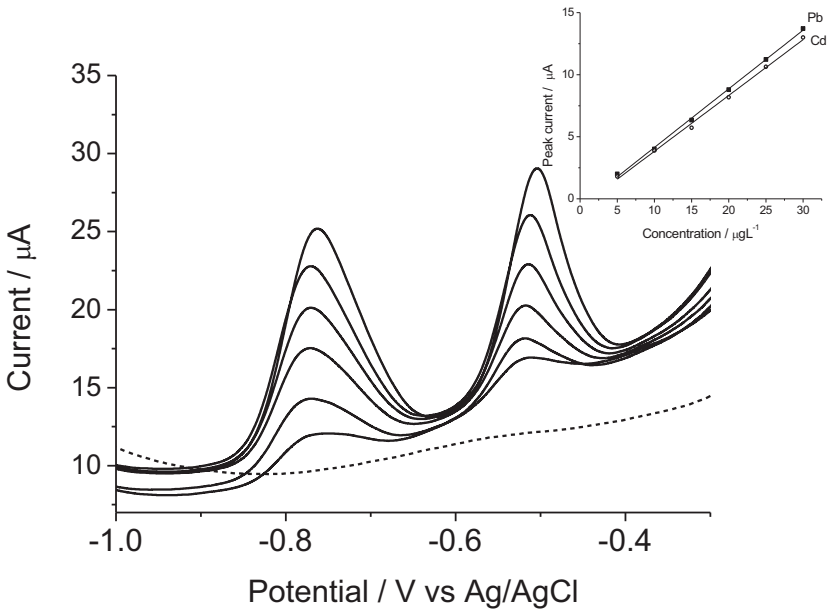

Figure 5.11. SW-ASV recorded at the in-situ prepared Bi-carbon electrode in 0.1 M acetate buffer (pH 4.5), 10 mg L^{-1} Bi(III) in the absence (dotted line) and presence of increasing concentrations of Pb(II) and Cd(II), from 5 to 30 μg L^{-1} (full lines). Deposition at -1.1V for 300 s. SWV parameters: frequency 25 Hz, amplitude 50 mV, potential step of 5 mV. Inset: corresponding calibration plots.

5.3.7 Adsorptive cathodic stripping voltammetry of Ni(II) and Co(II) at Bi modified PPCE

In-situ bismuth modified PPCE were also applied to the simultaneous determination of Ni(II) and Co(II) ions through adsorptive cathodic stripping voltammetry. As it was explained in the section 3.2.3, a two-step accumulation protocol, i.e. (i) -1.1 V for 60 s (in-situ deposition of bismuth) followed by (ii) -0.8 V for 60 or 120 s (accumulation of Ni-DMG and/or Co-DMG complexes) was applied.

Optimization of the experimental procedure

In order to optimize the electroanalytical performance of the proposed electrode, the operational parameters such as the in-situ bismuth concentration and bismuth deposition time were examined. The optimization of the bismuth concentration was carried out at fixed deposition time of 60 s and deposition potential of -1.1 V. During this step Bi was deposited on the PPCE electrode surface, whereas Ni(II)-DMG complex was not adsorbed. The concentration of Bi(III) in the measurement solution was changed in the range of 0 to 20 mg L^{-1}, and its effect upon the Ni(II) stripping signal is shown in Figure 5.12. The stripping peak current increased by increasing the concentration of Bi(III) from 2.5 mg L^{-1} and reached a

constant value when the Bi(III) concentration was ≥ 10 μg L^{-1}. It is important to note that, considering the higher overpotential for hydrogen evolution on carbon electrodes than on gold, at Bi(III) concentrations lower than 5 mg L^{-1} it is already detectable the Ni(II) signal.

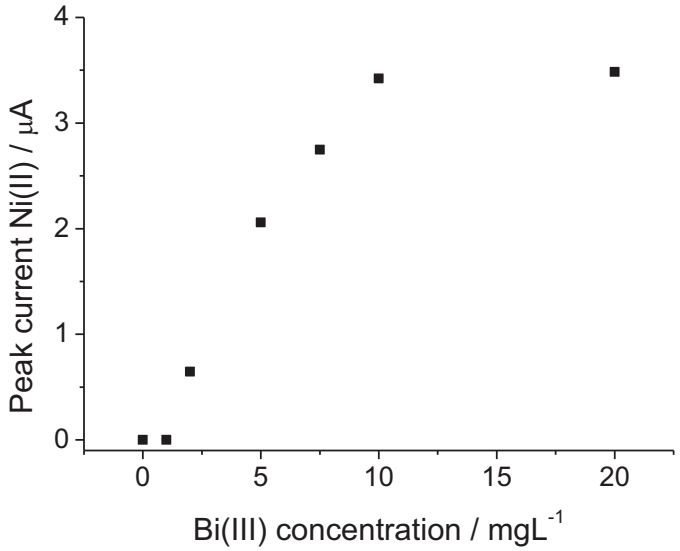

Figure 5.12. Effect of Bi(III) concentration on the Ni(II) peak current. Concentration of Ni(II): 10 mg L^{-1}, accumulation time: 60 s.

The optimization of the bismuth deposition time was carried out at fixed bismuth concentration (10 mgL^{-1}) and deposition potential of -1.1 V. The Bi(III) deposition time was changed in the range of 10 to 120 seconds, and its effect upon the Ni(II) stripping signal is shown in Figure 5.13A. The highest peak is recorded between 30 and 60 seconds of deposition time while at higher deposition time the signal decreases.

In order to further investigate the relationship between bismuth deposition time and Ni(II)-DMG reduction peak we performed 10 independent determinations with Bi(III) deposition time of 10, 30, 60, 120 seconds, and studied the relative standard deviation (RSD) of each set of measurements. As is it visible in Figure 5.13B, the RSD associated to short bismuth deposition time (60, 30 and 10 seconds) is lower than 5% but has a remarkable increase if a deposition of 120 s is performed. We indeed decided to use 60 s as optimized deposition time for further investigation of Ni(II) and Co(II) signal on PPCE.

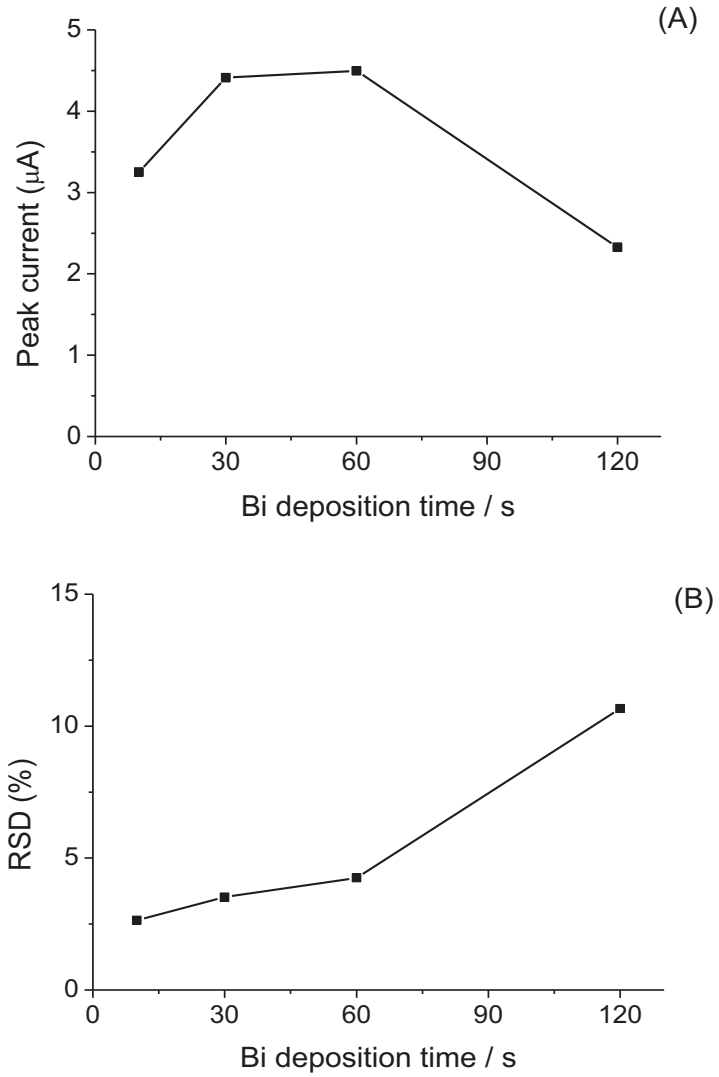

Figure 5.13. A) Effect of Bi(III) deposition time on the Ni(II) peak current. Concentration of Ni(II): 10 mg L^{-1}, accumulation time at -0.8V: 60 s. B) Effect of Bi(III) deposition time on the Ni(II) peak reproducibility. Concentration of Ni(II): 10 mg L^{-1}, accumulation time at -0.8V: 60 s.

Calibration

The electroanalytical performance of the bismuth modified PPCE was further studied while increasing the concentration of Ni(II) in the range of 0.5 to 5.0 μg L^{-1}, as shown in Figure 5.14 and in the inset. The electrode gave a good linear behavior in combination with 120 s accumulation time. A detection limit (DL) of 20 ng L^{-1} was calculated by using the $3\sigma_b$ /m criterion. The calculated DL was comparable to the one obtained with bulk gold substrate [47] and lower compared with other electroanalytical methods reported in the literature [48-52].

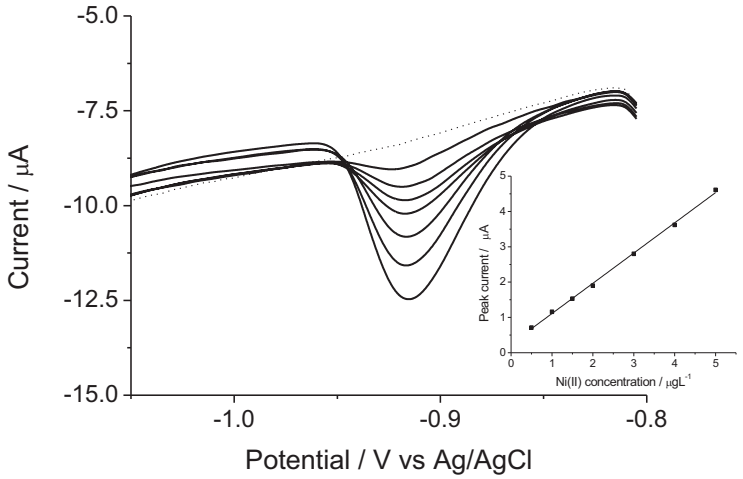

Figure 5.14. AdSVs of the in-situ prepared Bi-PPCE for increasing concentration of Ni(II) in the range of 0.5 – 5 μgL^{-1} in 0.1 M ammonia buffer solution containing 10 mg L^{-1} Bi(III), 1×10^{-5} mol L^{-1} DMG and 0.01 mol L^{-1} tartrate. Deposition at −1.1 V for 60 s followed by accumulation at −0.8 V for 120 s; equilibration time of 15 s.

We decided to follow the AdCSVs recorded at the Bi-PPCE while increasing both concentrations of Ni(II) and Co(II). As can be seen in this Figure 5.15, the stripping signals of both the analytes furnish two well-resolved stripping peaks. Ni(II) peak increased linearly from 5 to 45.0 μg L^{-1} while the Co(II) peak scaled with Co(II) concentration in the range 10 - 70 μgL^{-1} (see the corresponding inset). The calculated DLs (3σ/m) were 0.5 and 2.5 μg L^{-1} for Ni(II) and Co(II), respectively. In comparison with the gold substrate the DMG-Co signal gave a lower sensibility leading to a higher DL but it is stress worthy that these are preliminary results with a new kind of electrode material therefore better results are expected with further optimization.

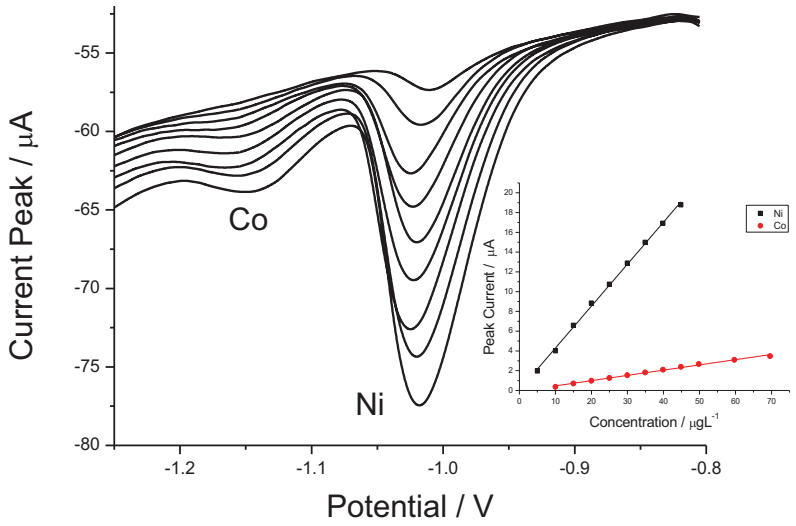

Figure 5.15. AdSVs of the in-situ prepared Bi-PPCE for increasing concentration of Ni(II) and Co(II). Ni(II) in the range of 0.5 – 45 μg L^{-1} and Co(II) 10 – 70 μg L^{-1} in 0.1 M ammonia buffer solution (pH = 9.0) containing 10 mg L^{-1} Bi(III), 1×10^{-5} mol L^{-1} DMG and 0.01 mol L^{-1} potassium sodium tartrate. Deposition at −1.1 V for 60 s followed by accumulation at −0.8 V for 60 s. Other parameters as in Fig. 5.14.

Certified reference material (NIST 1640a)

Bi-PPCEs were tested for measuring Ni(II) in NIST 1640a certified reference material. 1 mL of NIST 1640a was diluted 1 : 10 with 0.1 mol L^{-1} ammonium buffer solution, containing 0.01 mol L^{-1} sodium potassium tartrate, 1 x 10^{-5} mol L^{-1} DMG, and 10 mg L^{-1} Bi(III). The AdCSVs were characterized by a cathodic stripping peak at ca. -0.95V (Figure 5.16), which increased linearly with the additions of Ni(II). The sample concentration calculated by extrapolation of the calibration plots is shown in the inset of Figure 5.16 and considering the dilution factor were 26.3 ± 0.6 μg L^{-1} for Ni(II). This value is in satisfactory agreement with the values of 27.4 ± 0.8 μg L^{-1} certified for this reference material.

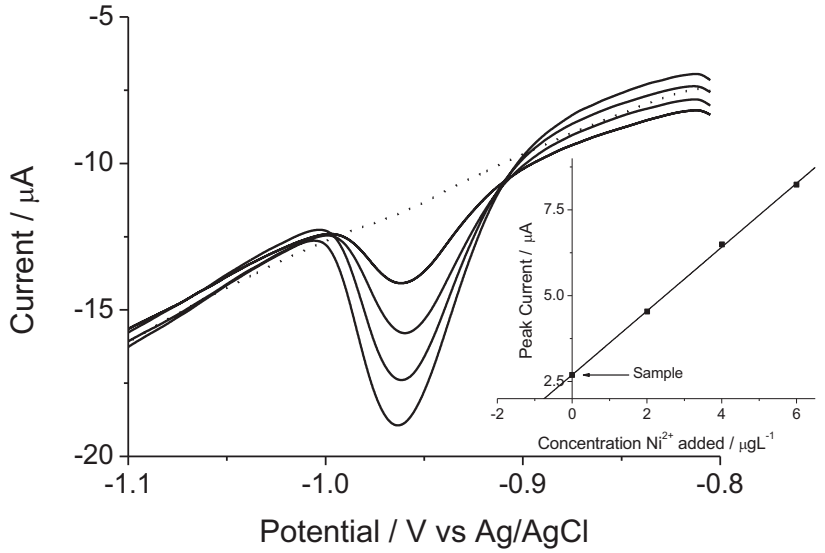

Figure 5.16. AdCSV for measuring NIST-1640a certified reference material via standard addition protocol. Conditions: -1.1 V for 60s, -0.8 V for 60 s. Other conditions as in Figure 5.14.

5.3.8 ASV of As(III) with GNP-modified PPCE

PPCE has also been modified with gold nanoparticles (GNP) in order to analyze As(III) trough ASV. Indeed it was already demonstrated that the modification of a carbon-based substrate with GNP brings to a reduced Cu interference [52] and higher sensitivity that the one obtained with a bulk gold electrode [9,10,53-56]. The Au-Nps can be deposited by mean of electroless [54] or electrochemical methods [52,55]. The so prepared modified electrodes showed detection limits (DL) as low as 0.01 μg L^{-1} [9].

Morphological characterization

Initially, gold nanoparticles were deposited from a solution containing 0.1 mM of $[AuCl_4]^-$ in 0.5 M H_2SO_4 with of a step potential between +1V and -0.045V vs Ag/AgCl as previously described by Compton et al. [9]. The step duration was fixed at 15 seconds.

Figure 5.17A and B show two SEM images of a PPCE modified with gold nanoparticles. Figure 5.17 A displays how the metal particles are organized on the carbon substrate. They are randomly arranged but the surface is uniformly covered. From a SEM image taken at higher magnification (Figure 5.17B), we also measured the diameter of the particles. These seems quite uniform also in the diameter dispersion (400 – 500 nm), proof that this kind of deposition is an efficient way to electro-deposit GNP.

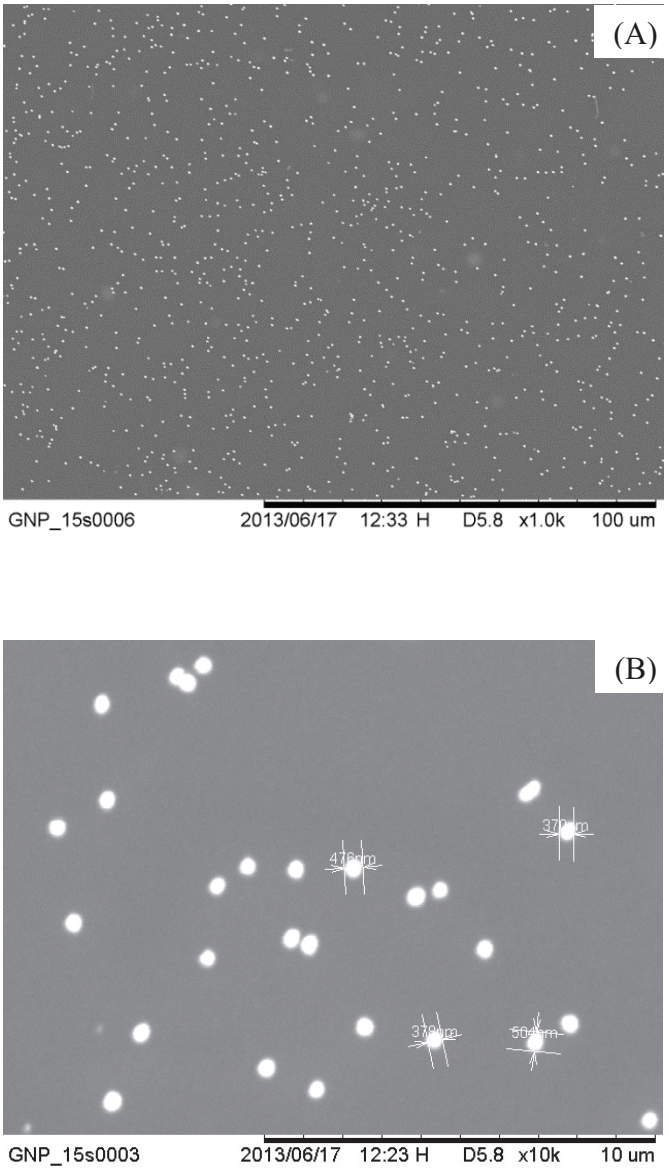

Figure 5.17. SEM images of PPCE modified with GNP from a solution containing 0.1 mM of $[AuCl_4]^-$ in 0.5 M H_2SO_4 with of a step potential between +1V and -0.045V vs Ag/AgCl. Step duration 15s.

Calibration

The electroanalytical performance of the GNP modified PPCE was studied in the ASV of As(III) while increasing its concentration in the range from 5 to 25 μg L^{-1}, as shown in Figure 5.18 and inset. As supporting electrolyte was used 0.2M HCl with 62mM hydrazine, which avoid the oxidation of As(III) to As(V) [57,58]. This media was also used in order to compare the results obtained with the GNP-PPCE with those obtained with NEEs, described and discussed in the chapter 2.

The electrode gave a good linear behavior in combination with 120 s accumulation time. A detection limit (DL) of 0.8 μg L^{-1} was calculated by using the $3\sigma/m$ criterion.

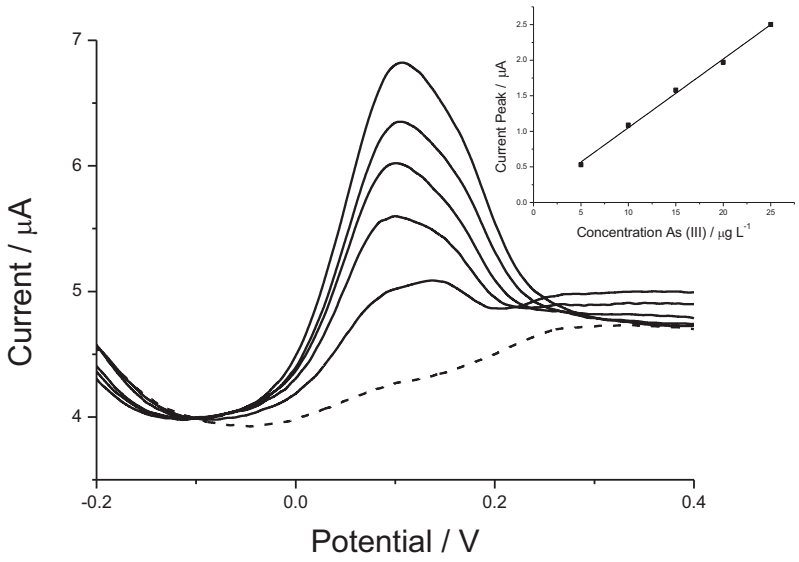

Figure 5.18. SW-ASV recorded at the GNP modified-PPCE in 0.2 M HCl, 2 g L^{-1} hydrazine in the absence (dotted line) and presence of increasing concentrations of As(III) from 5 to 25 μg L^{-1} (full lines). Deposition at -0.4V for 60 s. SWV parameters: frequency 25 Hz, amplitude 50 mV, potential step of 5 mV. Inset: corresponding calibration plots.

5.4 Conclusions

We carried out pyrolysis of SU-8 patterns at different temperatures and dwell times and demonstrated the effect of these conditions on the electrochemical behavior of the thus derived carbon. The electrodes are also characterized by Raman spectroscopy, XRD, and resistance measurements. Carbon electrodes pyrolyzed at 900°C for 4 hours display near-ideal electrochemical behavior. We also investigated the influence of substrate and electrode thickness on electrochemistry of carbon. We found that the electrodes fabricated on Si_3N_4 and SiO_2 substrates display better electrochemical response compared to those fabricated on bare silicon. We also tested electrode fabrication on to sapphire substrate, however a poor adhesion of carbon films on sapphire caused SU-8 films thicker than 2 μm to peel-off during pyrolysis. Carbon constitutes excellent material for electrochemical applications that can be optimized employing the pyrolysis conditions we reported. C-MEMS process can lead to various two and three dimensional electrode designs suitable for a wide range of next generation electrochemical sensors.

Finally, the above results demonstrate that PCCEs can be successfully applied to the determination of toxic inorganic ions such as Pb, Cd, Ni, Co and As. To this aim, Bi-modified PPCE were used to analyze trace concentration of Cd(II) and Pb(II) via anodic stripping voltammetry (ASV) and Ni(II) and Co(II) by adsorptive cathodic stripping voltammetry. PPCE modified with gold nanoparticles are developed for performing the ASV of trace As(III). For all the analytes detection limits as low as 1 μgL^{-1} are obtained, using a preconcentration time of only few minutes, so opening new prospects for the development of deployable electroanalytical chips.

5.5 References

[1] K. Kinoshita, *Carbon Electrochemical and Physico-chemical Properties*, John Wiley & Sons, New York (1988).

[2] R. J. Taylor, A. A. Humffray, *J. Electroanal. Chem. Interf. Electrochem.*, 42 (1973) 347-354.

[3] A. Adenier, M.M. Chehimi, I. Gallardo, J. Pinson, N. Vila, *Langmuir*, 20 (2004) 8243-8253.

[4] P. Allongue, M. Delamar, B. Desbat, O. Fagebaume, R. Hitmi, J. Pinson, J. M. Savéant, *J. Am. Chem. Soc.*, 119 (1997) 201-207

[5] T.M. Florence, *J. Electroanal. Chem. Interf. Electrochem.*, 27 (1970) 273-281.

[6] Y.C. Sun, J. Mierzwa, M.H. Yang, *Talanta*, 44 (1997) 1379-1387.

[7] I. Švancara, C. Prior, S.B. Hočevar, J. Wang, *Electroanalysis*, 22 (2010) 1405-1420.

[8] S.B. Hocevar, I. Švancara, B. Ogorevc, K. Vytřas, *Anal. Chem.*, 79 (2007) 8639-8643.

[9] X. Dai, O. Nekrassova, M. E. Hyde, R. G. Compton, *Anal. Chem*. 76 (2004) 5924-5929.

[10] X. Dai, R. G. Compton, *Anal. Sci*., 22 (2006) 567-570.

[11] P. Ugo, L.M. Moretto, G.A. Mazzocchin, *Anal. Chim. Acta*, 305 (1995) 74-82.

[12] P. Ugo, L.M. Moretto, *Electroanalysis*, 7 (1995), 1105-1113.

[13] J. Wang, *Electroanalysis*, 17 (2005), 7-14.

[14] C. Wang, L. Taherabadi, G. Jia, M. Madou, Y. Yeh, B. Dunn, *Electrochem. Solid-St.*, **7** (2004) A435-438.

[15] C. Wang, G. Jia, L. Taherabadi, M. Madou, *J. Microelectromech. S.*, 14 (2005) 348-358.

[16] T. Maitra, S. Sharma, A. Srivastava, Y.K. Cho, M. Madou, and A. Sharma, *Carbon*, 50 (2012) 1753-1761.

[17] K. Pan, H. Ming, Y. Liu, and Z. Kang, *New J. Chem.*, 36 (2012) 113-118.

[18] J. Dong, W. Shen, and B. Tatarchuk, *Appl. Phys. Lett.*, 80 (2002) 3733-3735.

[19] H. Shen, L. Zhang, M. Liu, and Z. Zhang, *Theranostics,* 2 (2012) 283-294.

[20] Q. He, S. Wu, Z. Yin, and H. Zhang, *Chem. Sci.*, 3 (2012) 1764-1772.

[21] K. Bosnick, N. Gabor, and P.L. McEuen, *Appl. Phys. Lett.*, 89 (2006) 163121-163123.

[22] S. Ilani, L.A.K. Donev, M. Kindermann, and P.L. McEuen, *Nat. Phys.*, 2 (2006) 687-691.

[23] V. Sazonova, Y. Yaish, H. Ustunel, D. Roundy, T.A. Arias, and P.L. McEuen, *Nature*, 431 (2004) 284-287.

[24] G.S. Bisht, S. Holmberg, L. Kulinsky, and M.J. Madou, *Langmuir*, 28 (2012) 14055-

14064.

[25] S. Sharma, A. Sharma, Y.-K. Cho, and M. Madou, *Appl. Mat. Interfaces*, 4 (2012) 34-39.

[26] G.T. Teixidor, R. Gorkin, P.P. Tripathi, G.S. Bisht, M. Kulkarni, T.K. Maiti, T.K. Battacharyya, J.R. Subramaniam, A. Sharma, B.Y. Park, and M Madou, *Biomed. Mater,* 3 (2008) 034116 (8pp).

[27] J.A. Lee, S. Hwang, J. Kwak, S. Park, S.S. Lee, and K.C.Lee., *Sensors and Actuators B*, 129 (2008) 372-379.

[28] M. K. Zachek, P. Takmakov, B. Moody, R. M. Wightman, and G. S. McCarty, *Anal. Chem.*, 81 (2009) 6258-6265.

[29] C. Wang, and M.J. Madou, *Biosens. Bioelectron*., 20 (2005) 2181-2187.

[30] http://microchem.com/pdf/SU82000DataSheet2025thru2075Ver4.pdf

[31] A.J. Bard, L.R Faulkner, *Electrochemical Methods Fundamentals and Applications,* second edition, Wiley, John Wiley & Sons, New York (2001)

[32] S. Ranganathan, R. McCreery, S. M. Majji, and M. Madou, *J. Electrochem. Soc.*, 147 (2000), 277-282.

[33] J. Kim, X. Song, K. Kinoshita, M. Madou, and R. White, *J. Electrochem. Soc.*, 145 (1998) 2314-2319.

[34] R.L. McCreery, *Chem Rev*., 108 (2008) 2646-2687.

[35] Y. Wang, D. Alsmeyer, and R. L. McCreery, *Chem. Mater.*, 2 (1990) 557-563.

[36] L. Binsheng, and L. Peichang, *J. High Resolution Chrom. & Chrom. Commun.*, 10 (1987) 449-454.

[37] J. Zhao, L. Yang, F. Li, R. Yu, and C. Jin, *Carbon*, 47 (2009) 744-751.

[38] G. M. Jenkins, and K. Kawamura, *Polymeric Carbons - Carbon Fibre, Glass and Char*, Cambridge University Press, 1976

[39] IUPAC Compendium of Chemical Terminology (second edition 1997), 67 (1995) 493.

[40] C. Beriet, and D. Pletcher, *J. of Electroanal. Chem.*, 361 (1993) 93-101.

[41] J. Kielland, *J. Am. Chem. Soc.*, 59 (1937) 1675-1678.

[42] B. Brunetti, P. Ugo, L.M. Moretto, and C.R. Martin, *J. Electroanal. Chem*, 491 (2000) 166-174.

[43] E.A. Hutton, B. Ogorevc, S.B. Hočevar, and M.R. Smyth, *Anal. Chim. Acta*, 557 (2006) 57-63.

[44] A. Mardegan, S. Dal Borgo, P. Scopece, L.M. Moretto, S.B. Hočevar, and P. Ugo, *Electrochem. Commun.*, 24 (2012) 28-31.

[45] A. Economou, TrAC *Trends in Anal. Chem.*, 24 (2005) 334-340.

[46] F. Arduini, J.Q. Calvo, A. Amine, G. Palleschi, and D. Moscone, TrAC *Trends in Anal. Chem.*, 29 (2010) 1295-1304.

[47] A. Mardegan, S. Dal Borgo, P. Scopece, L. M. Moretto, S. B. Hočevar, P. Ugo, *Electroanalysis*, 2013, in press.

[48] E.A. Hutton, B. Ogorevc, S.B. Hočevar, M.R. Smyth, *Anal. Chim. Acta,* 557 (2006) 57-63.

[49] E.A. Hutton, S.B. Hočevar, B. Ogorevc, M.R. Smyth, *Electrochem. Commun.,* 5 (2003) 765-769.

[49] J. Wang, J.M. Lu, *Electrochem. Commun.,* 2 (2000) 390-393.

[50] D. Ruhlig, A. Schulte, W. Schuhmann, *Electroanalysis,* 18 (2006) 53-58.

[51] L.A. Piankova, N.A. Malakhova, N.Y. Stozhko, K.Z. Brainina, A.M. Murzakaev, O.R.Timoshenkova, *Electrochem Commun.,* 13 (2011) 981-984.

[52] X. Dai, R.G. Compton, *Electroanalysis*, 17 (2005) 1325-1330.

[53] L. Xiao, G.G. Wildgoose, R.G. Compton, *Anal. Chim. Acta*, 620 (2008) 44-49

[54] M. Khairy, D. K. Kampouris, R. O. Kadara, C. E. Banks, *Electroanalysis*, 22 (2010) 2496-2501.

[55] M. Hossain, M. Islam, S. Fersousi, T. Okajiama, T. Ohsaka, *Electroanalysis*, 20 (2008) 2435-2441.

[56] E. Majid, S. Hrapovic, Y. Liu, K.B. Male, J.H.T. Luong, *Anal. Chem.*, 78 (2006) 762-769.

[57] Y.-C. Sun, J. Mierzwa, M.-H. Yang, *Talanta*, 44 (1997) 1379-1387.

[58] G. Dugo, L. L. Pera, V. L. Turco, G. D. Bella, *Chemosphere*, 61 (2005) 1093-1101.

Concluding remarks

This thesis demonstrates the advantages of the use of advanced materials such as Nanoelectrode Ensemble (NEEs) and Pyrolyzed Photoresist Carbon Electrodes (PPCE) in the electroanalysis of some inorganic priority pollutants.

In the first case, thanks to their particular geometry, NEEs allow the anodic stripping voltammetric determination of trace elements, in our case arsenic, by a simple method reaching detection limits (DLs) which are about 2 orders of magnitude lower that those achievable with conventional gold electrodes.

A method to chemically reduce As^{5+} into As^{3+} was developed allowing one to perform the speciation of the two oxidation states of inorganic arsenic which are different in toxicity.

The controlled increase of the active area of NEEs through chemical or plasma etching lead to the production of 3D-NEEs where gold nanowires protrudes from the polycarbonate template. These ensembles of nanowires didn't suffer from the surface saturation effect observed with nanodiscs NEEs; exploting such characteristic 3D-NEEs were applied to the redox speciation analysis of As^{3+} and As^{5+} in real samples (i.e. river water).

Moreover, NEEs were integrated in a prototype of a flow cell with the prospect of developing a portable sensing station.

In this thesis we also demonstrated that the potential window accessible with gold NEEs can be extended in the cathodic range via the deposition of bismuth; part of this work was developed during a stage at the National Institute of Chemistry, Lijubliana (SLO), in the group of Dr. Samo Hocevar.

Bismuth electrodes exhibit a cathodic part of the operational potential window very similar to that of mercury, with even superior performance in the presence of dissolved oxygen and presenting, at the same time, a non-toxic character and excellent electroanalytical performances.

In principle, the same gold substrate could be used as a bare electrode for the anodic determination of As, while after the modification of Au with bismuth, one could perform the determination of some metals whose stripping peak are too cathodic for being detectable with gold nanoelectrodes.

Bismuth modified NEEs have been applied here for the anodic stripping voltammetry of Pb(II) at trace concentration levels, using short accumulation time. Preliminary studies based on the comparison between the in-situ and ex-situ preparation of the Bi-NEEs indicated that the latter approach yielded improved electroanalytical performances.

When the analyte reacts irreversibly or forms intermetallic compounds or cannot form an amalgam/alloy, the adsorptive stripping protocols can be an interesting approach.
In this thesis we developed an analytical methodology for the in-situ modification of a gold substrate with bismuth which, with respect to the ex-situ one, van be easily applied for in-field or on-site monitoring. The results obtained in the adsorptive cathodic stripping determination of Nickel and Cobalt are improved with respect to those obtained with "conventional" glassy carbon substrate. The method is successfully applied for trace analysis of nickel in lagoon water samples.

Finally, during a stage spent in the BioMems Group at the University of California Irvine (UCI), group of Prof. Marc Madou, I studied the development of a new kind of carbon electrodes produced by the pyrolysis of a negative photoresist named SU-8.
We carried out the pyrolysis of SU-8 at different temperatures and dwell times and demonstrated the effect of these conditions on the electrochemical behavior of the thus derived carbon structures. The advantage of these electrodes is that they can be easily patterned in different shapes and geometries at the micro- and submicrometer scale. The electrodes obtained were characterized by Raman spectroscopy, XRD, and resistance measurements, demonstrating that it is possible to obtain glassy-carbon like structures. We investigated the influence of the nature of the substrate and electrode thickness. Finally, the so obtained pyrolyzed photoresist carbon electrodes (PPCEs) were applied to the stripping voltammetry of heavy metal ions (Pb(II),Cd(II), Ni(II), Co(II)), again after modfication with bismuth; for all the analytes detection limits as low as 1 μgL^{-1} are obtained, using a preconcentration time of only few minutes.

Further efforts should be done in order to find new applications for this advanced carbon materials which already displayed advantages compared to commercially available screen printed (SPCE) carbon electrodes. Between them we can list:

- The photolithographic process together with the pyrolysis allows the production of very smooth surfaces which display characteristics comparable to "bulk" glassy carbon. The electrodes are indeed more reproducible and stable than the SPCEs.
- 3-D structures with controlled active area can be obtained with a two-step photolithography process followed by pyrolysis. This carbon structures could find application in the field of catalysis and energy storage.
- By designing a proper mask, one can generate a wide range of diverse electrode geometries for many electroanalytical and electrochemical applications.

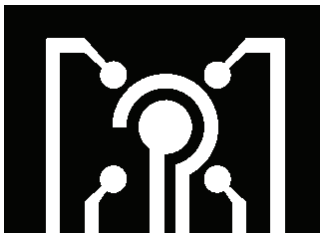

Figure A. Scheme of an array of single addressable electrodes.

Figure A shows the example of an array composed by 4 working microelectrodes (individually addressable) plus counter- and reference electrode, designed and obtained during my stage, which is now presently under characterization. Moreover, thanks to the special characteristics of SU-8, other geometries can be easily produced, so that there is plenty of room to further studies and improvements.

APPENDIX

Publications in international journals and books (peer-reviewed)

- A. Mardegan, P. Scopece, F. Lamberti, M. Meneghetti, L.M. Moretto, P. Ugo, Electroanalysis of trace inorganic arsenic with gold nanoelectrode ensembles, *Electroanalysis*, 24 (2012) 798-806.

- A. Mardegan, S. Dal Borgo, P. Scopece, L.M. Moretto, S.B. Hocevar, P. Ugo, Bismuth modified gold nanoelectrode ensemble for stripping voltammetric determination of lead, *Electrochem Commun.*, 24 (2012) 28-30.

- A. Mardegan, R. Kamath, S. Sharma, P. Scopece, P. Ugo, M. Madou, Optimization of Carbon Electrodes derived from Epoxy-based Photoresist, *J. Electrochem. Soc.*, 160 (2013) B132-B137.

- A. Mardegan, P. Scopece, L.M. Moretto, P. Ugo, An Electrochemical Sensor for Trace Inorganic Arsenic based on Nanoelectrode Ensemble, in *Sensors*, edited by F. Baldini et. al., chap. 81, Springer, New York, 2014. (ISBN: 978-1-4614-3859-5).

- A. Mardegan, S. Dal Borgo, P. Scopece, L.M. Moretto, S.B. Hocevar, P. Ugo, Simultaneous adsorptive cathodic stripping voltammetric determination of Nickel(II) and Cobalt(II) at the in-situ bismuth-modified gold electrode, *Electroanalysis,* 25 (2013), in press, DOI: 10.1002/elan.201300320.

Oral Presentation to National/International Scientific Meetings

- Communication to the 18th Young Investigators' Seminar on Analytical Chemistry (YISAC), held in Novi Sad (SRB) from 28 to 30 June 2011 entitled "*Arsenic determination with ensembles of nanoelectrodes: from batch to flow analysis*" by A. Mardegan, P. Scopece, S. Silvestrini, M. Maggini, P. Ugo.

- Communication to the 14th International Conference on Electroanalysis, ESEAC, held in Portoroz (SLO) from 3 to 7 June 2012 entitled "*Inorganic Arsenic Speciation with 3D-Nanoelectrode Ensemble in Real Samples*" by A. Mardegan, P. Scopece, M. Marchiori, E. Coraluppi, F. Zanon, L. M. Moretto, P. Ugo

- Communication to the 19th Young Investigators' Seminar on Analytical Chemistry (YISAC), held in Nova Gorica (SLO) from 27 to 30 June 2012 entitled "*Field Analysis of Inorganic Arsenic with 3D-Nanoelectrode Ensemble*" by A. Mardegan, P. Scopece, L.M. Moretto, P. Ugo.

- Communication to the 20th Young Investigators' Seminar on Analytical Chemistry (YISAC), held in Maribor (SLO) from 26 to 29 June 2013 entitled *"Preparation of Bismuth film electrode on gold substrate and its application for trace metal detection"* by S. Dal Borgo, A. Mardegan, P. Scopece, L.M. Moretto, P. Ugo, S.B. Hocevar.

- Communication to the 24th Congresso Nazionale di Chimica Analitica, held in Sestri Levante (ITA) from 15 to 19 September 2013 entitled "*Pyrolyzed photoresist carbon electrodes: application to heavy metal analysis*" by A. Mardegan, M. Cettolin, R. Kamath, P. Scopece, M. Madou, P. Ugo.

Poster Contribution to National / International Scientific Meetings

- Communication to ElecNano4 – 7th Echems, held in Paris (FRA) from 23 to 26 May 2011 entitled "*Determination of inorganic arsenic with ensembles of nanoelectrodes: from batch to flow analysis*" by A. Mardegan, P. Scopece, S. Silvestrini, M. Maggini, P. Ugo.

- Communication to Nanotechitaly, held in Venice (ITA) from 23 to 25 November 2011 entitled "*Nanostructured gold electrodes for arsenic determination*" by A. Mardegan, P. Scopece, P. Ugo.

- Communication to Convegno Nazionale Sensori, held in Rome (ITA) from 15 to 17 February 2012 entitled "*Determination of inorganic arsenic with gold nanoelectrode ensemble*" by A. Mardegan, P. Scopece, P. Ugo.

- Communication to the XXIII Congresso Nazionale di Chimica Analitica, held in Elba Isle (ITA) from 16 to 20 September 2012 entitled "*Extension of the potential window accessible to gold nanoelectrode ensembles through deposition of bismuth film*" by L. M. Moretto, A. Mardegan, S. Dal Borgo, P. Scopece, S. B. Hočevar, P. Ugo.